To the Graduate Council:

I am submitting herewith a thesis written by Frank James Dworak entitled "Characterizing Turbulence Structure along Woody Vegetated Banks in Incised Channels: Implications for Stream Restoration." I have examined the final electronic copy of this thesis for form and content and recommend that it be accepted in partial fulfillment of the requirements for the degree of Master of Science, with a major in Environmental Engineering.

John Schwartz
Major Professor

We have read this thesis
and recommend its acceptance:

Randy Gentry

Carol Harden

Accepted for the Council:

Anne Mayhew
Vice Chancellor and
Dean of Graduate Studies

(Original signatures are on file with official student records.)

Characterizing Turbulence Structure along Woody Vegetated Banks in Incised Channels: Implications for Stream Restoration

A Thesis
Presented for the
Master of Science
Degree
The University of Tennessee, Knoxville

Frank James Dworak
December 2005

Acknowledgements

I would like to thank Dr. John Schwartz for serving as my major professor. His help and expertise played an essential role in this project and my graduate education. I would also like to express my gratitude to Dr. Randy Gentry and Dr. Carol Harden for sitting on my committee and taking the time to help with my thesis defense.

I would also like to thank Dr. Michael Sale at the U. S. Department of Energy, Hydropower Program, Oak Ridge National Laboratory, for partially funding this research through the UT-Battelle Subcontract No. 4000035554. Additional funding for this project came from the University of Tennessee. Many thanks to Dr. Fotis Sotiropoulos and Dr. Joongcheol Paik at the Georgia Institute of Technology for their help and knowledge in computational fluid dynamics.

This project could not have been possible without the help of Kelley Williams, Brantley Thames, Robert Sain, and Dr. John Schwartz in gathering field data at the Beaver Creek Research site.

Likewise, I would like to thank my family, who have always supported me and helped me throughout the many years of my college education.

Abstract

The impacts of urbanization have modified natural watersheds and stream hydraulic, hydrologic, and geomorphic processes that have lead to geomorphic and ecological disturbances in natural stream systems. These alterations have resulted in channel incision and the loss of channel-scale hydraulic characteristics responsible for initiating and maintaining pool-riffle bedforms, which are capable of supporting diverse biological stream ecosystems. Through the use of FLOW-3D, a 3-dimensional computational fluid dynamics model, three scenarios of an urban, incised, and channelized stream were simulated to characterize the turbulent, hydraulic structure during bankfull discharge. The simulations were conducted with trees inhibiting bankfull flow (representing the channel's current state), trees removed from the channel, and a restoration design using three clusters of the original trees to initiate flow acceleration-deceleration regions. These simulations suggested that hydraulic processes found to initiate and maintain pool-riffle sequences can be restored to impaired urbanized channels for which these processes have been lost. This research can be applied to stream restoration design in hopes to establish less invasive procedures that can promote the development and maintenance of natural stream processes. If the natural processes can be restored to the channel, it is likely the project will have a higher degree of success in the future of the stream system.

Table of Contents

Chapter 1: Introduction 1

Chapter 2: Literature Review 8

Channel Evolution 8
Macro-bedforms 13
Hydrodynamics 14
Turbulence 18
Pool-Riffle Maintenance for Stream Restoration Design 27

Chapter 3: Methods 31

Study Design 31
Study Area 32
Topographic Characterization 35
3-Dimensional Hydrodynamic Model 38
Model Preparation 41
Finite Element Grid Generation 43
Hydraulic Criteria and Boundary Conditions 45
Post Processing 49

Chapter 4: Results 56

Channel with Trees 56
Channel without Trees 62
Channel with Restoration Design 65

Chapter 5: Discussion of Results 73

List of References 77

Appendices 82

Appendix A 83
1-Meter y-z Cross-Sections of the Channel with Trees 84
Appendix B 104
1-Meter y-z Cross-Sections of the Channel without Trees 105
Appendix C 125
1-Meter y-z Cross-Sections of the Channel with Restoration Design 126

Vita 146

List of Figures

Figure 1.1: Helical flow patterns occurring in a sinuous channel 5
Figure 1.2: Helical flow patterns experienced in a channel bend 5
Figure 2.1: Models of (A) channel evolution and (B) bank-slope development for disturbed alluvial channels 9
Figure 2.2: Coefficient of drag for spheres (CD) relative to Particle Reynolds Number (Re_p), based on the best-fit equation from White, 1974 12
Figure 2.3: The morphology of single-row alternate bars in straight channels 15
Figure 2.4: A fluid element, A, subjected to shear stresses τ and P 20
Figure 2.5: The development and growth of an eddy with high and low velocity flow regions 22
Figure 2.6: The destruction process of a macroturbulent eddy 23
Figure 2.7: Examples of several turbulent flows illustrating the growth rate in terms of θ 25
Figure 2.8: The bursting processes in a vertical sequence to illustrate a possible relationship between macroturbulent bursting processes and alternating bedforms 26
Figure 3.1: Research watershed and site scaled from a Tennessee county map created in Arcmap 33
Figure 3.2: Land-use map of the research watershed generated in Arcmap 34
Figure 3.3: Photo of Beaver Creek research site during bankfull flow 36
Figure 3.4: Photo looking down the channel of the Beaver Creek research site during bankfull flow 37
Figure 3.5: Tecplot image of research site (channel only) 39
Figure 3.6: Tecplot image of research site (channel and trees) 40
Figure 3.7: FLOW-3D interpolated image of the research site (with trees) 42
Figure 3.8: FLOW-3D image of the mesh generating process 44
Figure 3.9: A FLOW-3D image of a simulation in progress showing the stabilization of the “stability limit vs. time” and “time step size vs. time”, indicating steady state conditions 47
Figure 3.10: A FLOW-3D image of the 3-dimensional analysis window setup for a 10-second velocity magnitude display 51
Figure 3.11: A FLOW-3D image of the 2-dimensional analysis window setup for a 10-second velocity magnitude display, in the x-y plane, with plain vectors scaled to a factor of 2 52
Figure 3.12: A FLOW-3D image of an example of a 3-dimensional display 53
Figure 3.13: A FLOW-3D image of an example of a 2-dimensional display in the y-z plane 55
Figure 4.1: Modeled positive and negative y and z-velocities (m/s) in the channel with the trees present 57
Figure 4.2: Tecplot image of the channel with all of the trees present to better illustrate the location of the trees with relation to the study site 58

List of Figures Continued

Figure 4.3: Modeled velocity magnitude and velocity magnitude vectors illustrated in y-z cross-sections in the channel with the trees present 59
Figure 4.4: Modeled turbulent kinetic energy diagram of the channel with the trees present 61
Figure 4.5: Modeled positive and negative y and z-velocities (m/s) in the channel with the trees removed 63
Figure 4.6: Modeled velocity magnitude and velocity magnitude vectors illustrated in y-z cross-sections in the channel with the trees removed 64
Figure 4.7: Modeled turbulent kinetic energy diagram of the channel with the trees absent 66
Figure 4.8: Modeled positive and negative y and z-velocities (m/s) in the channel with the restoration design implicated 67
Figure 4.9: Tecplot image of the channel with restoration design to better illustrate the location of the trees with relation to the study site 69
Figure 4.10: Modeled velocity magnitude and velocity magnitude vectors illustrated in y-z cross-sections in the channel with the restoration design implemented 70
Figure 4.11: Modeled turbulent kinetic energy diagram of the channel with the restoration design implemented 71

Chapter 1: Introduction

The effects of urbanization on natural stream morphology and habitat are a growing concern. Impacts from urbanization modify the natural watershed and stream hydraulic, hydrologic and geomorphic processes by altering the landscape, modifying vegetation and soil characteristics, and introducing impervious surfaces and drainage (Palhegyi et al. 2003). Urban changes to watersheds lead to greater peak flows and increased frequency storm events, resulting in hydraulic and hydrologic changes that can initiate channel incision (Doerfer and Urbonas 2003). An effect of channel incision is the disconnection between the stream and its floodplain, leading to simplified streambed morphology (Schwartz and Herricks 2005A). Unlike simple streambeds, complex pool-riffle sequences provide a variety of hydraulic flow patterns and structural environments able to support diverse ecosystems (Bombardelli et al. 2000, Sear and Newson 2004, Rodriquez et al. 2000). The flow and substrate diversity seen in natural channels with pool-riffle streambed morphology diminishes in the incised streams (Sear and Newson 2004, Schwartz and Herricks 2005A).

Channel incision occurs when there is an imbalance between sediment transport and sediment supply that alters channel morphology through bed and bank erosion (Bledsoe et al. 2002). Incision is especially evident in channels disturbed by urbanization and channelization, a straightening and shortening of a stream. When a channel is straightened, hydraulic changes occur. The total energy available to the channel increases overall and is coupled with increases in the velocity magnitude (Rychborst 1980, Booker et al. 2000). This causes instability in the system, resulting in erosion by

means of channel incision as riffles erode and pools aggrade (Rychborst 1980, Schwartz and Herricks 2005A, MacRae 1996). Other hydraulic changes historically recognized in incised channels are decreases in energy slope, decreases in upstream water surface elevations, increases in lateral and longitudinal flow patterns, increases in downstream water surface elevations, and increases in sediment loads downstream of the channel incision and straightening (Rychborst 1980). Channels with these characteristics have diminishing bank stability and are synonymous with Stage III streams in the Channel Evolution Model (Simon 1995). Prior to bank failure, woody vegetation and root structure occupy the banks and provide temporary stability and decrease bank erosion (Simon 1995). While the woody vegetation aids in bank protection, it modifies turbulence structure and decreases lateral kinetic energy along the banks, therefore, possibly contributing to the destruction of the pool-riffle sequence within these channels.

Pool-riffle sequences are the dominant macro-bedforms in alluvial channels of intermediate slope (Sear and Newson 2004, Gregory et al. 1994, Richards 1976). The sequences routinely occur between 5 to 7 channel widths in succession in both sinuous and non-sinuous channels, and are strongly influenced by width to depth ratios (Keller and Melhorn 1978, Gregory et al. 1994, Dietrich 1987). Pool-riffle bed morphology controls hydraulic patterns, which in turn control bed scour, sediment transfer and deposition in streams, playing an important role in the geomorphic characteristics of the channel (Heritage and Milan 2004).

Equally important, pool-riffle sequences offer a variety of flow fields and substrates that provide an environment capable of supporting a diverse biological ecosystem (Sear and Newson 2004, Schwartz 2002, Rhoads et al. 2003). Naturally, there is an acceleration of flow over riffles and a deceleration within pools. Riffles tend to support benthic macro-invertebrate populations and small fish, while pools can support larger fish and provide critical habitat during low flows (Thompson 2002). Complexities in morphological character, including heterogeneous distributions in bed substrates, provide adequate cover for protection from predators and high flow events (Thompson 2002, Schwartz and Herricks 2005). Together, these characteristics make pool-riffle sequences dominant features in stream restoration. Although the pool-riffle sequence is well understood for its importance to stream health and aquatic habitat, little is known about the lack of maintenance in pool-riffle sequences within incised channels.

There are many theories supporting the maintenance of pool-riffle sequences that stem from sedimentological and hydraulic based processes. It has been proven that these process-based theories cannot stand alone to explain the maintenance of pool-riffle sequences in every case, while on the other hand, literature has supported pool-riffle maintenance through a combination of both, process and hydraulics (Dietrich 1987, Sear and Newson 2004). Phase shifts are process-based and begin when bar height is gradually decayed by lower flows, scouring fine sediment from riffles and depositing it into pools (Wilkinson et al. 2004). Conversely, higher flows scour pools and buildup riffles, increasing riffle height and maintaining pool depth (Wilkinson et al. 2004). Similarly, velocity reversals center on sediment transport capacities, increasing during

high flow and decreasing in low flows (Wilkinson et al. 2004). As these are major contributions to pool-riffle maintenance, the hydraulic characteristics of the stream provide the actual work necessary for the preservation process (Dietrich 1987). The continuously changing velocity patterns, as flow increases over riffles and decreases in pools, are primary hydraulic characteristics within pool-riffle sequences, but helical flow patterns govern hydraulic maintenance (Dietrich 1987). Helical flow patterns are caused by velocity profiles, pressure gradients, free-surface elevations, and near-bed shear stresses (Dietrich 1987, Rychborst 1980). These flow patterns are 3-dimensional regimes that are seen in both sinuous and non-sinuous channels.

The concepts governing helical flow are most obvious in sinuous channels, but are also experienced in straight channels. Dietrich offers a comprehensive description of helical flow within a stream bend, while Figures 1.1 and 1.2 help to visualize the patterns. Stream bends result in centrifugal forces acting in cross-channel patterns. These forces are counter-balanced by a cross-channel slope of the free surface, causing a cross-channel pressure gradient. Near surface flow is conveyed outward against the opposing pressure gradient, while slower, near bed velocities are turned inward. Within straight channels, alternate bar development influences the cross-stream and near bed velocity distributions, invoking helical flow patterns (Dietrich 1987). Near bed shear stresses also play important maintenance roles as they increase in pools when discharge approaches bankfull levels (Booker et al. 2000). During low flow conditions riffles experience the high near bed shear stresses while bed shear stresses decrease in pools (Booker et al.

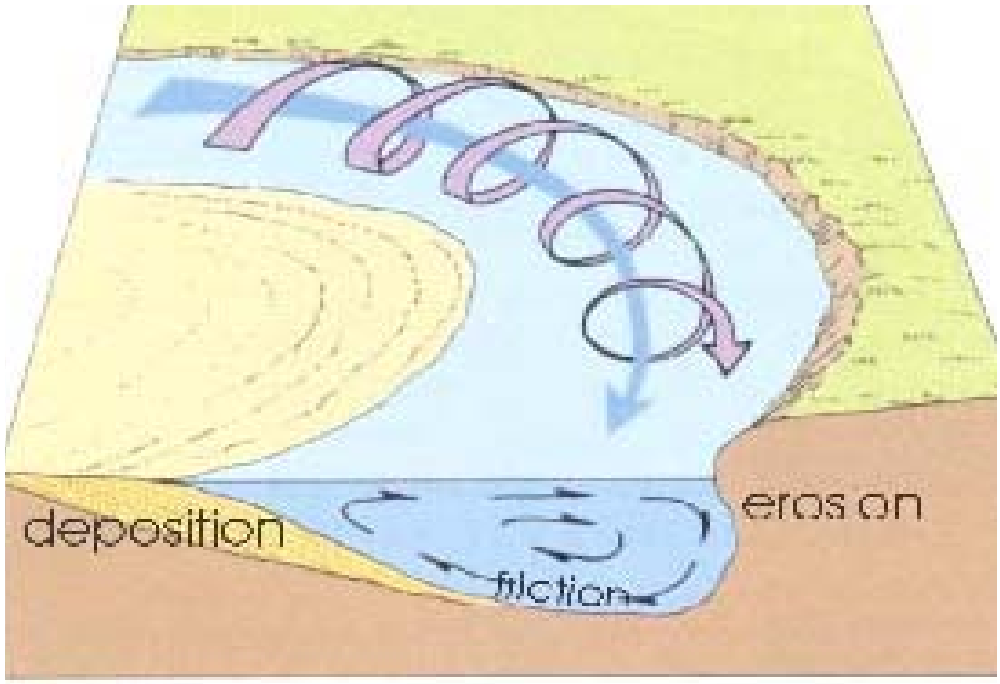

Figure 1.1: Helical flow patterns occurring in a sinuous channel (Tuysuz 2002).

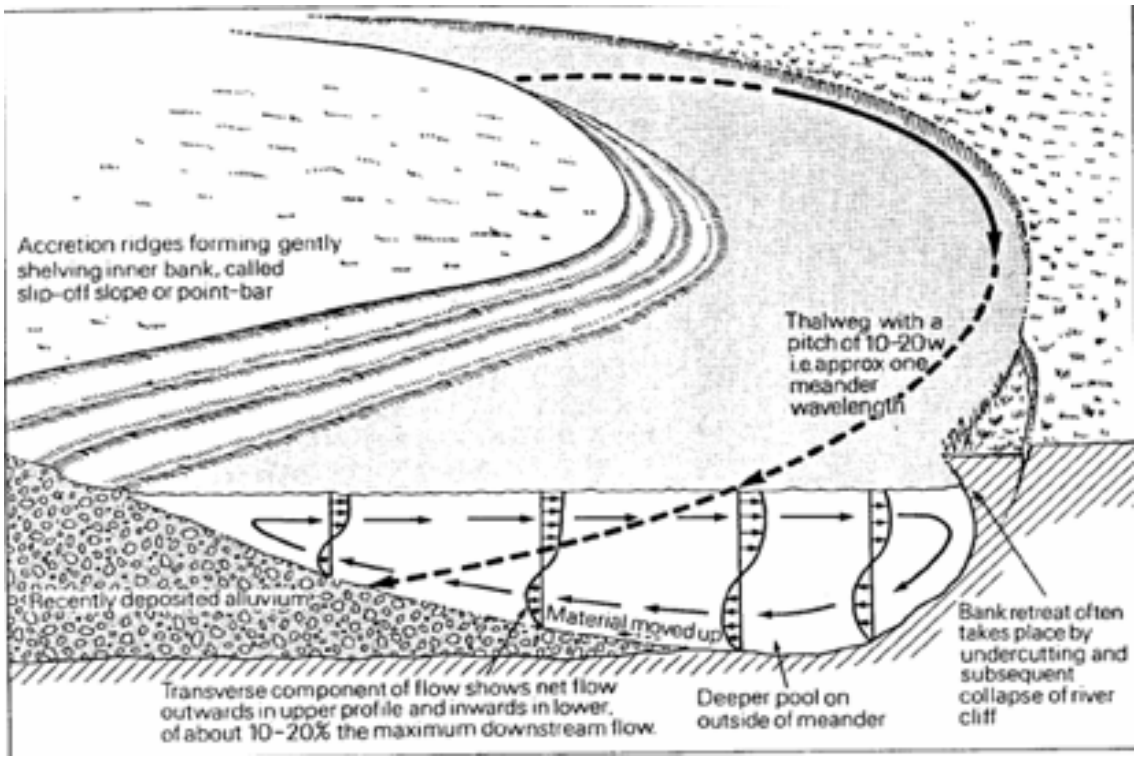

Figure 1.2: Helical flow patterns experienced in a channel bend (Smith and Stopp 1978).

2000). Similarly, there are consistent observations of progressive declines in bed roughness as flow increases (Sear and Newson 2004). Overall, the complexity of the special patterns of near-bed velocities and boundary shear stresses decline as flow increases (Booker et al. 2000). This information can be a valuable resource when evaluating stream restoration techniques.

Modern approaches suggest that the creation of pool-riffle habitat is one of the most important criteria for evaluating the success of channel restoration projects (Thompson 2002, Sear and Newson 2004, Emery et al. 2003, Schwartz and Herricks 2005A). The current problem exists that there are not adequate design criteria for the development and maintenance of pool-riffle streambed morphology. While it is common to construct pool-riffle bedforms within stream restoration projects, it does not necessarily restore the sustainable hydraulic functioning needed to maintain these bedforms (Emery et al. 2003, Gaboury 1997). Characterizing the hydraulic properties of flow over pool-riffle sequences in open channels is critical for understanding sediment transport and morphological evolution processes of unaltered streams, and therefore, is relevant to stream rehabilitation and management (Cao et al. 2002).

The objective of this research is to characterize the turbulence structure experienced by an urban, incised stream in order to understand the hydraulics associated with pre-bank failure conditions of Stage III channels and the degradation of pool-riffle sequences. Beaver Creek in north Knox County, Tennessee, has been impacted by urban sprawl within its watershed. The stream has been channelized, incised, and separated from its

floodplain. Trees that were once part of the floodplain interrupt bankfull flows, causing increases in bank roughness. Mass bank-failures have not yet occurred due to the cohesive properties of the soil in this region and the elaborate root systems of the vegetation lining the banks. According to the Channel Evolution Model, the banks will ultimately fail as lateral erosion exceeds the bank stability threshold and cause considerable degradation within this section of channel, further degrading the quality of the stream as a whole (Simon 1995). Additionally, this research supports a hydraulic design approach for stream restoration with the goal to test an ecohydraulic design that initiates and provides natural maintenance of pool-riffle sequences.

Chapter 2: Literature Review

Channel Evolution

Alluvial channels react to physical and hydrologic disturbance by altering their geomorphic, sedimentologic, and hydraulic properties in order to create and follow the path of least resistance (Palhegyi et al. 2003, Simon 1995). These reactions are systematic in nature and have been categorized in channel evolution models in order to help recognize and understand channel responses to impacts from urbanization and changing environments (Simon 1995, Bledsoe et al. 2002). Simon (1995) has documented six different evolutionary stages of channel development and has summarized the findings in the Channel Evolution Model, see Figure 2.1. The evolution of the Beaver Creek research site has followed Simon's Channel Evolution Model with evidence of the first three stages of development.

Stage I is evident within the research site only when considering the entire domain of Beaver Creek in Knox County. Some sections of the stream upstream of the research site are still in the pre-disturbed stage, characterized by stable bars, convex top-bank shape, high flow lines relative to the top of the bank, and vegetated banks down to the flow lines (Simon 1995). Stage II has occurred through channelization, evident in the linear bank surfaces, similar riparian species and age, and separation between the stream and its floodplain (Simon 1995). The sections of channel in and around the research site are currently experiencing the pinnacle of the Stage III evolutionary process, with signs of severe incision and increasing bank instability.

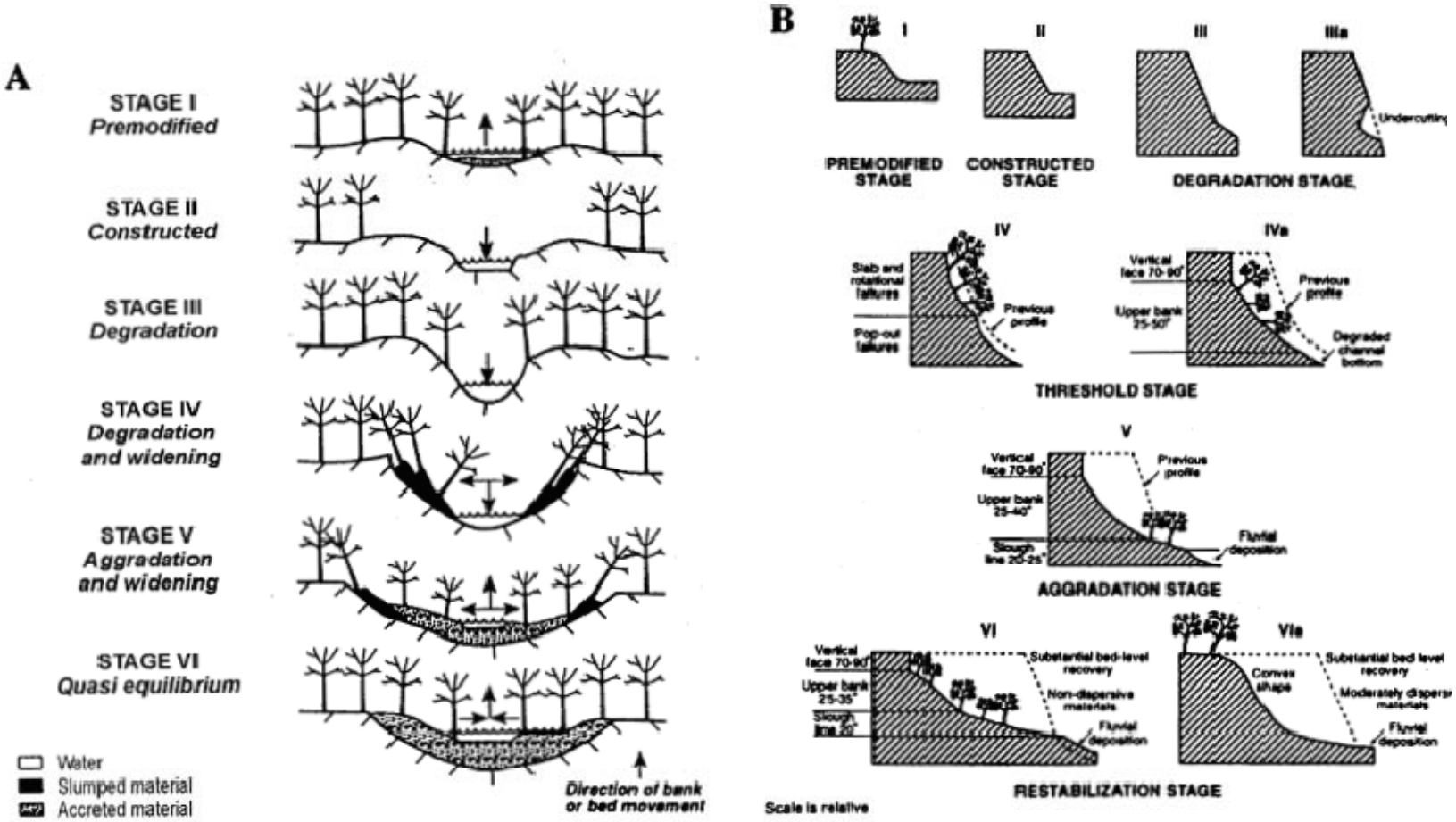

Figure 2.1: Models of (A) channel evolution and (B) bank-slope development for disturbed alluvial channels (Simon and Hupp 1986).

Stage III is considered the degradation stage and is prominent in urbanized watersheds (Simon 1995, Bledsoe et al. 2002). Channel incision is the dominant characteristic within Stage III channels and is evident through heightening and steepening of the banks, erosion of alternate bars, riparian vegetation is high on the banks relative to the flow lines, and the flow lines are lower relative to the top of the bank (Simon 1995). Overall stream power is increased in incised channels, changing their sediment transport and sediment supply characteristics (Bledsoe et al. 2002, Rychborst 1980).

Sediment transport and supply are directly related to properties of flow hydraulics, streambed and bank material compositions, and upstream sediment contributions (Langendoen 2000, Julien 1998, Sturm 2001). The stability of the bed and banks of an alluvial channel can be determined through the threshold of sediment movement (Sturm 2001). This threshold of motion is most often linked to the Shields parameter and is most easily defined in terms of critical shear stress, τ_c. Critical shear stress is described as a function of the following variables:

$$\tau_c = f_1(\gamma_s - \gamma, d_s, \rho, \mu)$$

where γ_s-γ is the submerged specific weight of the sediment, d_s is the sediment grain size, ρ is the fluid density, and μ is the dynamic viscosity of the fluid. These terms can be linked through dimensional analysis and expressed as:

$$\frac{\tau_c}{(\gamma_s - \gamma)d_s} = f_2\left(\frac{u_{*c}d_s}{\nu}\right)$$

in which u_{*c} is the critical value of the shear velocity and is equal to $(\tau_c / \rho)^{1/2}$, while the kinematic viscosity, v, is equal to (μ / ρ). This equation cannot be solved directly, but critical shear stress and velocity can be solved for iteratively. Once a particle reaches the threshold of motion, if the stream velocity is greater than the fall velocity of the particle, the sediment will be transported downstream. The fall velocity of sediment is defined by Sturm (2001) as the terminal speed of a sediment grain in water at a specified temperature in an infinite expanse of quiescent water. An expression has been developed for fall velocity based on a spherical particle defined by:

$$w_f = \sqrt{\frac{\frac{4}{3}(\gamma_s / \gamma - 1) g d_s}{C_D}}$$

where w_f is the fall velocity, g is the acceleration due to gravity, and C_D is a drag coefficient related to the sphere. Similar to the equation for the threshold of motion, this equation cannot be solved explicitly because C_D is a function of Particle Reynolds Number, Re_p ($Re_p = w_f d_s / v$). To make an iterative solution easier to solve, C_D vs. Re_p diagrams have been developed. The plot shown in Figure 2.2 was developed from a best-fit equation by White (1974) and expressed as:

$$C_D = \frac{24}{Re_p} + \frac{6}{1 + \sqrt{Re_p}} + 0.4$$

The sediment movement equations support the theory that increased shear stresses and velocities experienced in incised channels encourage sediment erosion and transport. In natural alluvial stream systems, sediment transport and deposition are necessary

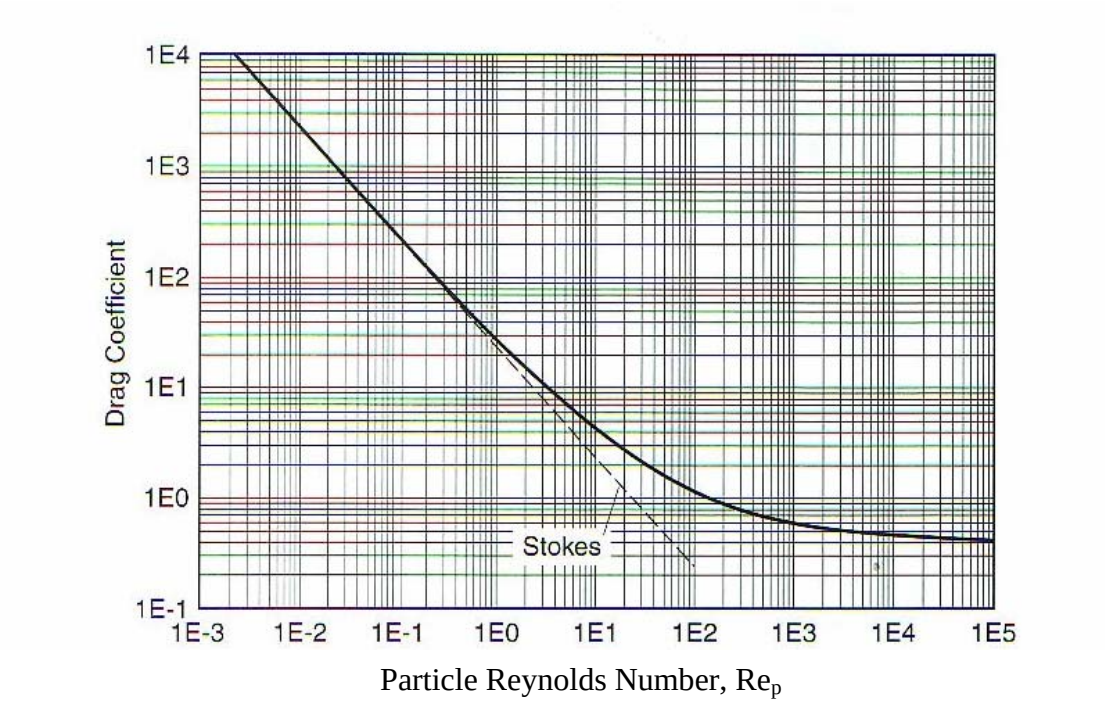

Figure 2.2: Coefficient of drag for spheres (CD) relative to Particle Reynolds Number (Re_p), based on the best-fit equation from White, 1974 (Sturm 2001).

conditions for meander initiation, however they are the effects of some original cause, like high flow events, but not the cause itself (Rhoads and Welford 1991).

Macro-bedforms

Pool and riffle macro-bedforms are created from mobile beds in alluvial channels and have been discovered in both straight and meandering channels with heterogeneous bed material (Knighton 1998). Pools have been defined as topographically low areas produced by scour, which generally contain relatively fine grained bed-material, whereas riffles are topographically high areas produced by the accumulation of relatively coarse grained bed-material (Gregory et al. 1994). The variation in bed material between pools and riffles suggest local sorting mechanisms (Knighton 1998). They also exhibit distinct channel and flow geometries, where riffles tend to be wider and shallower at all stages of flow (Knighton 1998). Furthermore, a significant property of pool-riffle geometry is the recurrent spacing of successive pools or riffles at a distance of 5 to 7 times the channel width (Knighton 1998, Keller and Melhorn 1978).

Considerable research has been done to define the relationship between pool-to-pool, or riffle-to-riffle spacing, and channel width (Dietrich 1987). The most extensive data set for this research comes from Keller and Melhorn, 1978, who found pool-to-pool spacing ranging from 1.5 to 23.3 channel widths, with an overall mean of 5.9 channel widths (Knighton 1998). Further research has supported this spacing trend, with inter-pool or inter-riffle spacing ranging from 5 to 7 channel widths. The regularity of the pool-riffle

sequence has sometimes led to its definition as a single bed-form at times referred to as the bar unit (Dietrich 1987).

Pool-riffle sequences spaced 5 to 7 channel widths have been found in all types of streams, from sand and gravel beds, to bedrock and boulder-bed courses (Knighton 1998). Even in channels disturbed by channelization, the inter-riffle distance generally falls within the range of 5 to 7 channel widths (Gregory et al. 1994). However, with a wide variety of disturbances, negatively impacted streams do not always conform to the 5 to 7 width guidelines (Gregory et al. 1994). Gregory et al. further suggest that more research should be conducted on establishing the relationship between pool-riffle spacing and channel width for particular types of influence on the channel environment in order to define the degree to which each channel conforms to the 5 to 7 channel width spacing. The accurate scale at which pool-riffle sequences occur is needed for further investigation into the processes that form and maintain these bedforms.

Hydrodynamics

Mechanisms that produce flow oscillation in straight channels are based on hydrodynamic theories of meander initiation (Rhoads and Welford 1991). In straight, erodible channels, the initial motion of bed material occurs parallel to the stream banks, causing scour holes to develop rapidly along the bed. The material is scoured at regular intervals occurring along alternate sides of the channel. The eroded sediment is deposited downstream in fan-shaped bars that overlap in a regular pattern forming alternate bars, Figure 2.3 (Dietrich 1987). Rhoads and Welford (1991) continue by trying to explain the

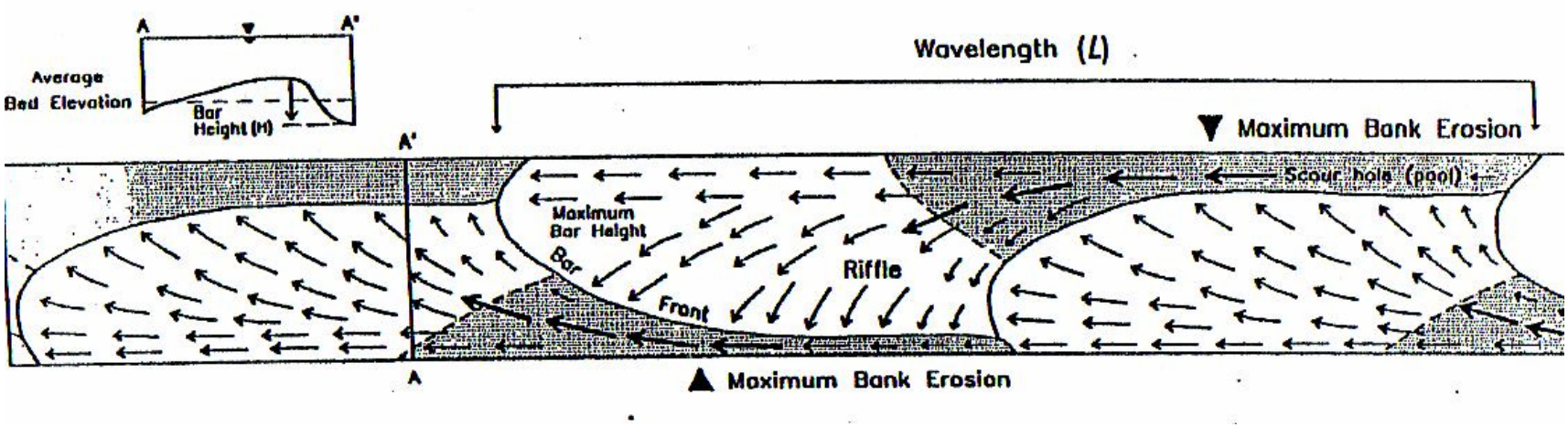

Figure 2.3: The morphology of single-row alternate bars in straight channels. Shaded areas are below reach-averaged bed elevation, arrows indicate patterns of flow, and heavy arrows mark position of the thalweg (Rhoads and Welford 1991).

initial development of the alternating bars in straight channels using the research available at the time of the publication. The formation of alternate bars during low values of excess shear stress and high width to depth ratios suggests that low-flow dictates the phenomenon. This has been observed in channels consisting of coarse, heterogeneous bed material. However, when armoring has occurred, this phenomenon ceases at low values of excess shear stress and 3-dimensional flow regimes dominate the process of alternate bar initiation.

Periodically reversing helical flow patterns have consistently been recognized as a fundamental characteristic of flow in meandering rivers and have recently been conceptualized as a mechanism for initiating periodic, alternating bed deformation of the channel bed and banks (Rhoads and Welford 1991, Dietrich 1987). Continuing with the Rhoads and Welford (1991) research, they have linked the occurrence of helical flow patterns in straight channels to anisotropic turbulence initiating bed scour at recurring intervals. Both gradual and abrupt variations in boundary roughness have been found to produce helical flow in straight channels. Models have been constructed with channels consisting of coarse materials lining the center and finer materials along the banks to produce contra-rotating, surface convergent, circulation cells along opposite sides of the channel further producing helical patterns. Other theories use low-velocity, high vorticity eddies shed continuously from wall boundaries into the outer region of flow. These eddies form a horseshoe shaped flow regime moving up along the banks and toward the center of the channel surface. If these flow regimes develop along both banks, twin surface convergent helical flow patterns result. When these helical flow patterns occur at

regular intervals, they may be capable of transporting sediment laterally across the channel to produce alternate bars. Instability, caused by rising stage flood events within the flow regime, could provide cell asymmetry and periodic reversal. These dominant circulation patterns may eventually lead to alternating bars and a meandering thalweg. This metamorphosis from a straight channel has been theorized in the bar theory and starts as infinitesimal harmonic perturbations in the bed that grow at various rates to ultimately create a meandering stream. Dissimilarities among theories stem from variations in hydrodynamics, channel morphology, and sediment properties.

The theories developed to account for meander initiation and alternate bar formation have been supported by laboratory and/or field research. Many of these theories are case-specific and criticized for generating non-repeatable results in varying channels. Rhoads and Welford (1991) concluded that a universal theory of meander initiation had not emerged and that it is likely that a combination of theories can explain the occurrence. In this thesis research, the hypothesis of incessant incision due to stream bank stability does not allow the formation of alternating bars at the Beaver Creek research site. With greater shear stresses occurring at the bed, channel incision will progress until a threshold is reached and the erosive properties of the bank exceed that of the bed and its increased shear stress combined.

The banks along the research site are resistant to erosion, in part due to the cohesive properties of the bank material and the structured vegetation and root systems covering the banks. The soils around the research site, as well as the Tennessee Valley region, are

high in clay and are more cohesive than those high in sand (Coduto 1998). Cohesive properties of clays cause particles to bond and resist hydraulic erosion, while further bank stability is achieved when root systems are combined with cohesive soils (Simon and Thomas 2002, Simon and Collison 2002). Soils are generally strong in compression but weak in tension, whilst root fibers are strong in tension and weak in compression forming a matrix for the bonding soil (Simon and Collison 2002, Coduto 1998). In addition to providing a structural matrix, the riparian vegetation also helps to lower pore pressure, additionally increasing the strength of the streambank (Simon and Collison 2002). This increased stability not only resists erosion but also allows the trees to remain low enough on the bank to participate in bankfull discharges. These trees increase turbulence along shores dissipating energy and stunting the progression of the channel evolution process.

Turbulence

Turbulence is best characterized as highly disordered and chaotic fluid motion over a wide range of length scales and frequencies (Ziaei et al. 2005). In turbulent flow, an individual particle will follow a very irregular and erratic path, with no two particles having identical or even similar paths, causing its behavior to be stochastic in nature (Franzini and Finnemore 1997, Keshavarzi et al. 2005). The structure of fully developed turbulent flow consists of a hierarchy of eddies and vortices of various sizes and disorders (Ziaei et al. 2005, Yalin 1992, Keshavarzi et al. 2005). The nature of the eddies and vortices is best described in a quote from L. F. Richardson's *Whether prediction by numerical process*, as "big whorls have little whorls, which feed on their velocity; and little whorls have lesser whorls, and so on to viscosity…" (Keshavarzi et al. 2005).

Although a great deal of research has been conducted on the bursting process and coherent structure of turbulence, little is still agreed upon its detailed mechanism (Yalin 1992). However, their general patterns have been summarized and well explained in detail by Yalin (1992).

Yalin (1992) defines turbulence as a living entity consisting of birth, life, and death. Previous theories stressed the importance of the large eddies that break down in an energy cascade and give rise to smaller eddies. It wasn't until researchers discovered the bursting process, which proved that the largest eddies started as much smaller eddies produced near flow boundaries. In fact, the closer to the boundary the eddy is born, the smaller its initial size. Immediately after its generation, the eddy is carried upward and conveyed downstream. The upward velocity decreases while the size of the eddy increases, due to coalescence and engulfment. The eddy continues to grow until it contacts the boundary layer, when it is destroyed, giving rise to the next eddies in succession. This process of eddies originating, growing, being destroyed, and therefore giving rise to new eddies is known as the bursting process.

Yalin gives an excellent explanation of the bursting process starting at the fluid element. Figure 2.4 is an illustration of a fluid element, A, subjected to shear stresses τ at P. If the value of τ is sufficiently large, instead of deforming into a highly strained parallelogram shown as B, the element chooses to roll up into an eddy, which can be considered the path of least resistance for the element.

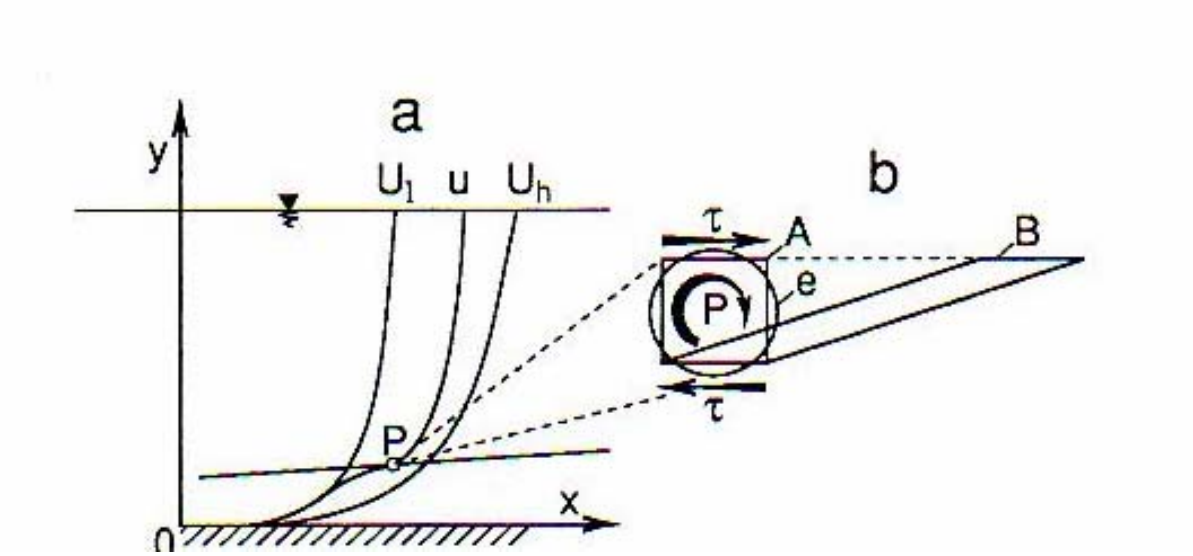

Figure 2.4: A fluid element, A, subjected to shear stresses τ at P (Yalin 1992).

Yalin then simplifies the growth and destruction of the newly formed eddy, as shown in Figures 2.5 and 2.6. The eddy e is formed by both high and low velocity fluids. It travels upward in the low velocity region, just alongside the region of high velocity, growing in size as it progresses in the trajectory s. The displacement of fluid mass as e moves along s instigates circulatory motions within the low velocity regions, expressed as e' and e". The interface between e" and the region of high velocity acts as a high shear zone and a region of instability. Together these secondary circulatory motions act opposite one another to form an ejection motion from m to e. The high velocity fluid continues to be capable of overtaking the eddy in the gap formed between the eddy and the free surface. The continual upward displacement and growth of the eddy weakens the ejection force while reducing the gap between the eddy and the free surface. This causes the high velocity fluid to suddenly change its configuration and pass under the eddy, known as the sweep. Following the sweep, the high velocity region widens and interacts with e', reducing the velocity. This causes the flow around the eddy to be neutralized, while the eddy continues to grow in size. Figure 2.6 shows the events as the eddy progresses in the neutralized flow and becomes a macroturbulent eddy E, characterized by the eddy size being nearly equal to the flow thickness, h. The macroturbulent eddy continues to grow until it interacts with the free surface. This interaction causes the eddy to deflect downward toward the bed, resulting in the disintegration of the eddy. The disintegration progresses through an energy cascade, where there is a successive break up into smaller and smaller eddies until it is dissipated through viscous friction. The disintegration of the eddy signifies the disappearance of stress relief in the fluid at that location.

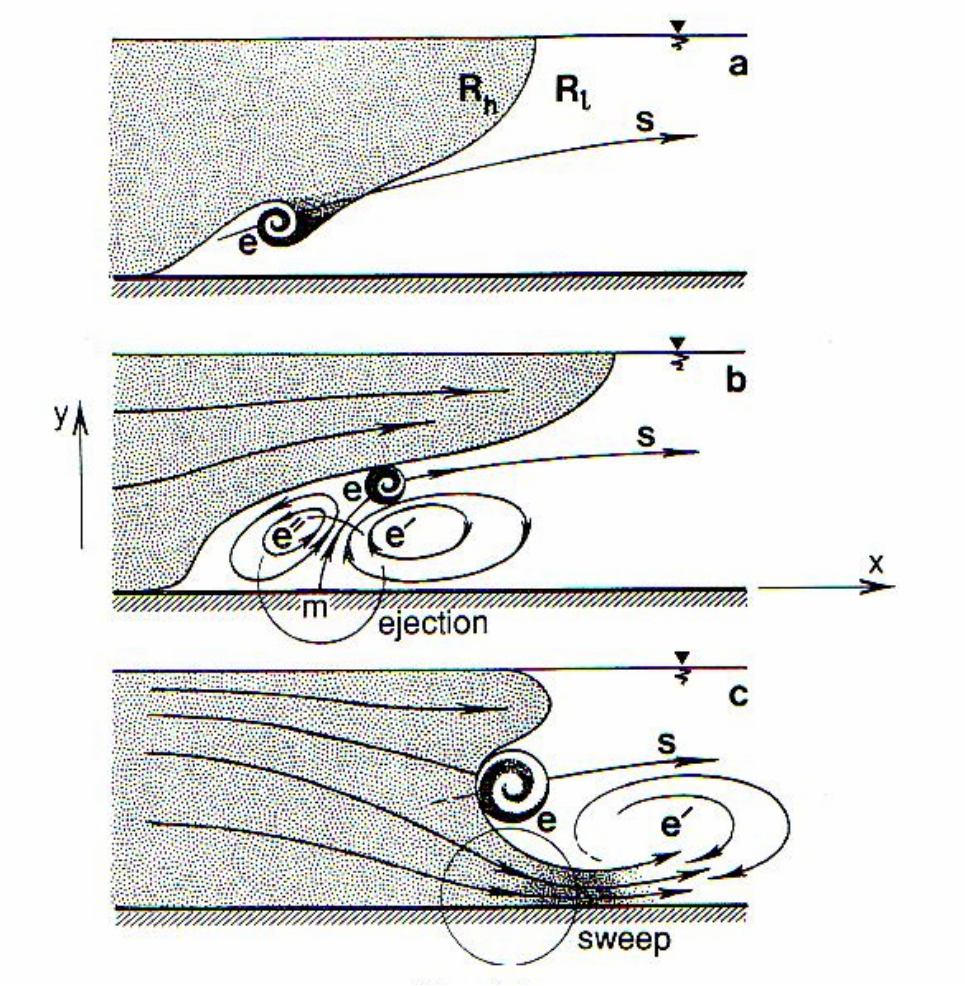

Figure 2.5: The development and growth of an eddy with high and low velocity flow regions (Yalin 1992).

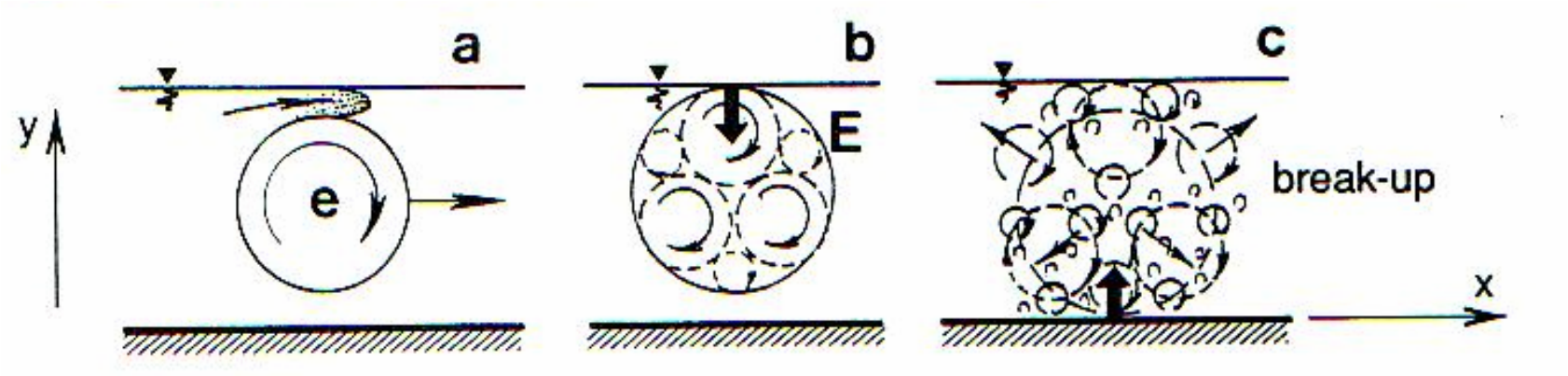

Figure 2.6: The destruction process of a macroturbulent eddy (Yalin 1992).

Yalin continues the discussion of turbulent eddies, pointing out that the growth rate of the turbulent eddies occurs in a distinct pattern in the direction of flow. Observation of several turbulent flows, Figure 2.7, result in a burst length, l, being approximately equal to the tan θ, and equal to 1/6 the distance in the flow direction, x. Normalizing this observation to a burst-forming eddy, the expression can be written as:

$$L \approx 6h$$

This indicates that the burst length, L, is approximately equal to six flow depths, h. Note the significance of the burst length in comparison to the bar unit, being 5 to 7 channel widths. Assuming accuracy sufficient for macroturbulent eddies and channels with large friction factors, the burst forming eddy being conveyed downstream can be identified with an average period, T. The relationship in terms of an average flow velocity, v, can be expressed as:

$$\frac{L}{h} = \frac{vT}{h} \approx 6$$

Similar to the patterns of burst length, burst width, L', has been defined as being approximately equal to two flow depths, based on observations in natural channels and experimental data. These patterns are only reasonable for large-scale patterns and are expressed as:

$$L' \approx 2h \text{, which can also be stated as } L' \approx \frac{1}{3}L.$$

Yalin further pieces together successive periods of the bursting process in a vertical sequence in order to illustrate a possible relationship between macroturbulent bursting processes and alternating bedforms, as shown in Figure 2.8.

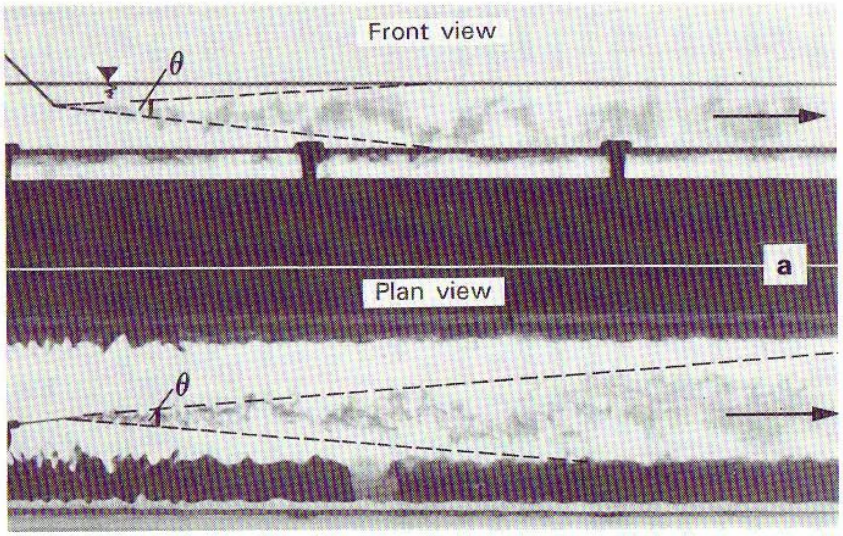

Fig. 2.6

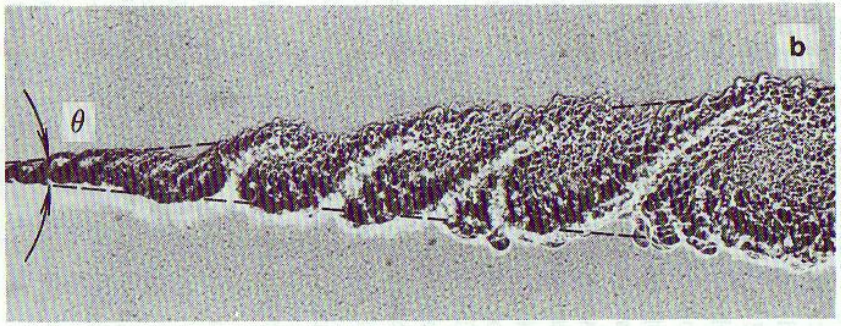

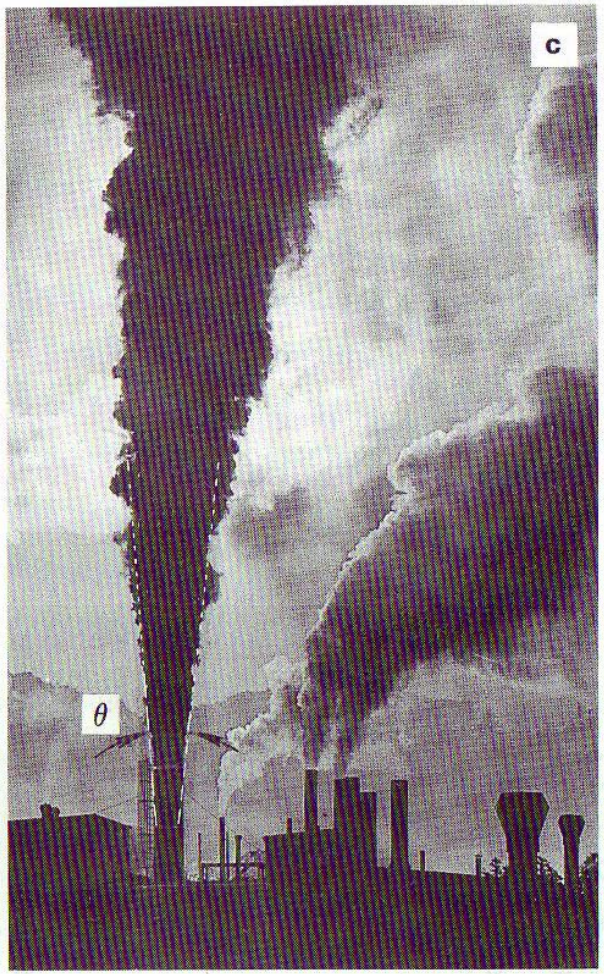

Figure 2.7: Examples of several turbulent flows illustrating the growth rate in terms of θ (Yalin 1992).

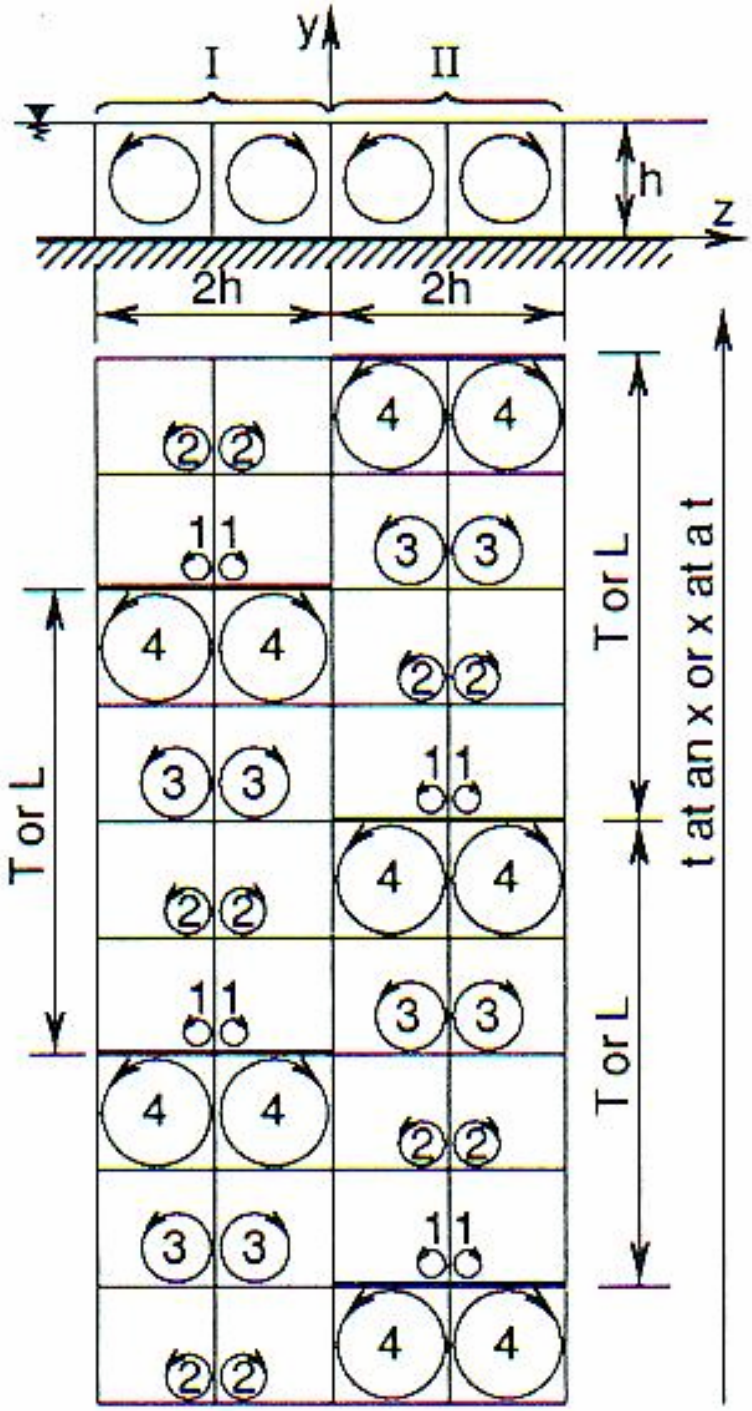

Figure 2.8: The bursting processes in a vertical sequence to illustrate a possible relationship between macroturbulent bursting processes and alternating bedforms (Yalin 1992).

Pool-riffle Maintenance for Stream Restoration Design

Stream hydrodynamics, bed and bank morphology, and turbulence are interrelated in processes that initiate and maintain pool-riffle sequences. Continually associated with natural, non-impacted streams, the importance of the pool-riffle habitat is well recognized for its role in habitat and biodiversity; however, the means by which these sequences are initiated and maintained are not well understood. With steady, and sometimes exponential human population increases, urbanization and urban sprawl has resulted in negatively impacted streams, destroying pool-riffle habitats and abolishing processes capable of initiating and maintaining these systems. Channel restoration projects, which have increased in number across the country to try to restore habitat and natural processes within these stream systems, have had varying degrees of success (Brown 2000, Niezgoda and Johnson 2005, Sear and Newson 2004, Thompson 2002).

Much of the successes of stream restoration projects rely on their individual design goals. When focused on restoring habitat and process, the creation of pool-riffle sequences is one of the most important criteria for evaluating the success of the channel restoration projects (Thompson 2002). There are several design mechanisms used to achieve simulated pool-riffle habitat in channel restoration.

Brown (2000) summarizes these design techniques in two groups: the grade control group and the flow deflection/concentration group. The grade control structures are designed to maintain a desired streambed elevation. Rock vortex weirs, rock cross vanes, step pools, log drops, and v-log drops are examples of some of the structures often used to attain the

grade desired. The flow deflection/concentration designs are used to change the direction of flow, to concentrate flow to protect eroding banks, redirect flows in meanders, or enhance pool-riffle habitats. Common design features to these approaches include wing deflectors, log vanes, rock vanes, J-rock vanes, cut off sills, and linear deflectors. These design groups make up a design technique commonly referred to as the morphologically-based natural channel design method (Brown 2000, Niezgoda and Johnson 2005).

These morphological, or form-based design methods focus on restoring or recreating natural channel characteristics (Brown 2000, Niezgoda and Johnson 2005). The natural channel characteristics are often gauged from reference streams reflecting predisturbed conditions, which may suggest that stream behaviors can be predicted from their appearance (Niezgoda and Johnson 2005). Niezgoda and Johnson summarize a number of assumptions often overlooked and involved in this type of design method:

- the reference channels used to develop the design equations are stable channels that have completely adjusted to their load.
- the bankfull discharge is assumed to be the channel forming discharge.
- sediment loads in the channel to be designed and the reference channel fall within a similar range.
- climate and geology (physiography) of the channels are similar.
- sediment load in the design channel is unchanging or that the stabilized channel is resilient to change.
- process and stream function can be inferred from the current form of the stream.

Complicated hydraulic concerns are often left out of stream restoration designs. Scour and fill dynamics, channel stability, flow resistance, and roughness at cross sections are often unique to each project and difficult to predict (Niezgoda and Johnson 2005, Rhoads and Welford 1991). Urban streams differ from natural streams in that they typically have highly altered water and sediment flow regimes and are constrained both laterally and longitudinally by infrastructure (Niezgoda and Johnson 2005, Schwartz and Herricks 2005B). Similarly, design parameters such as bankfull discharge obtained from regional curves may be unreliable due to dynamic hydrology and urbanization (Niezgoda and Johnson 2005). Although there have been many successes in stream restoration, there are also many failures.

Numerous stream restoration projects fail when the designed channel continues to adjust to the dynamic urbanizing watershed conditions (Niezgoda and Johnson 2005, Thompson 2002). There are many examples of failures in morphologically-based restoration designs that attempted to reestablish or recreate natural channel geometry in urban streams without accounting for changing environment and hydrodynamics (Niezgoda and Johnson 2005). Brown (2000) reported in a study of the performance of over 24 different restoration practices, that projects that attempted to reestablish or recreate natural channel geometry in urban streams had the highest tendency to fail. Likewise, many of the rehabilitated features are sedimentologically too homogeneous and well sorted to mimic natural riffles (Sear and Newson 2004). There is a need for more rigorous design, performance, and installation criteria to ensure functional attributes, which vary among stream systems and ecosystems (Sear and Newson 2004, Schwartz et al. 2001).

Much of the problem in stream restoration today is the lack of research on improving design criteria (Wade et al. 2002, Schwartz et al. 2003). There has been an overwhelming request for structured monitoring and evaluation techniques and plans for stream restoration projects. The evaluations of projects to date have seen local successes and failures. Many of the successes have been short-term studies of the return of habitat structure, increases in target species abundances, and increases in biodiversity (Brown 2000, Garboury 1997, Sear and Newson 2004, Thompson 2002). Few studies have documented the long-term responses (Thompson 2002). The future success of stream restoration design relies on increased research, field evaluation, and models to produce tangible design parameters and methods to approach channels on an individual basis and assure greater success.

Chapter 3: Methods

Study Design

The focus of this research is to characterize the turbulence structure in bankfull flow regimes and design hydraulic alterations to the channel that create helical flow patterns, furthermore generating and maintaining pool riffle bedforms. Three hypotheses have been drawn for this study:

- Channel incision with trees inhibiting bankfull discharge has caused a flow regime lacking channel-scale helical patterns.
- Channel incision without trees inhibiting bankfull discharge has caused a flow regime possessing channel-scale helical patterns.
- Channels with incised streambed morphology and trees inhibiting bankfull discharge can be modified to create flow acceleration-deceleration patterns to induce channel-scale helical flow patterns.

These hypotheses will be explored by experimentally modeling a Stage III incised channel with FLOW-3D, a 3-dimensional hydrodynamic model, and imposing the three bank morphologies and monitoring the flow patterns induced.

The site selection for this research was based on finding a Stage III incised channel with cohesive bank material capable of supporting trees obstructing bankfull flow. The length of the channel needed to exceed 14 channel unit-widths in order to naturally develop two pool-riffle sequences. The field data collection comprised a detailed topographic survey of the site. FLOW-3D was used to model three scenarios within the research site: a

bankfull event with trees, a bankfull event without trees, and a bankfull event with three tree clusters spaced 5 to 7 channel widths apart, based on the restoration design to create flow acceleration and deceleration.

Study Area

Beaver Creek in north Knox County, Tennessee, was selected as the research stream. Beaver Creek is recognized as being negatively impacted by urbanization and has been the object of recent studies by TDEC, Tennessee Department of Environment and Conservation. The watershed draining to the site is 72 square kilometers and is illustrated in Figure 3.1. The land-use designation is primarily subdivisions and small businesses. Much of the upper watershed is farmland being developed into subdivisions, a trend seen throughout the United States. Figure 3.2 is a GIS land-use map of the watershed generated in Arcmap. The site is a 16-kilometer drive from the University of Tennessee and is part of the Knox County Parks and Recreation Department. It has easy access from both banks with a greenway path that has recently been constructed along the east bank, providing access without impacting the stream itself. The west bank is bordered by the back of a Food City grocery store and consists of a paved loading dock within 15 meters of the stream. Permission to use the site for research was granted by the Knox County Parks and Recreation Department.

The section of channel is a classic Stage III stream based from the Channel Evolution Model, Figure 2.1. It has been channelized and straightened for greater than 200 meters long with an average slope of 0.0001 meters/meters. The section of channel that was

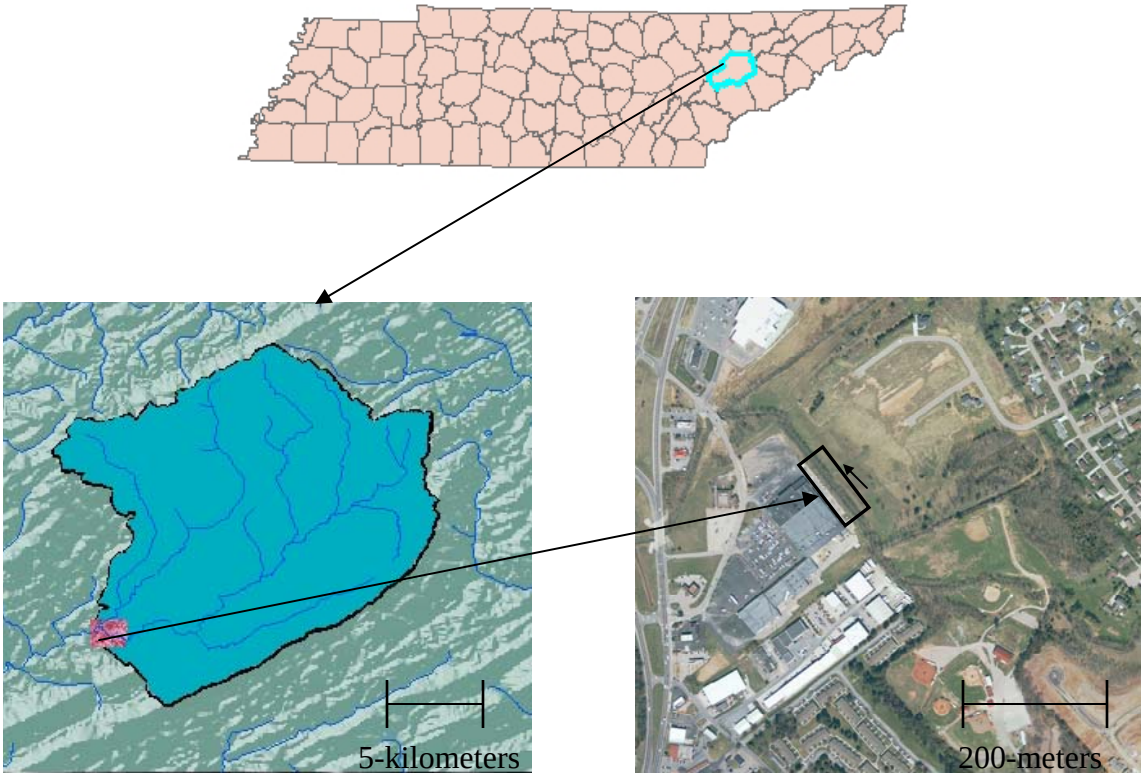

Figure 3.1: Research watershed and site scaled from a Tennessee county map created in Arcmap. The top map highlights Knox County within the state of Tennessee. The map located at the bottom left is the research site watershed boundary and tributaries. The illustration in the bottom right is a high-resolution orthoimagery photo of the research study area from the USGS Internet website. The most upstream point of the research site is located at coordinates:

Latitude	36 04 52.34	North
Longitude	083 55 24.70	West

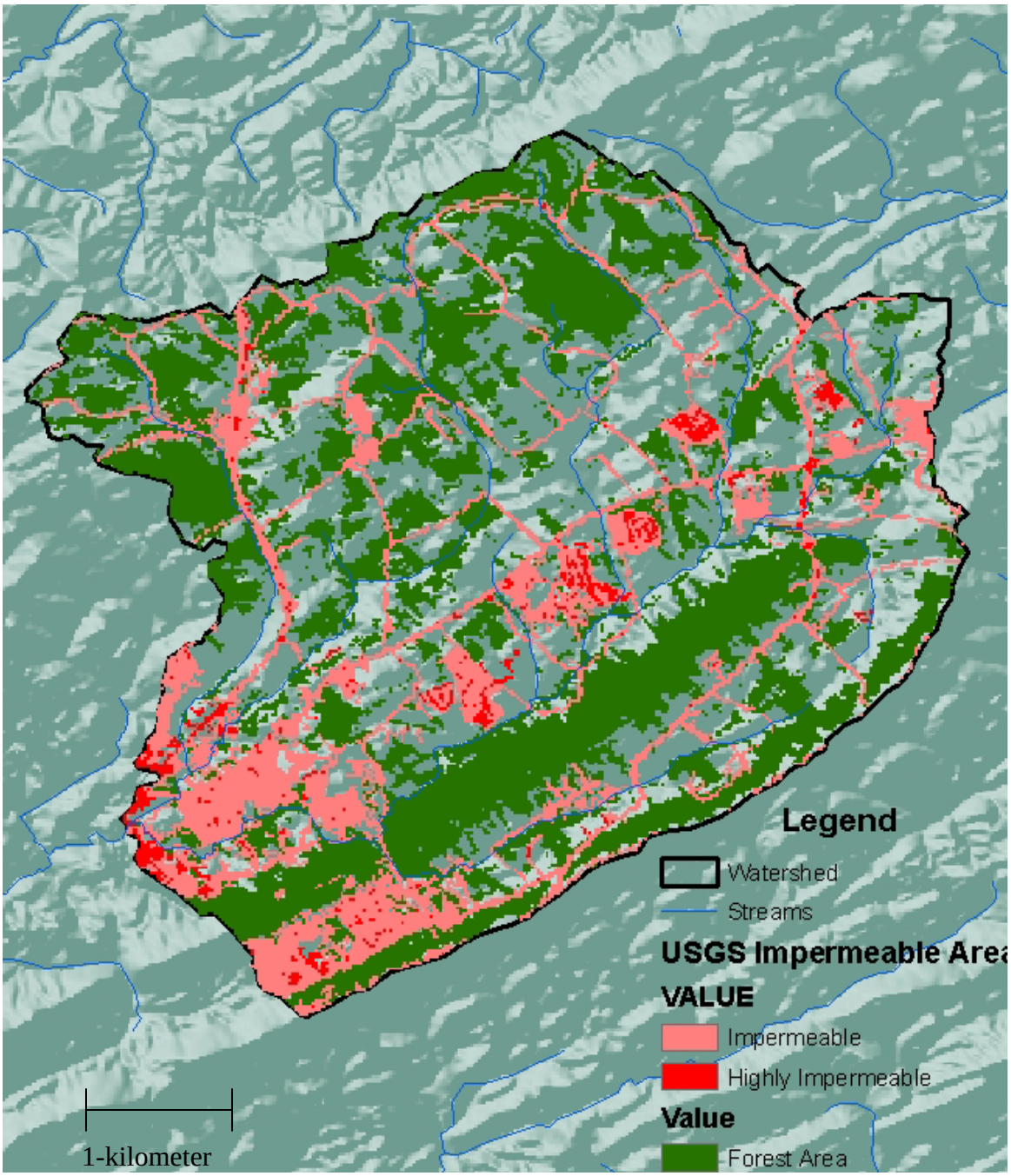

Figure 3.2: Land-use map of the research watershed generated in Arcmap. Impermeable areas represent housing and small businesses. The highly impermeable areas represent roadways and parking lots.

surveyed and modeled is 105 meters long and 6.5 meters wide. It is greater than 2 reaches long, sharply incised, and has diminished pool-riffle bed morphology. Trees line the channel on both banks and impede flows greater than 1.68 m^3/s. The research site during bankfull flow is pictured in Figures 3.3 and 3.4.

Topographic Characterization

A high-resolution survey of the stream topography was needed to generate the 3-dimensional hydraulic model. The survey was taken using a Trimble 3605-DR Total Station with TDS Recon data logger. The site was laid out with 9 benchmarks located at equal intervals along two reaches of the stream. The reference point of the survey was placed in an area that will not be disturbed. The channel was surveyed with an average width of 1-meter between cross-sections, starting at the greatest upstream point. The width between cross-sections was decreased when large topographic changes were present. The coordinates of each tree lining the channel were surveyed at the base of the tree, while their diameters were manually recorded. An option within the Trimble Total Station allowed the centroid of each tree to be surveyed based on the junction of the x and y-plane running through the tree.

The survey data were converted to an EXCEL spreadsheet where the data could be easily sorted and further converted to text files. In order for the data to be imported into FLOW-3D, it needed to be in an x, y, and z rectangular coordinate layout. Each tree was produced in FLOW-3D based on its radius and centroid coordinate. The trees were represented as separate subcomponents appearing as symmetric, vertical cylinders.

Figure 3.3: Photo of Beaver Creek research site during bankfull flow (01/14/2005).

Figure 3.4: Photo looking down the channel of the Beaver Creek research site during bankfull flow (01/14/2005).

A Tecplot image of the channel without trees is illustrated in Figure 3.5, and of the channel with trees is shown in Figure 3.6.

3-Dimensional Hydrodynamic Model

FLOW-3D was used for all the modeling applications. FLOW-3D is a commercial Computational Fluid Dynamic (CFD) 3-dimensional (3D) model with a graphical user interface. It is comprised of a pre-processor, finite element mesh generator, and a post-processor for display of simulations.

FLOW-3D approaches modeling by first dividing the flow region into variable sized rectangular cubes, or cells, in a finite element grid, also called a mesh. Each cell represents a control volume. For each cell, values are retained for basic flow quantities, such as velocity, pressure, and density. The model then uses finite difference approximations to the equations of motion to compute the spatial and temporal evolution of these values. Initial boundary conditions are needed to set up original flow characteristics on which to base the approximations. The governing differential equations used to calculate the approximations are also established from the initial depth and velocity boundary conditions.

The equations of motion used in FLOW-3D are based in terms of Cartesian Coordinates, are defined for the fluid velocity components (u, v, w) in the three coordinate directions by the Navier-Stokes equations, and maintain the conservation of momentum. All the variables related to the Navier-Stokes equations are located at the centers of the cells in

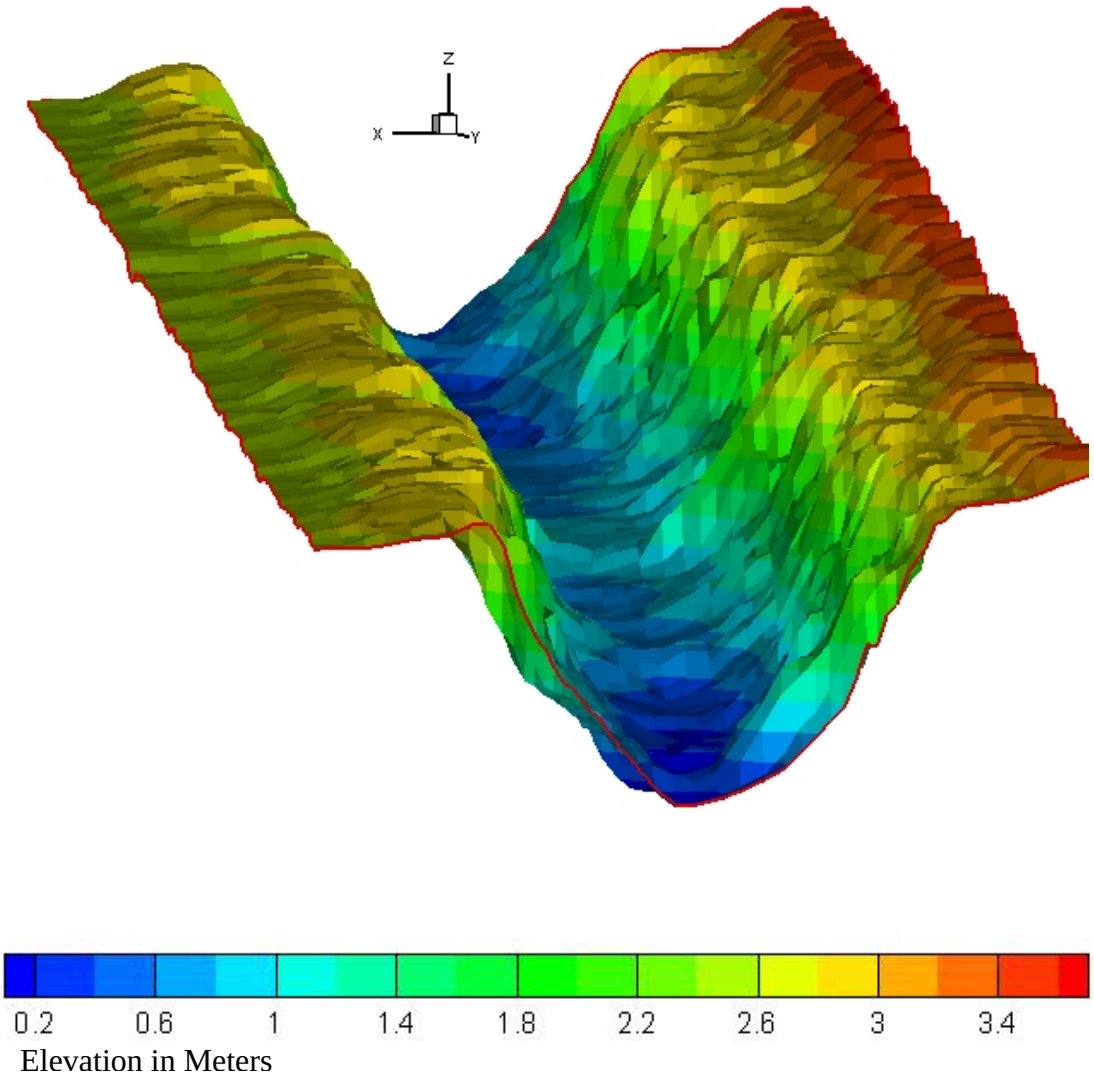

Figure 3.5: Tecplot image of research site (channel only).

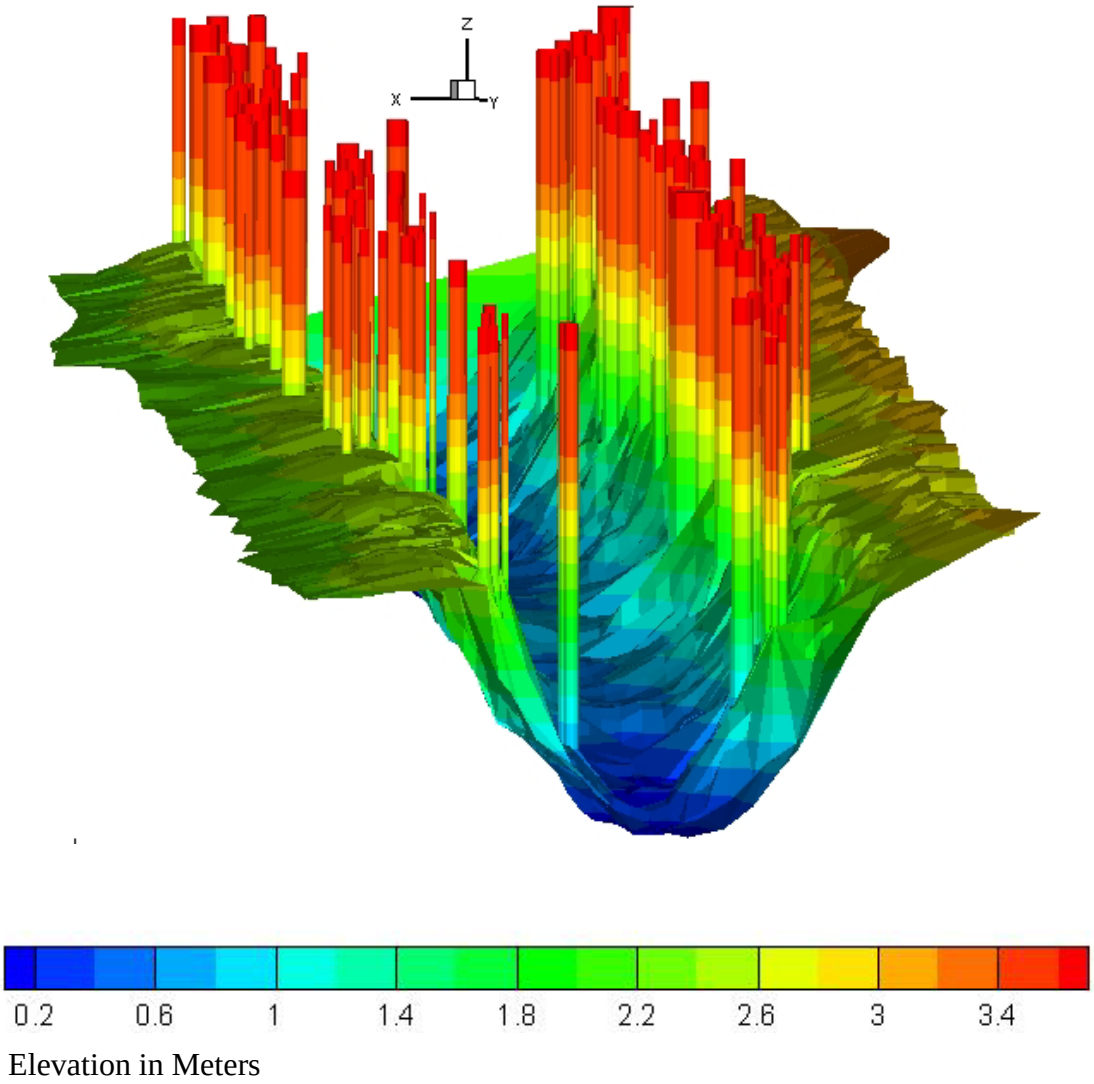

Figure 3.6: Tecplot image of research site (channel and trees).

the finite element grid except for the velocities, which are located at the faces of the cells. All calculations are based on a time-step and total-time, which is designated by the user. The Navier-Stokes equations with some additional terms used by FLOW-3D, and listed in their User's Manual are:

$$\frac{\partial u}{\partial t}+\frac{1}{V_F}\left\{uA_x\frac{\partial u}{\partial x}+vA_yR\frac{\partial u}{\partial y}+wA_z\frac{\partial u}{\partial z}\right\}-\xi\frac{A_yv^2}{xV_F}=-\frac{1}{\rho}\frac{\partial p}{\partial x}+G_x+f_x-b_x-\frac{RSOR}{\rho V_F}u$$

$$\frac{\partial v}{\partial t}+\frac{1}{V_F}\left\{uA_x\frac{\partial v}{\partial x}+vA_yR\frac{\partial v}{\partial y}+wA_z\frac{\partial v}{\partial z}\right\}+\xi\frac{A_yuv}{xV_F}=-\frac{1}{\rho}\left(R\frac{\partial p}{\partial y}\right)+G_y+f_y-b_y-\frac{RSOR}{\rho V_F}v$$

$$\frac{\partial w}{\partial t}+\frac{1}{V_F}\left\{uA_x\frac{\partial w}{\partial x}+vA_yR\frac{\partial w}{\partial y}+wA_z\frac{\partial w}{\partial z}\right\}=-\frac{1}{\rho}\frac{\partial p}{\partial z}+G_z+f_z-b_z-\frac{RSOR}{\rho V_F}w$$

where (G_x, G_y, G_z) are body accelerations, (f_x, f_y, f_z) are viscous accelerations, (b_x, b_y, b_z) are flow losses in porous media or across porous baffle plates, *RSOR* and the final terms account for the injection of mass at zero velocity.

Model Preparation

Initially, the topographic data were imported into FLOW-3D. ASCII formatted x-y-z data were directly loaded into FLOW-3D as a data file from which a surface was interpolated and based within a rectangular volume. Additional points and boundaries were added to the original topographic survey data in order to better represent the original channel, Figure 3.7. Once an acceptable channel was generated, the model was rotated -73.1º in order to orient the flow in the x-direction. The trees along the banks were generated as separate subcomponents in the model and represented as symmetric, vertical cylinders. The cylinders were equal in diameter to the base of the tree they represented.

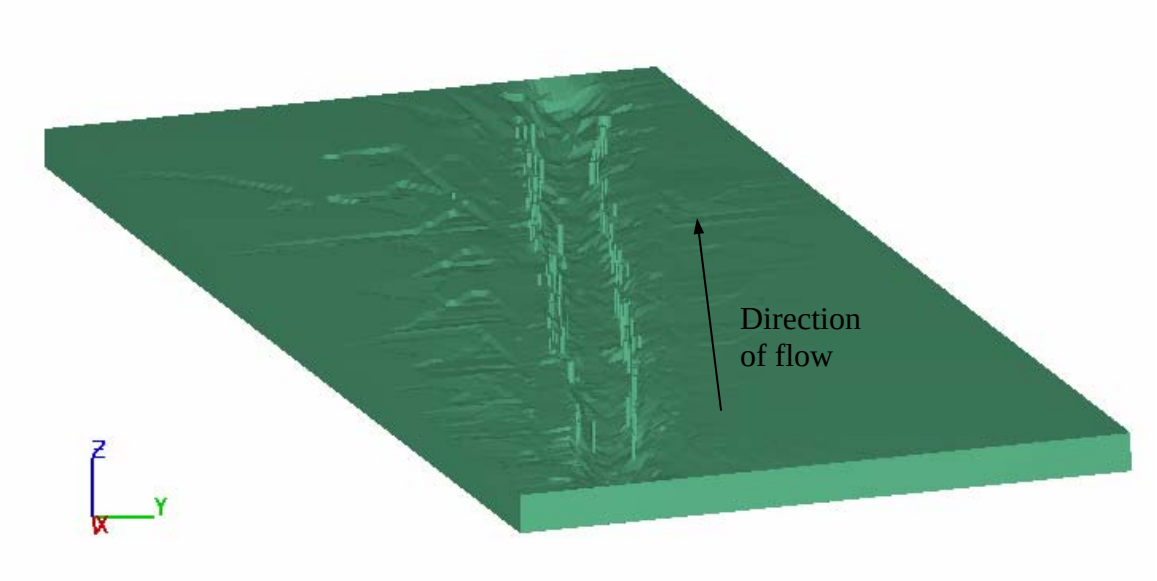

Figure 3.7: FLOW-3D interpolated image of the research site (with trees).

Finite Element Grid Generation

A 3-dimensional finite element grid, or mesh, was generated for all regions of flow within the research site. The mesh generator incorporated into FLOW-3D is very user friendly. Once the program is in the mesh generating mode, the procedure for producing the mesh consists of left clicking with the mouse and dragging the yellow boundary to produce the rectangular mesh block desired. The boundary seen during this procedure represents and establishes the i, j, k ordered minimum and maximum boundaries of the finite element grid. After the boundaries are established, the mesh can be manually altered within the menu tree. This is accomplished by entering changes to the x, y, and z properties along with the number of elements in each direction. Figure 3.8 is an illustration of the mesh generating procedure and the parameters within the menu tree.

Although the mesh and mesh boundaries could be easily manipulated, there were some considerations when developing the mesh. Licensing agreement for the version obtained required that each flow region needed to occupy less than 200,000 nodes. Each 200,000-node region was treated as a separate model, with the results of the previous model acting as the input of the current flow region. FLOW-3D recommends that there be no greater than a 1 to 2, or 2 to 1 scaling ratio between mesh blocks. The elements were made as "square" as possible to provide consistency among elements, resulting in fewer scaling issues during the calculations. All of the mesh blocks were produced with the same number of elements in each direction, allowing additional consistency between mesh blocks, although the volumes being modeled were different. Likewise, the same mesh

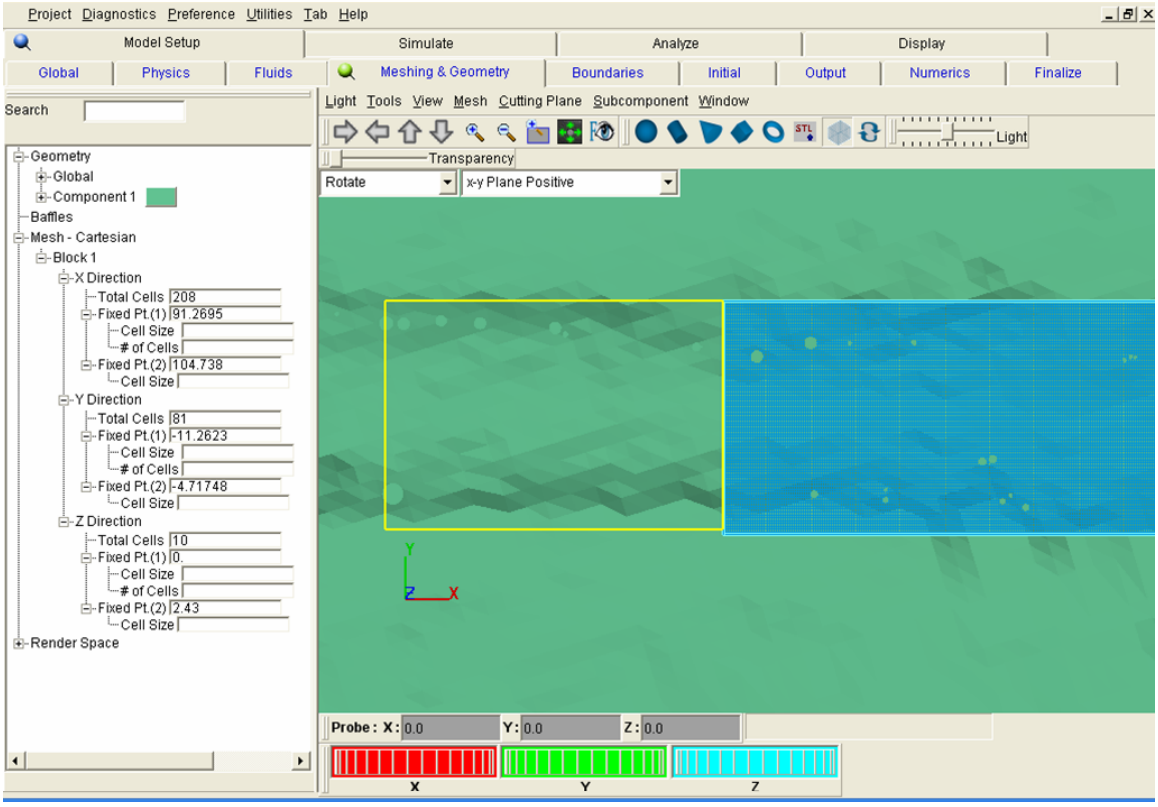

Figure 3.8: FLOW-3D image of the mesh generating process. The yellow box represents the mesh boundaries being generated.

parameters were used with each modeling scheme; bankfull with trees, bankfull without trees, and bankfull with restoration design applied.

In order for the cylinders, representing the trees, to be included into the model, they were required to occupy a minimum of two finite elements. This established a solid volume for the cylinder that could then be incorporated into the flow field. Because the trees were the smallest components in the model, they dictated the resolution of the mesh. The flow region for each individual model was decreased until the cell size was small enough to include each of the trees lining the bank.

Hydraulic Criteria and Boundary Conditions

The initial hydraulic criteria and boundary conditions are input manually along with default values built in to the model. This is a summary of the parameters used. All of the parameters of the model were defined in the International System of Units, which could be manually changed within FLOW-3D. Water at 20º Celsius was used as the single, Newtonian, incompressible fluid, selected from a list of several options. This fluid corresponded to a viscosity of 0.001 N s/m^2 and a density of 1000 kg/m^3. Gravity was user defined for the model as –9.8 m/s^2, implying the negative z-direction.

The simulations were run till steady state conditions were met for all three scenarios. The objective of this research was to characterize macro-turbulence structure, as opposed to turbulence on a micro-scale, which could be obtained with steady state conditions. There were multiple ways to determine when steady state conditions had been met. While the

simulation was in progress, the “Simulate” window allows the modeler to monitor the progress of the run. The FLOW-3D staff suggested when the “stability limit vs. time” and “time step size vs. time” become stable, it is an indicator that steady state conditions have been met (Figure 3.9). This technique proved to be accurate after 10 to 15 seconds of stability between these parameters. Steady state was also verified through a visual analysis of the data over the entire time frame of the simulation. When the change in velocity magnitude vs. time became very small, steady state conditions were met. This indicated that turbulence had converged on similar patterns at the scale of this research.

The turbulence closure for the model was selected from five different closure schemes. The options available were; Prandtl mixing length, one-equation turbulent energy model, two-equation k-e model, renormalized group model (RNG), and a large eddy simulation model. A turbulent mixing length can be manually entered when it applies. The turbulence in this research was scaled to the trees as opposed to the channel. This type of turbulence experiences an energy cascade, which in turn, dictated that the two-equation k-e model turbulence closure would be most appropriate for simulating this turbulence scheme.

The surface roughness k-value for the channel was manually entered within the “Geometry” window in the menu tree. A common surface roughness was defined for all of the subcomponents within component 1 of the geometry menu. Therefore, the surfaces of the trees were defined as the same roughness as the channel itself. Likewise,

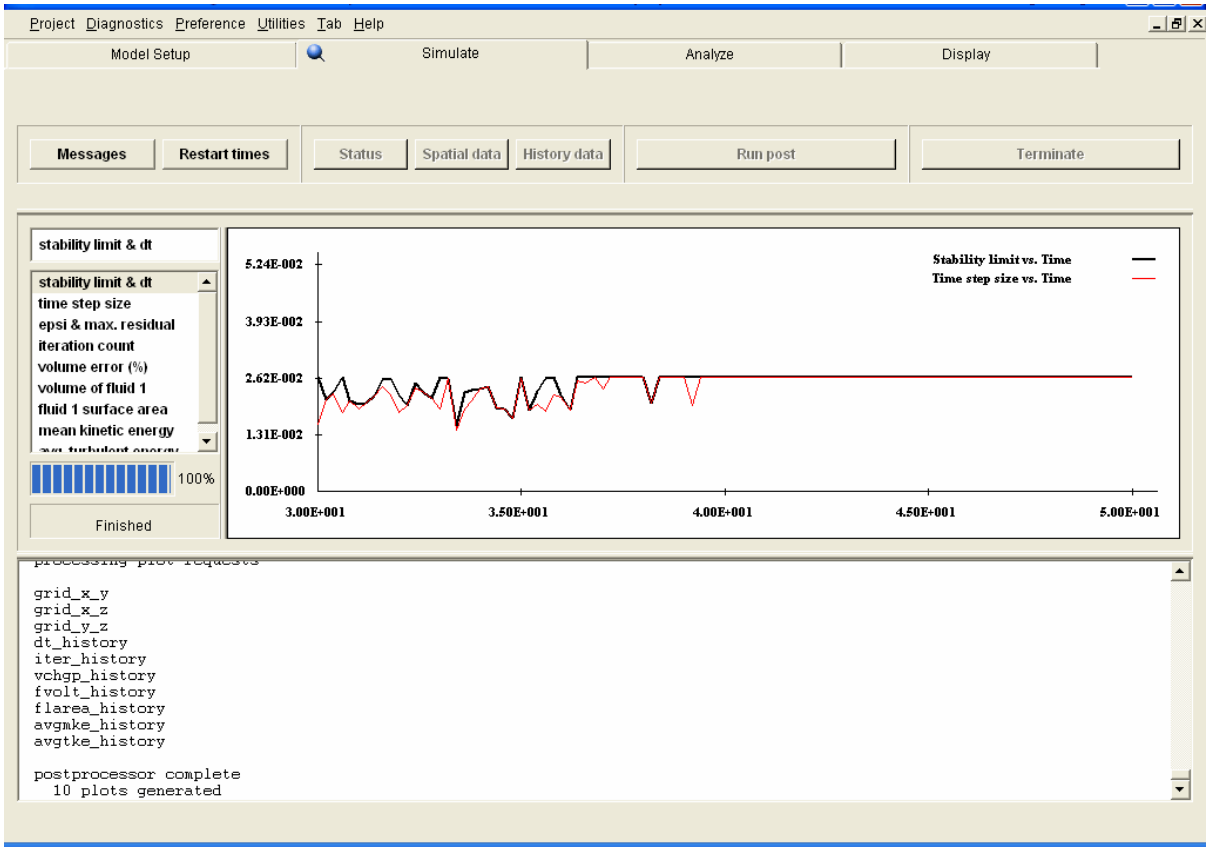

Figure 3.9: A FLOW-3D image of a simulation in progress showing the stabilization of the “stability limit vs. time” and “time step size vs. time”, indicating steady state conditions.

the channel bed had the same roughness coefficient as the banks. This could be altered if each geometry component was entered separately, but due to the scale of this research, similar roughness coefficients between the subcomponents were not a factor. The roughness coefficient "k" was a value unique to FLOW-3D and is defined below as:

$$k = \frac{R_h}{10^{\left[\left(\frac{0.046}{n} R_h^{\frac{1}{6}}\right) - 1.088\right]}}$$

where R_h is the hydraulic radius (area / wetted perimeter) and n is defined by values of Manning "n". The research channel had a value of k = 0.05, R_h = 2.78 meters, and n = 0.019. This value of "k" was determined by actual channel characteristics and confirmed through comparisons with actual flow properties.

The boundary conditions of the mesh were established under the "Boundary" tab. Boundary conditions are established for the minimum and maximum mesh boundaries of the x, y, and z-axes. The only mesh boundaries that changed between models were those in the x-direction, which was the direction of flow. A "Specified velocity" boundary was established at the most upstream location. This allowed the user to specify a uniform velocity at this boundary. However, the uniform velocity boundary was established in the channel five meters upstream of the study site. This allowed the streambed and bank roughness to set up a velocity gradient throughout the cross-section before the discharge reached the research site. An "Outflow" boundary was established at all downstream boundaries in the x-direction. Outflow boundaries represent a condition of continuation in the channel and flow, and all their related properties at that boundary. In essence, the

conditions remained constant if the channel was instantaneously severed at that point. "Grid Overlay" mesh boundaries were used at the upstream boundary when continuing a flow to a downstream model. The grid overlay boundary allowed the outflow conditions of the downstream boundary of the upstream simulation to begin the upstream conditions of the downstream simulation. This mimicked one continuous channel over several different models. The mesh boundaries in the y and z-directions were set as "Symmetry" boundaries. Symmetry boundaries imply there is no flux of any property across that boundary and no shear.

Initial conditions of the model were controlled within the "Initial" tab. The initial water level was set to a height of 1.72 meters. This depth was computed using HEC-RAS, a 1-dimensional hydrodynamic model, during a bankfull simulation of the research site. Hydrostatic pressure was applied in the z-direction, which was controlled by checking a box or specifying a uniform pressure. The time interval of the solutions was set to 0.05 seconds within the "Output" tab. This refers to the change in time for which each equation being solved and dictates 20 simulations for each second the model was operated.

Post Processing

FLOW-3D was used for all post-processing. The post processing was controlled from the "Analyze" tab in FLOW-3D. The data were analyzed as 2 and 3-dimensional displays. The output file was selected from the "Open results file" tab. The 3-dimensional data analysis was created with the fraction of fluid representing the entire mesh (Iso-surface)

as a solid volume component overlay. The color variable analysis was displayed in terms of velocity magnitude and x, y, and z-velocities. The times at which the simulation is displayed was controlled from the “Time frame” toggle. Figure 3.10 illustrates the 3-dimensional analysis window setup for a 10-second velocity magnitude display. The 2-dimensional analysis window could be set in terms of the x-y, y-z, or x-z planes. The contour variable was set similar to that of the 3-dimensional set-up with the capability of choosing a vector type. A plain vector type was used in this research. The x, y, and z limits were controlled to display only the areas desired for analysis. The time frame was controlled similar to the 3-dimensional analysis. The number of cells displaying vectors was controlled through the “Advanced” option and entering a “Vector frequency”. Likewise, the vector length was controlled with a scaling factor entered in the main window. The vector frequency and scale were commonly defined for all of the displays to produce results that could be easily interpreted. Figure 3.11 illustrates the 2-dimensional analysis window setup for a 10-second velocity magnitude display, in the x-y plane, with plain vectors scaled to a factor of 2. After completing the analysis set-up, the simulation is rendered and displayed in the “Display” window.

The display window has several options for viewing the simulation. For 3-dimensional displays, the image can be rotated, magnified, and viewed from several planes. A snapshot of any image can be saved or an animation can be made over a specified time period. The legend can be displayed anywhere on the screen and there are also options for controlling the light and transparency of the image. Figure 3.12 is an example of a 3-dimensional display. The 2-dimensional displays cannot be rotated or magnified,

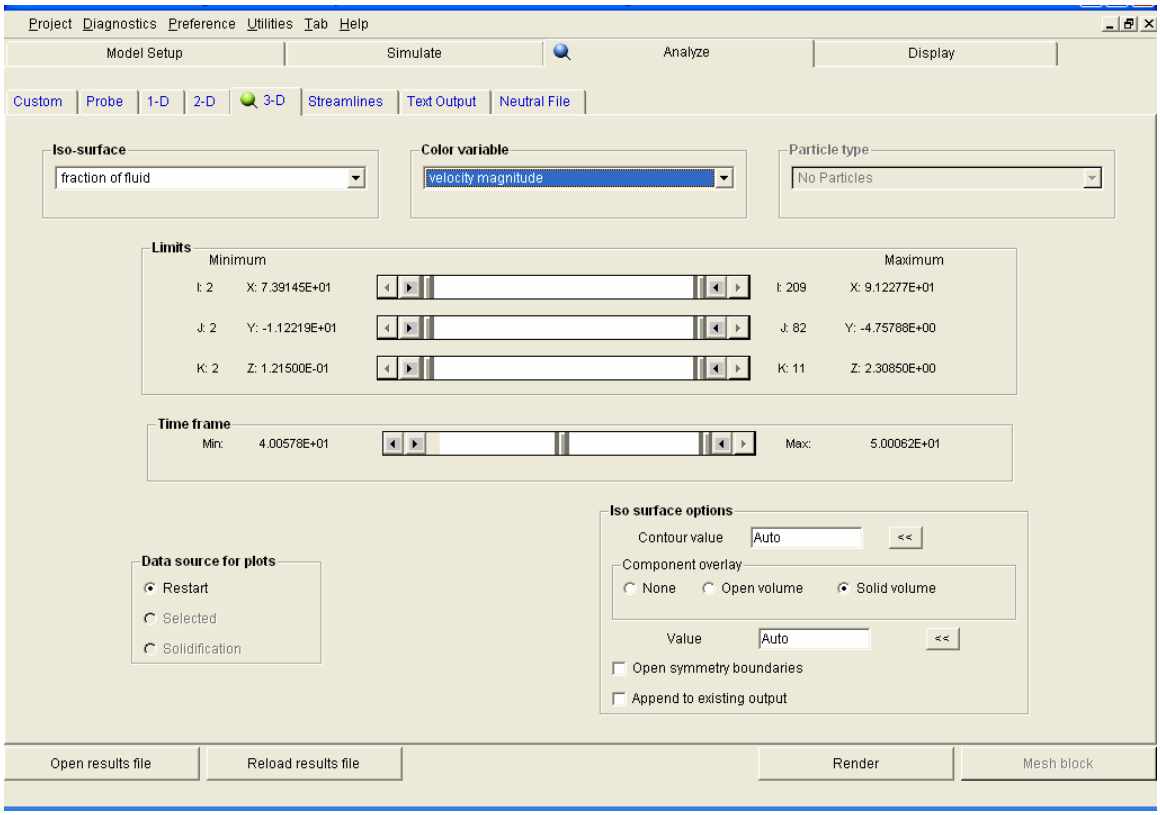

Figure 3.10: A FLOW-3D image of the 3-dimensional analysis window setup for a 10-second velocity magnitude display.

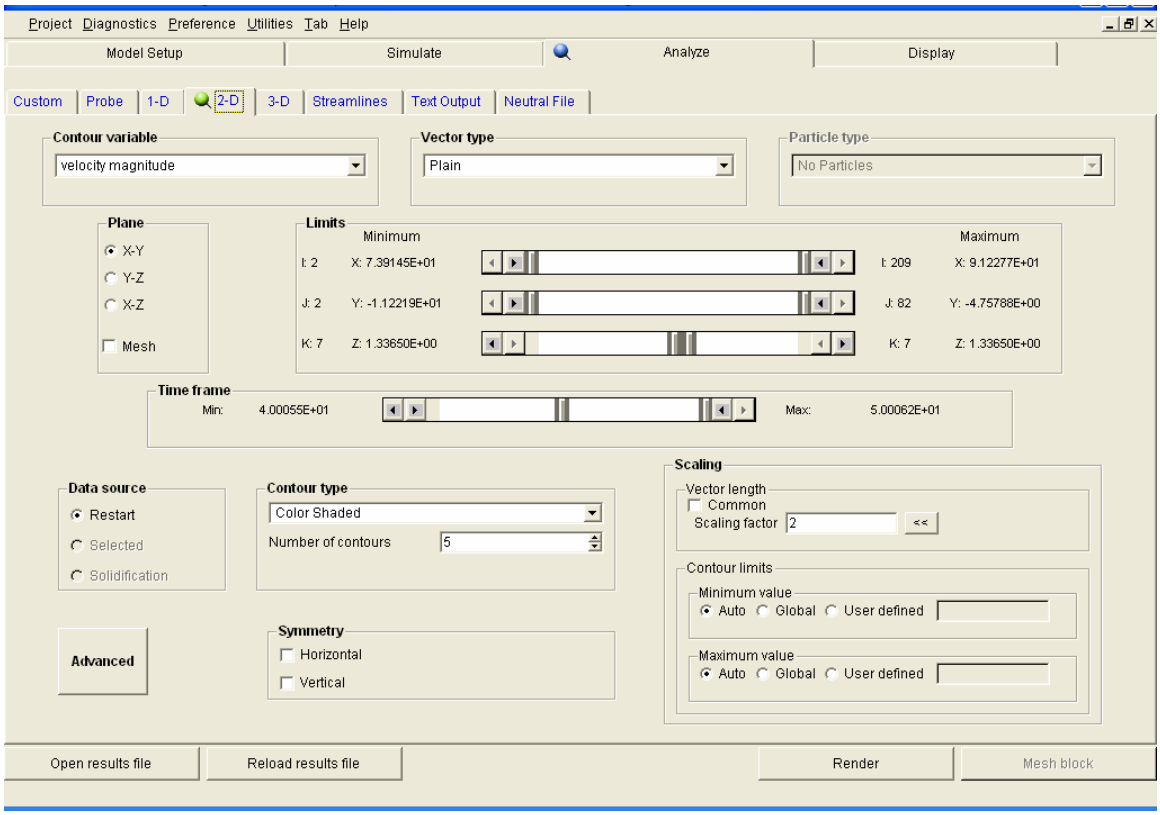

Figure 3.11: A FLOW-3D image of the 2-dimensional analysis window setup for a 10-second velocity magnitude display, in the x-y plane, with plain vectors scaled to a factor of 2.

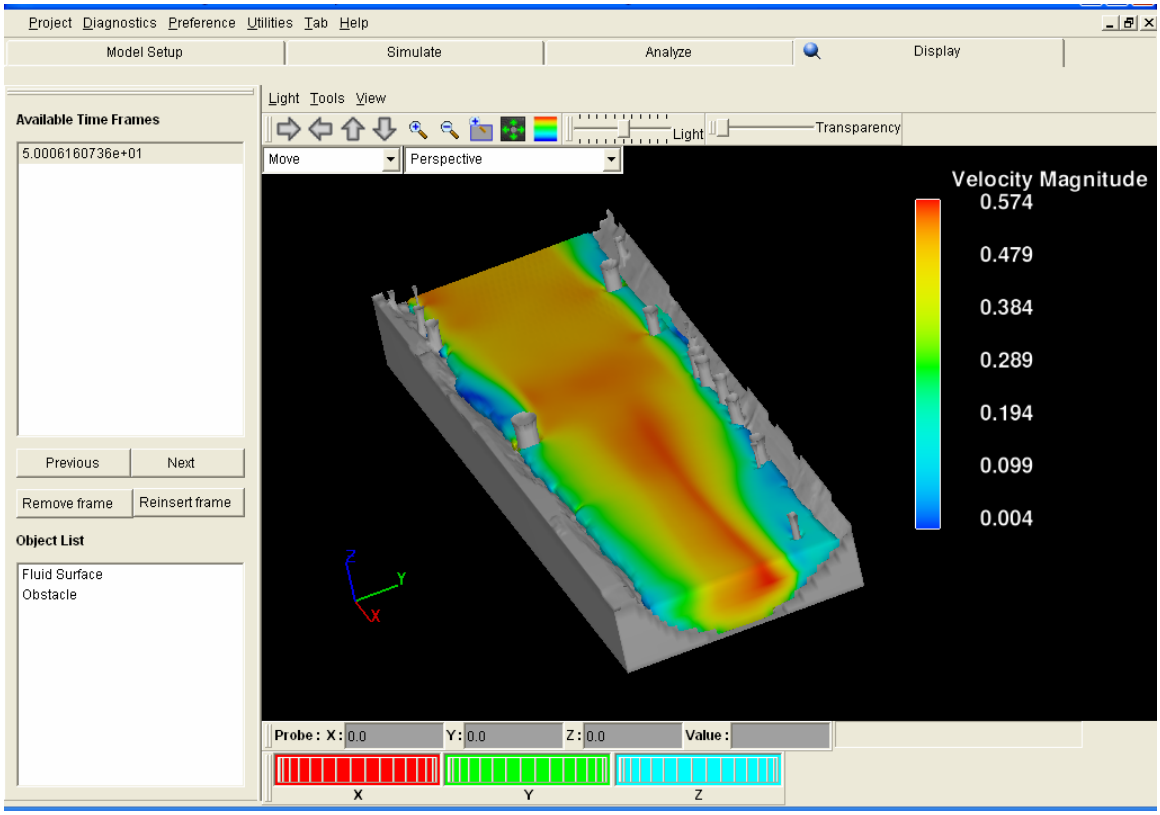

Figure 3.12: A FLOW-3D image of an example of a 3-dimensional display.

however it is easy to save an image and create animations. The vector lengths can also be formatted in the display window. Figure 3.13 is an example of a 2-dimensional display in the y-z plane.

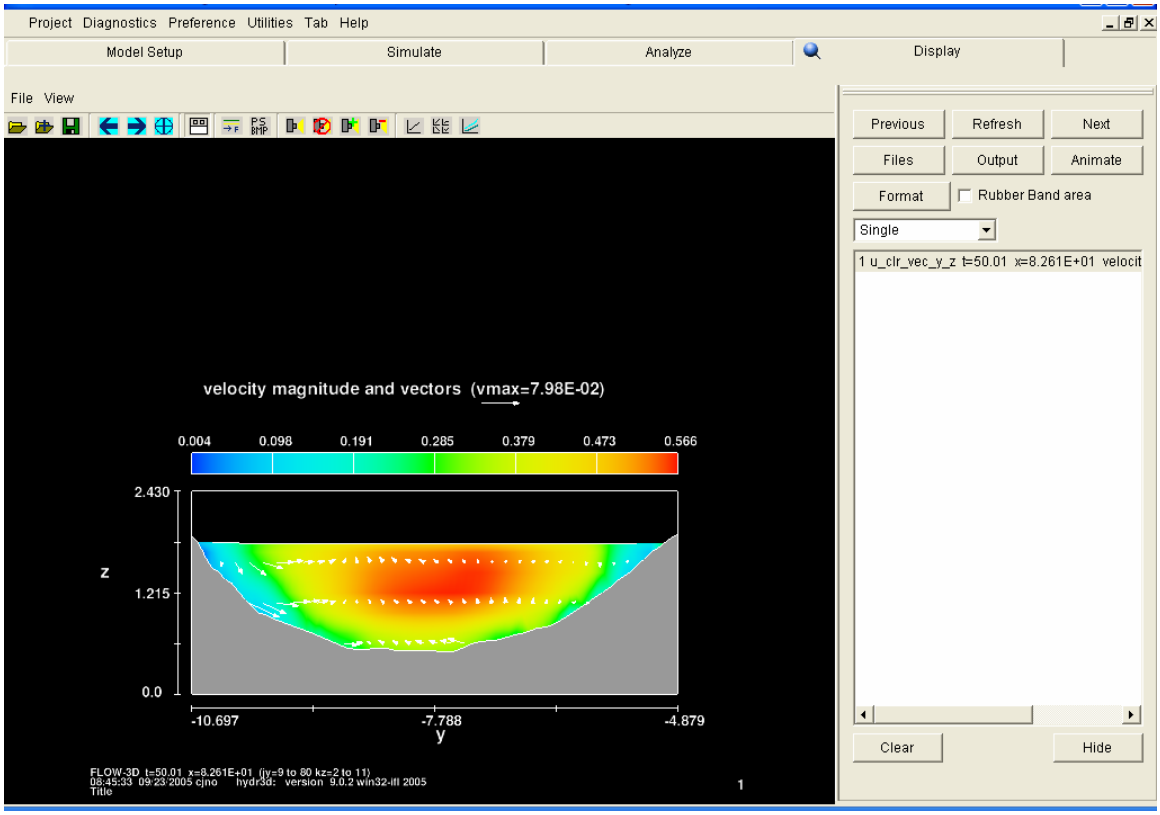

Figure 3.13: A FLOW-3D image of an example of a 2-dimensional display in the y-z plane.

Chapter 4: Results

There were three different scenarios for the Beaver Creek research site simulated in FLOW-3D. All of the simulations shared the exact same finite element grid, mean discharge, and initial boundary conditions. The initial conditions were set with a flow rate of 1.68 m^3/s, 1.72 meters of water height, and 0.4-meters/second velocities in the negative x-direction, which is in the downstream direction at the inflow cross-section for the modeled reach. These parameters were estimated using a HEC-RAS simulation of the research site in combination with a visual analysis of flow characteristics of an actual bankfull flow event.

Channel with Trees

The first simulation corresponded to the Beaver Creek reach with all of the trees present. This simulation represented the current conditions at the research site. Figure 4.1 illustrates the y and z-velocities experienced at three different water heights within the channel: 1.82 meters, 1.33 meters, and 0.85 meters. This pattern is consistent for all of the y and z-velocity figures. The y and z-velocities are characterized as being either in the positive or negative direction, with red symbolizing positive and blue symbolizing negative. The overall magnitudes of these velocities were small relative to the dominant x-velocities. A Tecplot image of the channel and trees is shown in Figure 4.2 to help show the locations of the trees and how they appear in the channel. The simulated velocity magnitudes were captured in y-z cross-sections and shown in Figure 4.3. The twelve cross-sections represented in the figure are irregularly spaced throughout the channel and were selected to show dominant flow patterns. The cross-sections are in

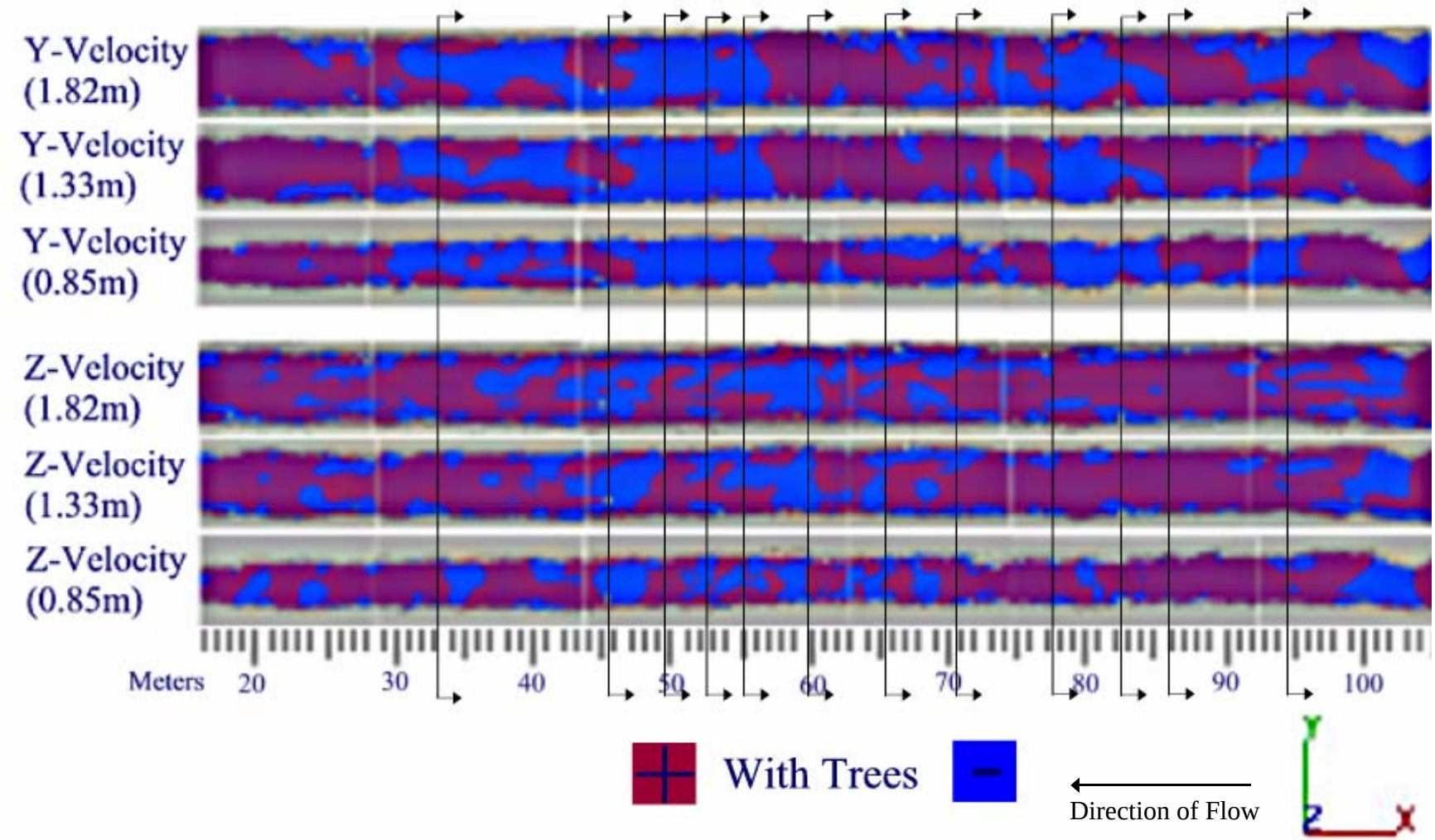

Figure 4.1: Modeled positive and negative y and z-velocities (m/s) in the channel with the trees present.

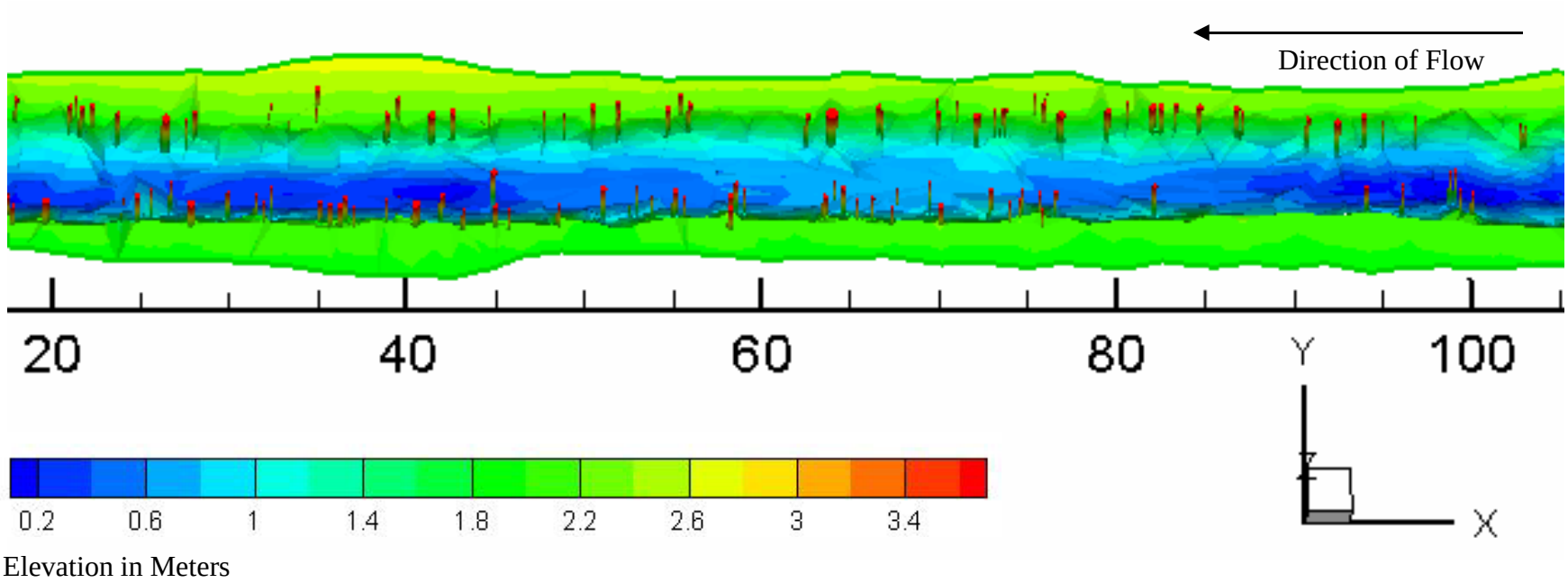

Figure 4.2: Tecplot image of the channel with all of the trees present to better illustrate the location of the trees with relation to the study site.

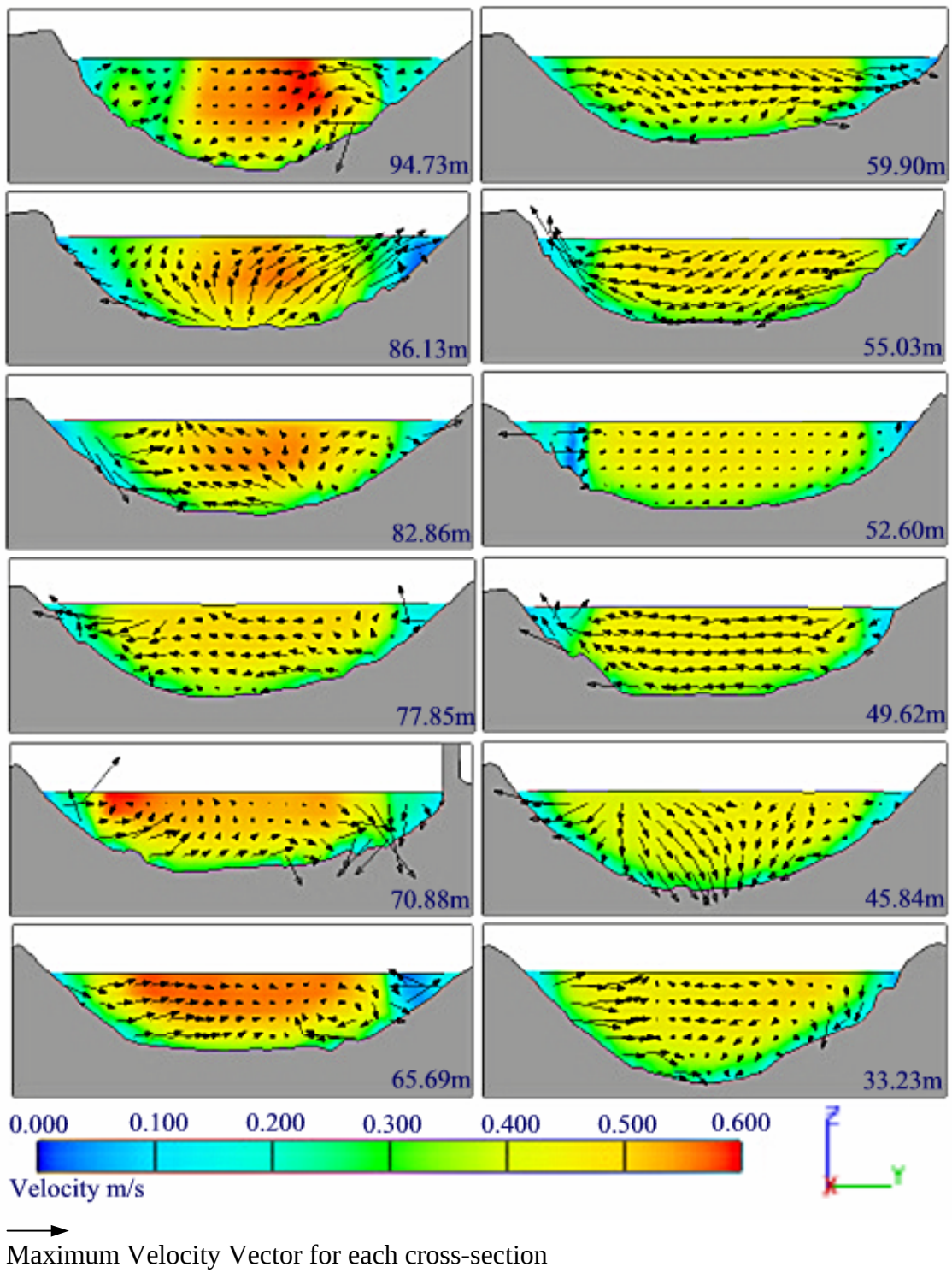

Figure 4.3: Modeled velocity magnitude and velocity magnitude vectors illustrated in y-z cross-sections in the channel with the trees present.

downstream order. Similarly, all of the figures consisting of y-z cross-sections will be represented in a consistent fashion.

The FLOW-3D simulation of the channel with the trees present, was visually analyzed using the velocity magnitude y-z cross-sections and flow vectors on 1-meter intervals downstream, (Appendix-A). The results showed a lack of channel-scale helical flow patterns. Instead, there were small, local circulation cells that scaled to the turbulence caused by the trees. The circulation cells developed rapidly and then dissipated upon approaching downstream trees. There were frequent, opposing cross-channel flow patterns caused by trees set directly across from one another. The flow would be directed toward the center of the channel by the trees and then dissipated when it came together in the center. The circular and cross-stream patterns were mostly confined to the outer banks of the cross-sections due to dominant downstream flows within the center of the cross-sections. The y and z-velocities were patchy in nature throughout the channel. They varied throughout the water column and demonstrated few distinct patterns.

The FLOW-3D simulation showed zones of high turbulent kinetic energy around the trees, Figure 4.4. Losses of energy due to the turbulence cause decreased flow within the areas following the impeding trees. Instead, the majority of the flow was concentrated within a zone in the center of the channel, where the trees were absent and the turbulent kinetic energy was small. This high-velocity zone showed little fluctuation in velocity and had a semi-uniform flow distribution. Although there were low flow regimes within

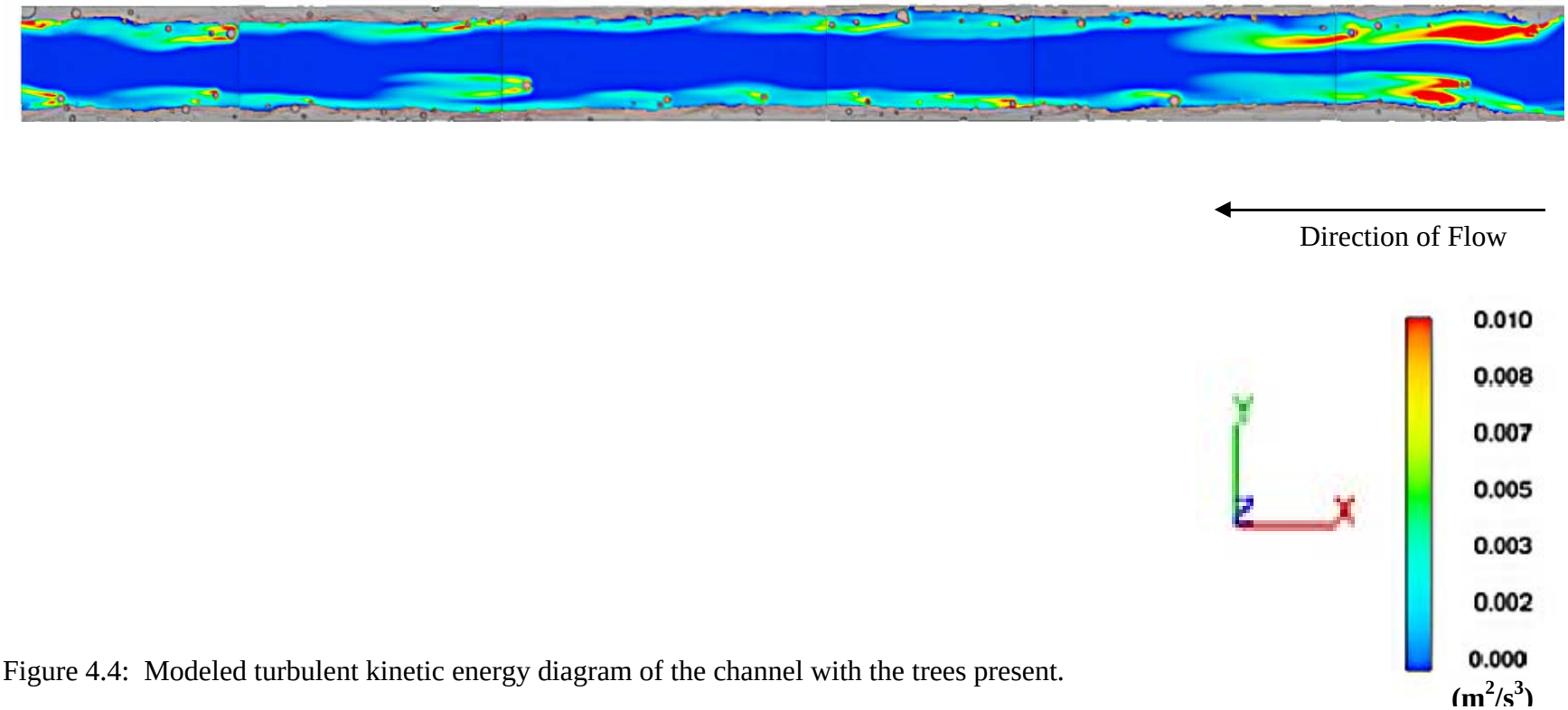

Figure 4.4: Modeled turbulent kinetic energy diagram of the channel with the trees present.

the impeding tree region, the flow areas immediately upstream and around the trees experienced high velocities, sometimes in excess of 0.82 m/s.

Large-scale heterogeneity in bed-topography, such as channel shape and ledges within the streambed, had moderate affects on the flow patterns in the channel with trees. A noticeable immediate depression in the streambed at meter 45 of the channel caused moderate changes to the velocity patterns. Differences between the bed-topography and bank-tree structure were difficult to differentiate.

Channel without Trees

The second scenario was identical to the first, except with all of the trees removed. This simulation was used as a control for the modeling experiment in order to represent flow patterns caused by bank and bed roughness only. Figure 4.5 illustrates the positive and negative y and z-velocities in the channel with the trees absent. The velocity magnitudes are represented in y-z cross-sections in Figure 4.6, stressing again that the cross-sections have been selected at locations within the research site that show dominant flow patterns and are not at regular intervals or similar between scenarios.

The channel with the trees absent was also visually analyzed using velocity magnitude y-z cross-sections and flow vectors on 1-meter intervals progressing downstream, (Appendix-B). The simulation showed strong, alternating cross-channel flow patterns resulting in channel-scale helical flow. There was obvious channel-scale flow acceleration and deceleration throughout the model. The accelerations and decelerations

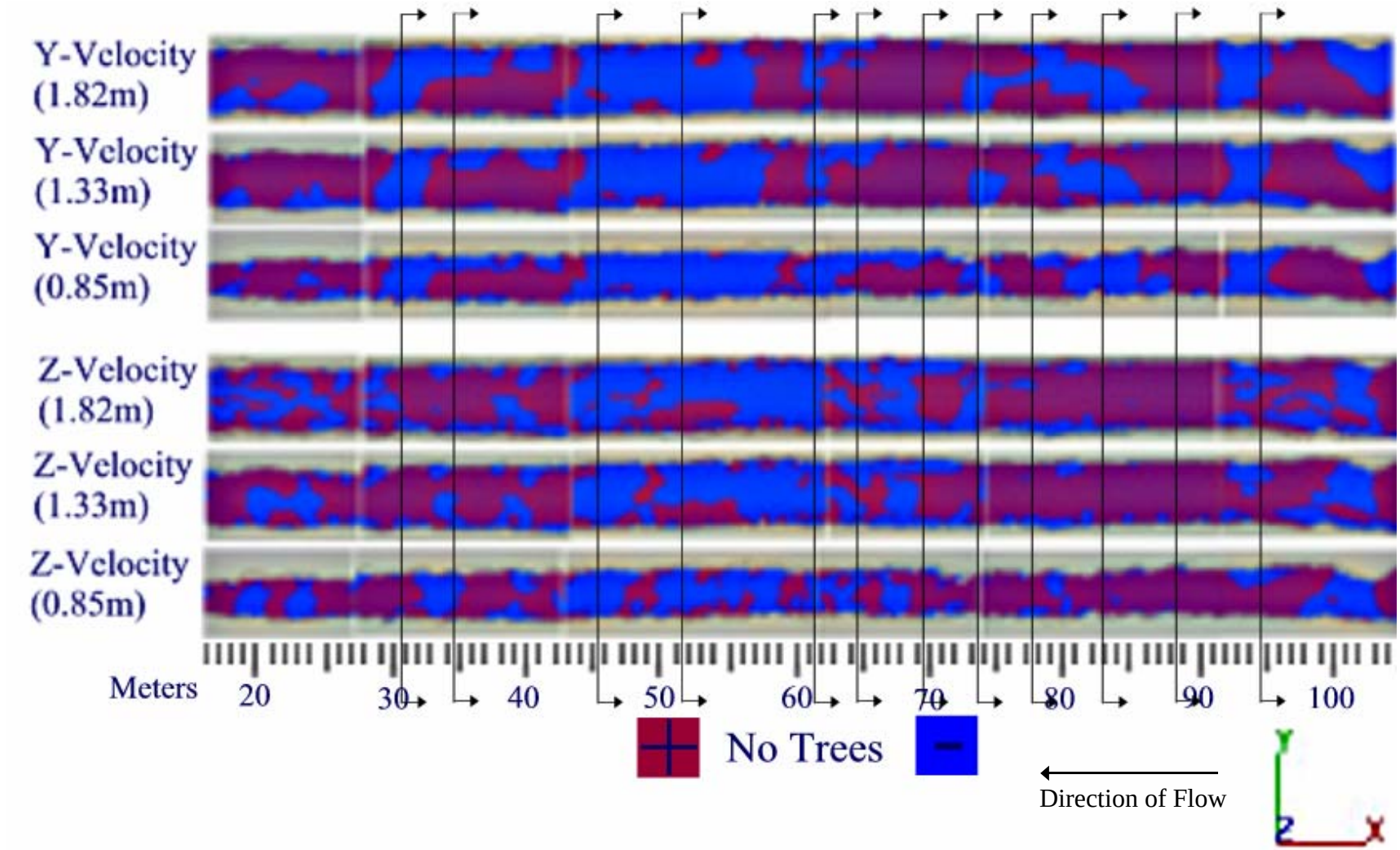

Figure 4.5: Modeled positive and negative y and z-velocities (m/s) in the channel with the trees removed.

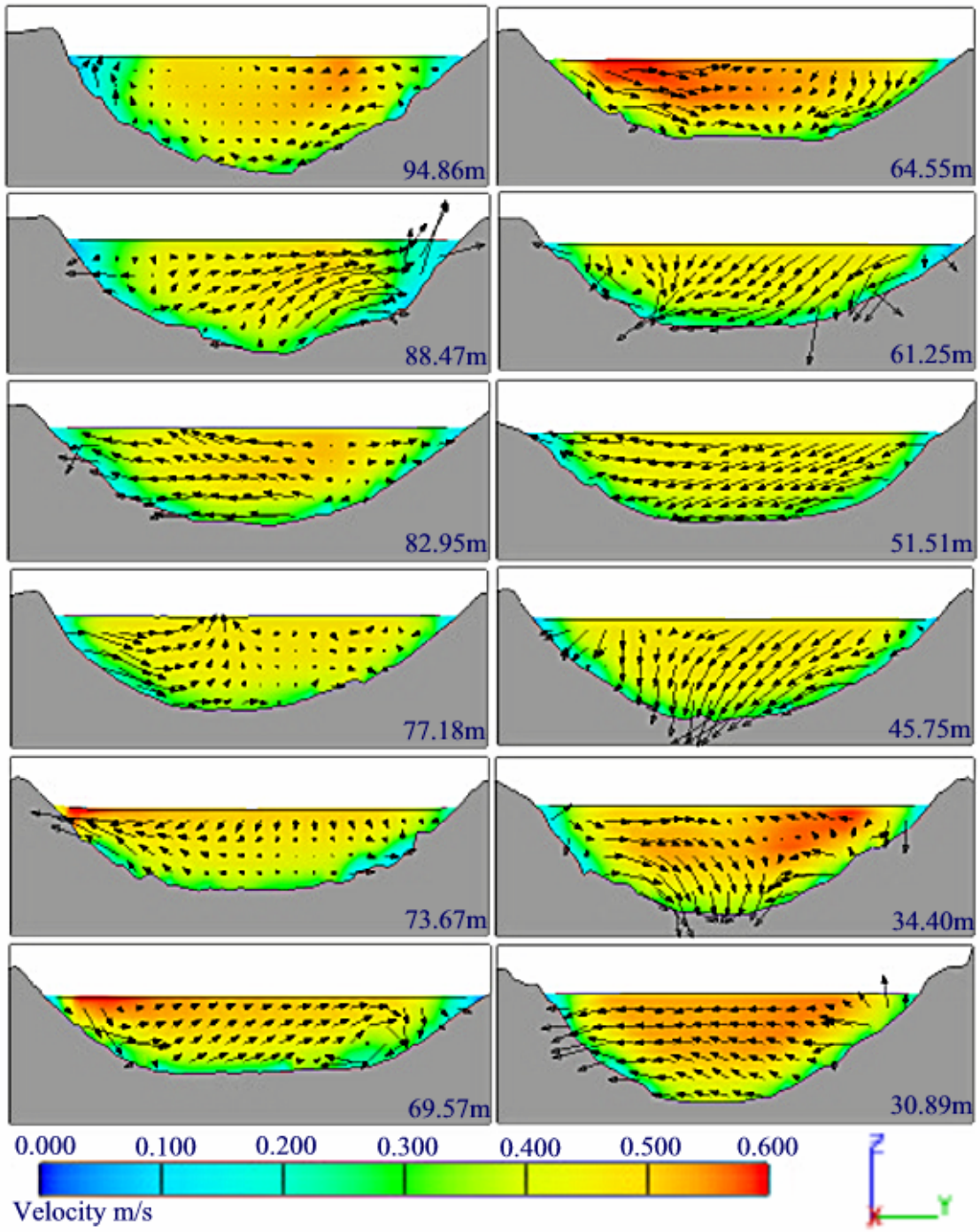

Maximum Velocity Vector for each cross-section

Figure 4.6: Modeled velocity magnitude and velocity magnitude vectors illustrated in y-z cross-sections in the channel with the trees removed.

were gradual, thus having moderate induction of cross-channel pattern caused by the changing velocities. Again, the y and z-velocities were patchy in nature throughout the channel. They varied throughout the water column and demonstrated few distinct patterns.

The majority of the flow was distributed across a greater part of the cross-section. This caused a uniform flow field with the highest velocity zone occurring within the centroid of the channel and having lower velocity magnitudes surrounding all sides of the high velocity zone. The vectors across the cross-section were also relatively uniform, indicating similar flow patterns.

Large-scale heterogeneity in streambed topography had a strong influence on flow patterns. At meter 42 of the model, a ledge along the channel bank initiated a localized high velocity zone. Likewise, the depression at meter 45 caused strong flow vectors toward the bed. However, the majority of the turbulent kinetic energy produced in this simulation was due to bed and bank roughness, therefore appearing to have a great influence on the flow regime, Figure 4.7.

Channel with Restoration Design

The third simulation exhibited a restoration design in which three patches of trees were left, spaced 5 to 7 channel widths apart, to initiate flow acceleration and deceleration. This simulation was designed to induce helical flow patterns in order to produce and maintain pool-riffle bedforms. Figure 4.8 shows the positive and negative y and z-

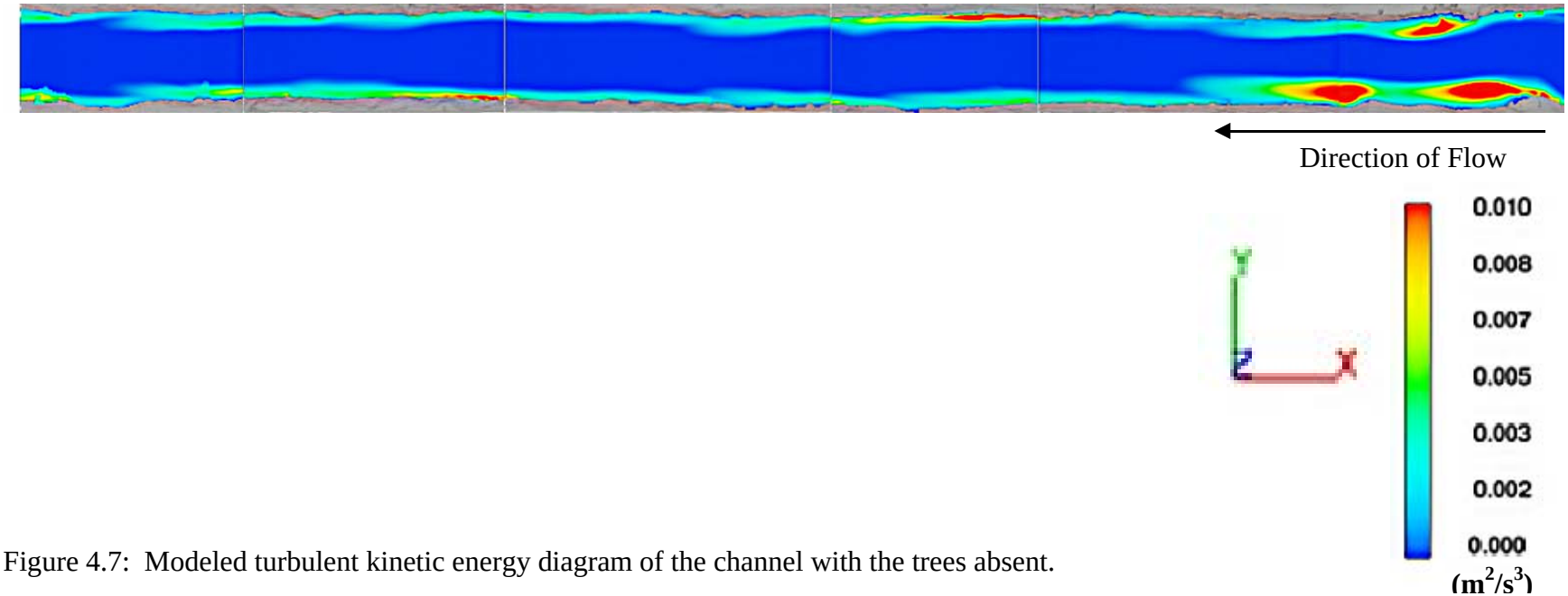

Figure 4.7: Modeled turbulent kinetic energy diagram of the channel with the trees absent.

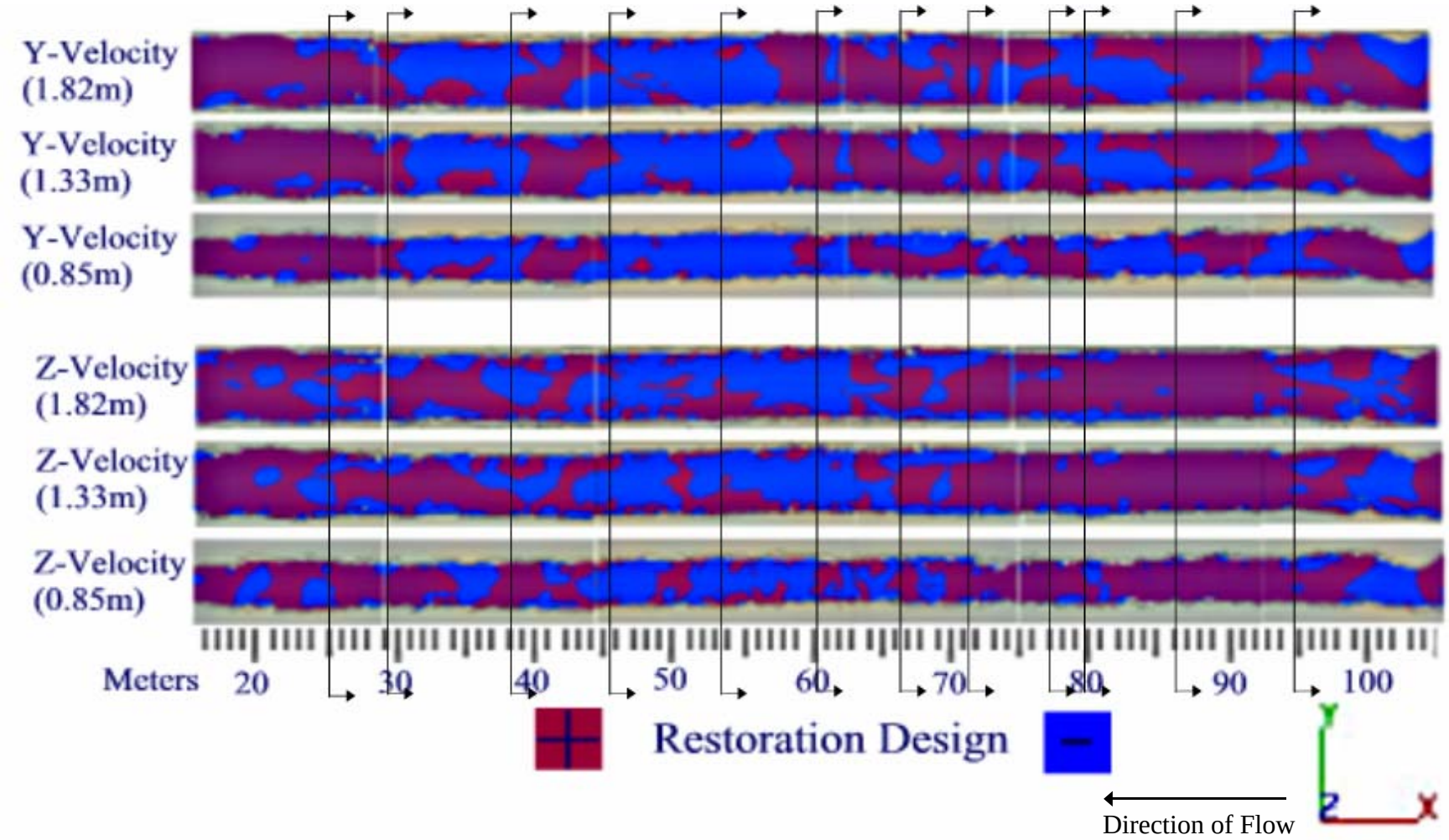

Figure 4.8: Modeled positive and negative y and z-velocities (m/s) in the channel with the restoration design implicated.

velocities in the channel with the restoration design. Again, Figure 4.9 is a Tecplot image of the channel with the restoration design implicated to better show the tree locations and the velocity magnitudes are illustrated in y-z cross-sections in Figure 4.10.

Similarly, the channel with the restoration design intact was visually analyzed using velocity magnitude y-z cross-sections and flow vectors on 1-meter intervals progressing downstream, (Appendix-C). The simulation showed strong, alternating cross-channel flow patterns resulting in channel-scale helical flow. The flow acceleration and deceleration was controlled by the restoration design, producing acute changes in velocity patterns upon entrance and exit of the restoration structure. The flow accelerations were concentrated toward the center of the cross-sections, while the deceleration areas were distributed more uniformly. The rapid changes in velocity patterns initiated strong cross-channel vectors. The near bed velocities also exhibited defined, channel-scale accelerations and decelerations. However, the y and z-velocities were still patchy in nature throughout the channel, varying throughout the water column and demonstrating few distinct patterns.

The majority of the turbulent kinetic energy was recognized within the flow constrictions, causing the flow to converge toward the center of the cross-section, Figure 4.11. However, bed and bank roughness also revealed moderate turbulent kinetic energy. The large-scale heterogeneity in streambed topography showed high turbulent kinetic energy and strongly influenced flow patterns. Similar to previous results, a ledge along the

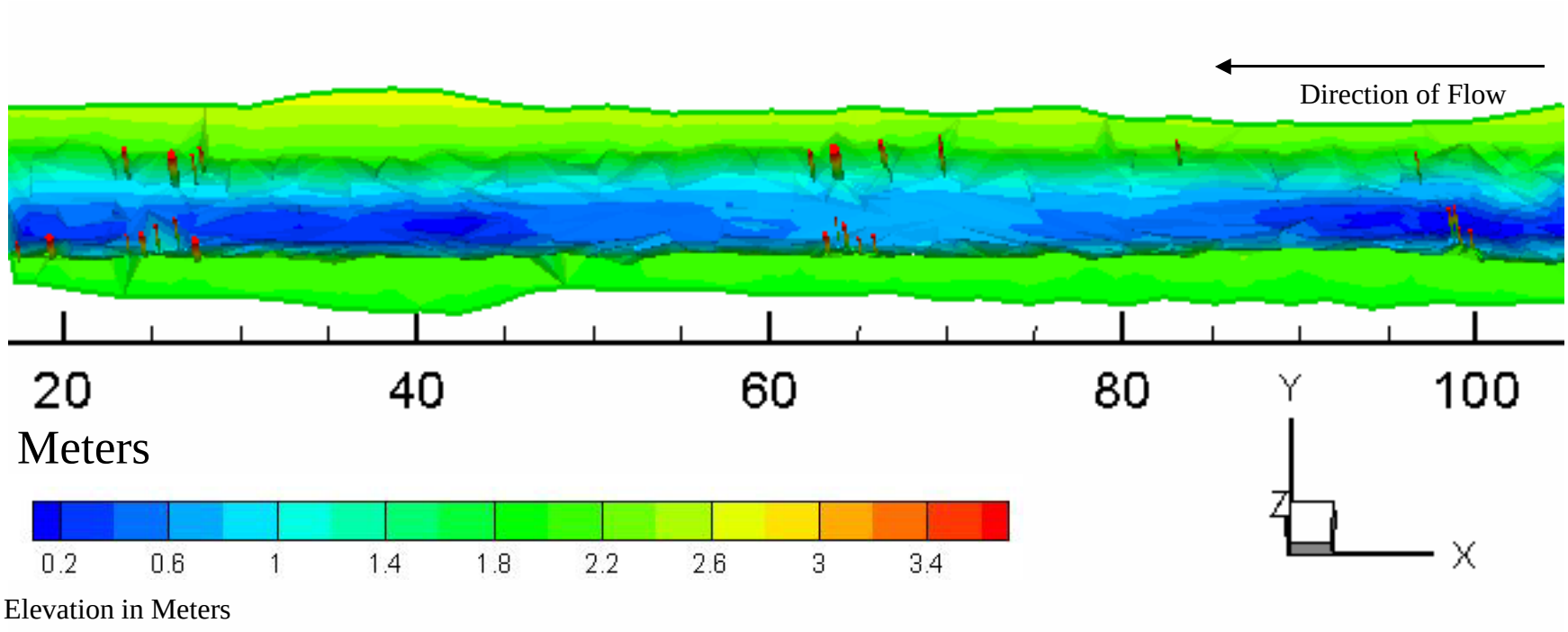

Figure 4.9: Tecplot image of the channel with restoration design to better illustrate the location of the trees with relation to the study site.

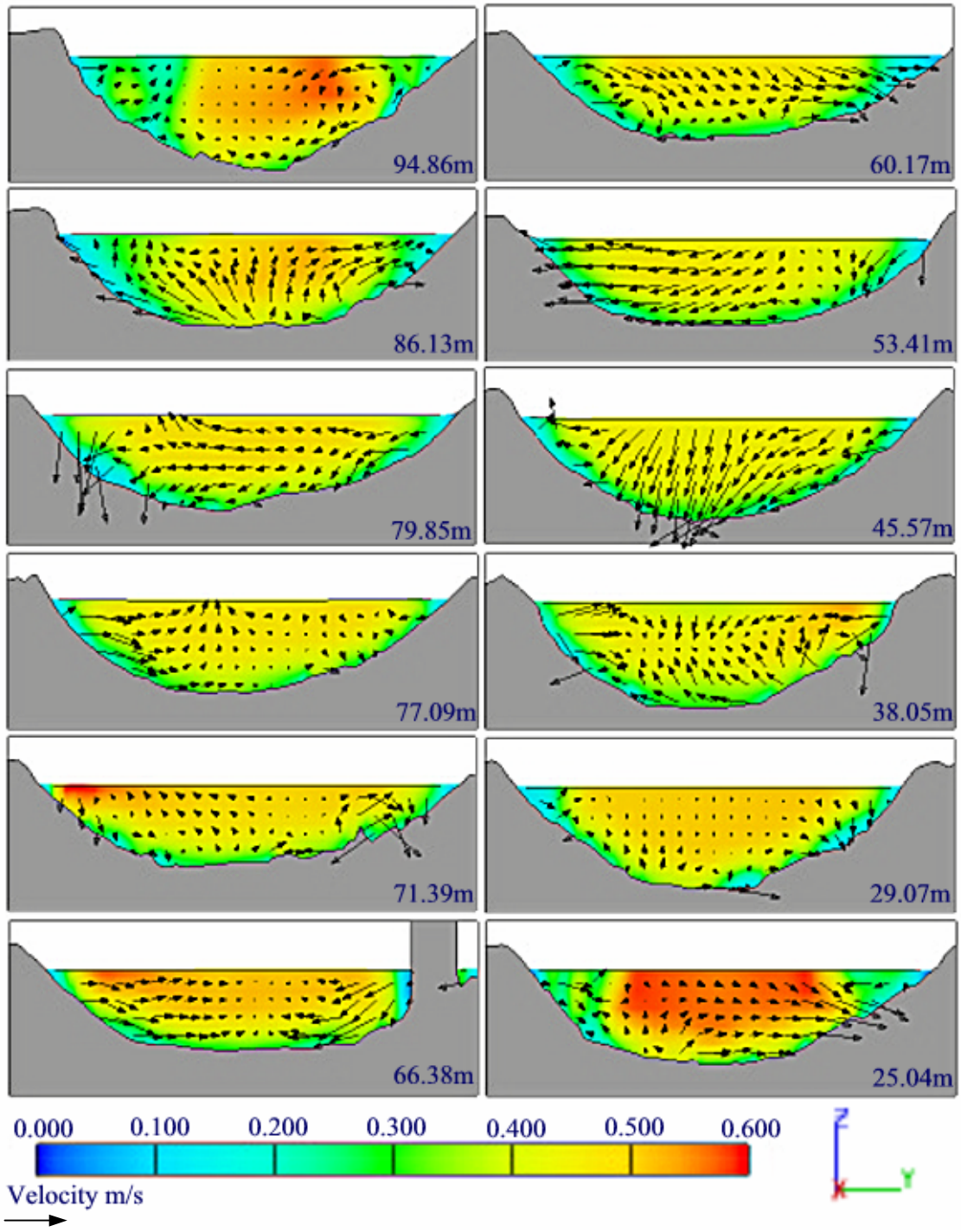

Figure 4.10: Modeled velocity magnitude and velocity magnitude vectors illustrated in y-z cross-sections in the channel with the restoration design implemented.

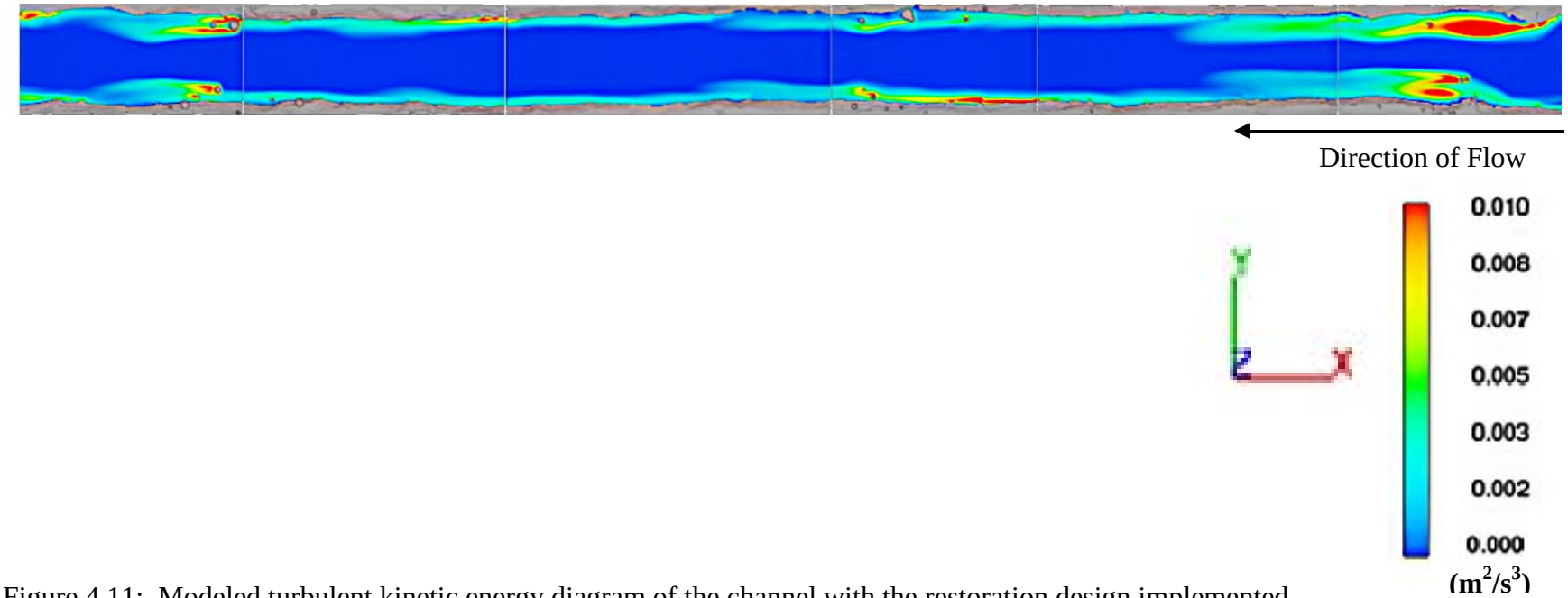

Figure 4.11: Modeled turbulent kinetic energy diagram of the channel with the restoration design implemented.

channel bank at meter 42 of the model, initiated a localized high velocity zone while the depression at meter 45 produced very large, defined flow vectors toward the bed.

Chapter 5: Discussion of Results

The results of the FLOW-3D simulations supported the objectives of this research in characterizing the turbulent structure within three different scenarios of the Beaver Creek research site. FLOW-3D was capable of establishing steady state flow regimes that represented the three scenarios in question. The simulation of the incised channel with trees inhibiting bankfull discharge did not show evidence of channel-scale helical flow patterns. The simulation of the incised channel with the trees removed did possess channel-scale helical flow patterns during bankfull discharge. Likewise, the simulation of the channel with three tree clusters spaced 5 to 7 channel widths apart, exhibiting channel restoration modifications, showed strong alternating velocities and channel-scale helical flow patterns during bankfull discharge.

The FLOW-3D simulation of the channel with trees inhibiting bankfull flow behaved much differently than the other two scenarios, as expected. The trees lining the bank produced excessive turbulent kinetic energy, which decreased the total available energy for the system. The turbulence in this channel was scaled to the trees, preventing channel-scale helical patterns to develop. As a result, large circulation cells evolved along the banks while the majority of the flow was directed toward the center of the channel. This was the region free from excessive roughness and essentially the path of least resistance. The increased velocities within the center of the channel would be expected to further incise the channel in order to create more uninhibited flow field (Simon 1995, Palhegyi et al. 2003). Although the majority of the discharge was directed toward the center of the channel, localized high velocity zones were recognized directly

around many of the trees. These localized high velocity zones could induce scour and erosion around the trees and increase their rate of failure (Sturm 2001). The failure of these trees would subject the channel to increased sediment loads and decreased stream power, causing the channel to progress into a Stage IV channel within the Channel Evolution Model, Figure 2.1 (Bledsoe et al. 2002, Rychborst 1980, Simon 1995).

The simulation of the channel with the trees removed displayed results consistent with current research in straight, alluvial channels. The model-developed channel-scale helical flow patterns, and flow acceleration-deceleration patterns on a 5 to 7 channel width basis (Dietrich 1987, Keller and Melhorn 1978, Rhoads and Welford 1991). These processes are consistent with producing and maintaining pool-riffle sequences (Dietrich 1987, Rhoads and Welford 1991). The velocities within this simulation were distributed relatively evenly across much of the cross-sections, demonstrating the possibility of increased shear stresses at the boundaries, a trait commonly observed in incised channels (Bledsoe et al. 2002, Rychborst 1980). Heterogeneity within the streambed and banks exhibited greater releases of turbulent kinetic energy and had strong influences on flow characteristics. These characteristics were also noticeable in the channel with the restoration design present. Likewise, the altered channels revealed very pronounced flow vectors into the bed of the depression at meter 45, supporting the theories of increased shear stresses in pools during bankfull discharges (Dietrich 1987, Rychborst 1980, Sear and Newson 2004, Wilkinson et al. 2004). The y and z-velocities were very patchy in nature throughout all of the channels. This demonstrated the highly disordered macro-structure of turbulence due to heterogeneous boundary layers experienced in natural

channels (Keshavarzi et al. 2005, Yalin 1992, Ziaei et al. 2005). This lack of uniformity was expected within the channel with trees, but more regular patterns were expected in the channels without trees and restoration design. These observations further stress how flow regimes are strongly affected by the irregular bed and bank topography commonly experienced in natural channels.

The simulation with the restoration design applied to the channel exhibited highly defined velocity acceleration-decelerations zones. These alternating velocity patterns were more exaggerated in the channel with the restoration design implemented than in the other two models. These discrete flow fields are apparent in pool-riffle sequences and are capable of supporting diverse biological ecosystems (Sear and Newson 2004, Schwartz 2002). Likewise, the initiation of cross-channel flow patterns was also more pronounced in the channel with the restoration design implemented, and concurred with results of Rhoads and Welford's research in 1991, which showed that abrupt variations in boundary roughness produce helical flow in straight channels. Along the same path, the abrupt anisotropic nature of the turbulence in this channel, demonstrated in the turbulent kinetic energy diagram, has been connected with processes encouraging bed scour at recurring intervals (Rhoads and Welford 1991). The acute nature of the hydraulic patterns that were recognized within the channel containing the implemented restoration design have also been demonstrated to initiate and maintain pool-riffle sequences in straight channels (Dietrich 1987, Gregory et al. 1994, Knighton 1998, Rhoads and Welford 1991).

Many characteristics of the results of the three simulations were consistent with current literature. The simulation of the channel with the trees present had more hydraulic differences than the simulations of the other two scenarios. Although both of the modified channels displayed characteristics responsible for the initiation and maintenance of pool-riffle sequences, these characteristics were more pronounced in the channel with the restoration design implemented. While these restoration structures initiated defined patterns, the hydraulic behaviors varied greatly between the sequences of the tree clusters. The degree and length of the constriction dictated the hydraulic characteristics of the stream. Therefore, future research to characterize the hydraulic affects of differing channel constrictions is necessary to optimize the benefits of the restoration design. The fate of successful channel restoration designs requires less invasive techniques that do not completely modify the channel geometry and cannot be destroyed by continuously changing systems. The success of these designs should not be determined through trial and error, but must be tested beforehand and proven scientifically. The establishment of pool-riffle sequences is the most important criterion for evaluating the success of channel restoration projects, so the hydraulic maintenance dictating the sediment transport and morphological evolution processes of these sequences should be the most important criteria in the channel restoration design (Thompson 2002, Cao et al. 2002).

List of References

List of References

Bledsoe, B. P., Watson, C. C., Biedenharn, D. S. (2002). "Quantification of Incised Channel Evolution and Equilibrium." Journal of the American Water Resources Association, Vol. 38, No. 3, 861-870.

Bombardelli, F. A., Garcia, M. H., Caisley, M. C. (2000). "2-D and 3-D Numerical Simulation of Abrupt Transitions in Open Channel Flows. Application to the design of canoe chutes." Proc., 4th Int. Conference on Hydroinformatics (CD-Rom), International Association for Hydraulic Research, Iowa City, IA.

Booker, D. J., Sear, D. A., Payne, A. J. (2000). "Modeling Three-Dimensional Flow Structures and Patterns of Boundary Shear Stress in a Natural Pool-Riffle Sequence." Earth Surface Processes and Landforms, Vol. 26, 553-576.

Booth, D. B., Montgomery, D. R., Bethel, J. (1997). "Large Woody Debris in Urban Streams of the Pacific Northwest." Proc., Effects of watershed development and management on aquatic ecosystems: Engineering Foundation Conference, Snowbird, UT, 178-197.

Brown, K. B. (2000). "Urban Stream Restoration Practices: An Initial Assessment." US EPA Office of Wetlands, Oceans, and Watersheds: 87, Ellicott City, MD.

Cao, Z., Carling, P., Oakey, R. (2002). "Flow Reversal Over a Natural Pool-Riffle Sequence: A Computational Study." Earth Surface Processes and Landforms, Vol. 28, 689-705.

Coduto, D. (1998). "Geotechnical Engineering, Principles and Practices." Prentice Hall, Inc., Upper Saddle River, NJ.

Dietrich, W. E. (1987). "Mechanics of Flow and Sediment Transport in River Bends." Institute of British Geographers Special Publication No. 18, Basil Blackwell, Inc., 179-227.

Doerfer, J., Urbonas, B. (2003). "Urban Watershed Master Planning for Stream Protection in the Denver Metropolitan Area." Proc., The Symposium-Protection and Restoration of Urban and Rural Streams, Philadelphia, PA, 51-60.

Emery, J. C., Gurnell, A. M., Clifford, N. J., Petts, G. E., Morrissey, I. P., Soar, P. J. (2003). "Classifying the Hydraulic Performance of Riffle-Pool Bedforms for Habitat Assessment and River Rehabilitation Design." River Research and Application, Vol. 19, 533-549.

Franzini, J. B., Finnemore, J. E. (1997). "Fluid Mechanics." The McGraw-Hill Companies, Inc., New York, NY.

Gaboury, M.N., Janusz, R. A., Broughton, K. E. (1997). “Stream Channel and Riparian Rehabilitation in the Dauphin Lake Watershed, Manitoba.” Water Qual. Res. J. Canada, Vol. 32, No. 2, 257-272.

Gregory, K. J., Gurnell, A. M., Hill, C. T., Tooth, S. (1994). “Stability of the Pool-Riffle Sequence in Changing River Channels.” Regulated Rivers: Research and Management, Vol. 9, 35-43.

Heritage, G. L., Milan, D. J. (2004). “A Conceptual Model of the Role of Excess Energy in the Maintenance of a Riffle-Pool Sequence.” Catena 58, 235-257.

Julien, P. Y. (1998). “Erosion and Sedimentation.” Cambridge University Press, Cambridge CB2 2RU, United Kingdom.

Keller, E. A., and Melhorn, W. M. (1978). “Rhythmic Spacing and Origin of Pools and Riffles.” Geological Society of America Bulletin, Vol. 89, 723–730.

Keshavarzi, A. R., Ziaei, A. N., Homayoun, E., Shirvani, A. (2005). “Fractal-Markovian Scaling of Turbulent Bursting Process in Open Channel Flow.” Chaos, Solitons and Fractals, Vol. 25, 307-318.

Knighton, D. (1998). “Fluvial Forms and Processes: A New Perspective.” Oxford University Press Inc., New York.

Langendoen, E. J., and Simon, A. (2000). "Stream channel evolution of Little Salt Creek and North Branch West Papillion Creek, eastern Nebraska." Report, US Department of Agriculture, Agricultural Research Service, National Sedimentation Laboratory, Oxford, MS.

MacRae, C. R. (1996). “Experience from Morphological Research on Canadian Streams: is Control of the Two Year Frequency Runoff Event the Best Basis for Stream Channel Protection?” Effects of Watershed Development and Management on Aquatic Ecosystems, Engineering Foundation, New York, NY, 144-162.

Niezgoda, S. L., Johnson, P. A. (2005). “Improving the Urban Stream Restoration Effort: Identifying Critical Form and Processes Relationships.” Environmental Management, Vol. 35, No. 5, 579-592.

Palhegyi, G., Mangarella, P., Strecker, E., Bicknell, J., Sen, D. (2003). “Developing Management Plans to Address Impacts from Urbanization on Stream Channel Integrity.” World Water and Environmental Resources Congress and Related Symposia, Philadelphia, PA.

Rhoads, B. L., Welford, M. R. (1991). “Initiation of River Meandering.” Progress in Physical Geography, Vol. 15, 2, 127-156.

Rhoads, B. L., Schwartz, J. S., Porter, S. (2003). "Stream Geomorphology, Bank Vegetation and Three-Dimensional Habitat Hydraulics for Fish in Midwestern Agricultural Streams." Water Resources Research, Vol 39(8), 1218-1230.

Richards, K. S. (1976). "The Morphology of Riffle-Pool Sequences." Earth Surface Processes, Vol. 1, 71-88.

Rodriquez, J. F., Garcia, M. H., Bombardelli, Guzman, J. M., F. A., Rhoads, B. L., Herricks, E. (2000). "Naturalization of Urban Streams Using In-Channel Structures." Proc., Joint Conference on Water Resources Engineering and Water Resources Planning and Management 2000, Minneapolis, MN.

Rychborst, H. (1980). "Geomorphological Changes After River-Meander Surgery." Geol. Mijnbouw, Vol. 59, 121-128.

Schwartz, J. S. (2002). "Stream Habitat Characterized by Stage-Specific Flows and Three-Dimensional Geomorphical Complexity: Development of Ecological Criteria for Stream Restoration Design." PhD Dissertation, University of Illinois, Urbana-Champaign, IL.

Schwartz, J. S., Carpenter, D. D., Slate, L. O., Sinha, S. K., Brennen, K., MacBroom, J. (2003). "Research Needs for Improvement for Principles and Practices in Urban Stream Restoration." Proc., Symposium on the Protection and Restoration of Urban and Rural Streams, Philadelphia, PA, 15-28.

Schwartz, J. S., Herricks, E. E. (2005A). "Evaluation of Pool-Riffle Naturalization Structures on Habitat Complexity and the Fish Community in an Urban Illinois Stream." River Research and Applications, (In Press).

Schwartz, J. S., Herricks, E. E. (2005B). "Fish Use of Stage-Specific Fluvial Habitats as Refuge During a Flood in a Low-Gradient Illinois Stream." Canadian Journal of Fisheries and Aquatic Science, Vol. 62, 1540-1552.

Schwartz, J. S., Herricks, E. E., Rhoads, B. L. (2001). "Integrating Geomorphology, Hydraulics, and Ecological Criteria to Support Stream Naturalization in East-Central Illinois." Proc., World Water and Environmental Resources Congress, Orlando, FL.

Sear, D. A., Newson, M. D. (2004). "The Hydraulic Impact and Performance of a Lowland Rehabilitation Scheme Based on Pool-Riffle Installation: The River Waveney, Scole, Suffolk, UK." River Research and Applications, Vol. 20, 847-863.
Simon, A., Thomas, R. E. (2002). "Process and Forms of an Unstable Alluvial System with Resistant, Cohesive Streambeds." Earth Surface Processes and Landforms, Vol. 27, 699-718.

Simon, A. (1995). "Adjustment and Recovery of Unstable Alluvial Channels: Identification and Approaches for Engineering Management." Earth Surface Processes and Landforms, Vol. 20, 611-628.

Simon, A., Collison, J. C. (2002). "Quantifying the Mechanical and Hydrologic Effects of Riparian Vegetation on Streambank Stability." Earth Surface Processes and Landforms, Vol. 27, 527-546.

Smith, D. I., Stopp, P. (1978). "The River Basin." Cambridge University Press, Cambridge, MA.

Sturm, T. W. (2001). "Open Channel Hydraulics." The McGraw-Hill Companies, Inc., New York, NY.

Thompson, D. M. (2002). "Long-Term Effect of Instream Habitat-Improvement Structures on Channel Morphology Along the Blackledge and Salmon Rivers, Connecticut, USA." Environmental Management, Vol. 29, No. 1, 250-265.

Tuysuz, O. (2002). "Fluvial Systems." International Technological University, [Online], http://www.eies.itu.edu.tr/dersnotlari/notlar/Y%C3%BCksek_lisans/Jeomorfoloji_Okan/Fluvial%20systems.pdf (Accessed: 28 October 2005).

Wade, R. J., Rhoads, B. L., Rodriquez, J., Daniels, M., Wilson, D., Herricks, E. E., Bombardelli, F., Garcia, M., Schwartz, J. S. (2002). "Integrating Science and Technology to Support Stream Naturalization Near Chicago, Illinois." Journal of the American Water Resources Association, Vol. 38, 931-944.

Wilkinson, S. N., Keller, R. J., Rutherfurd, I. D. (2004). "Phase-Shifts in Shear Stress as an Explanation for the Maintenance of Pool-Riffle Sequences." Earth Surface Processes and Landforms, Vol. 29, 737-753.

Yalin, M. S. (1992). "River Mechanics." Pergamon Press Ltd., Headington Hill Hall, Oxford OX3 0BW, England.

Ziaei, A. N., Keshavarzi, A. R., Homayoun, E. (2005). "Fractal Scaling and Simulation of Velocity Components and Turbulent Shear Stress in Open Channel Flow." Chaos, Solitons and Fractals, Vol. 24, 1031-1045.

Appendices

Appendix A

Channel With Trees

→ Maximum Velocity Vector for each cross-section

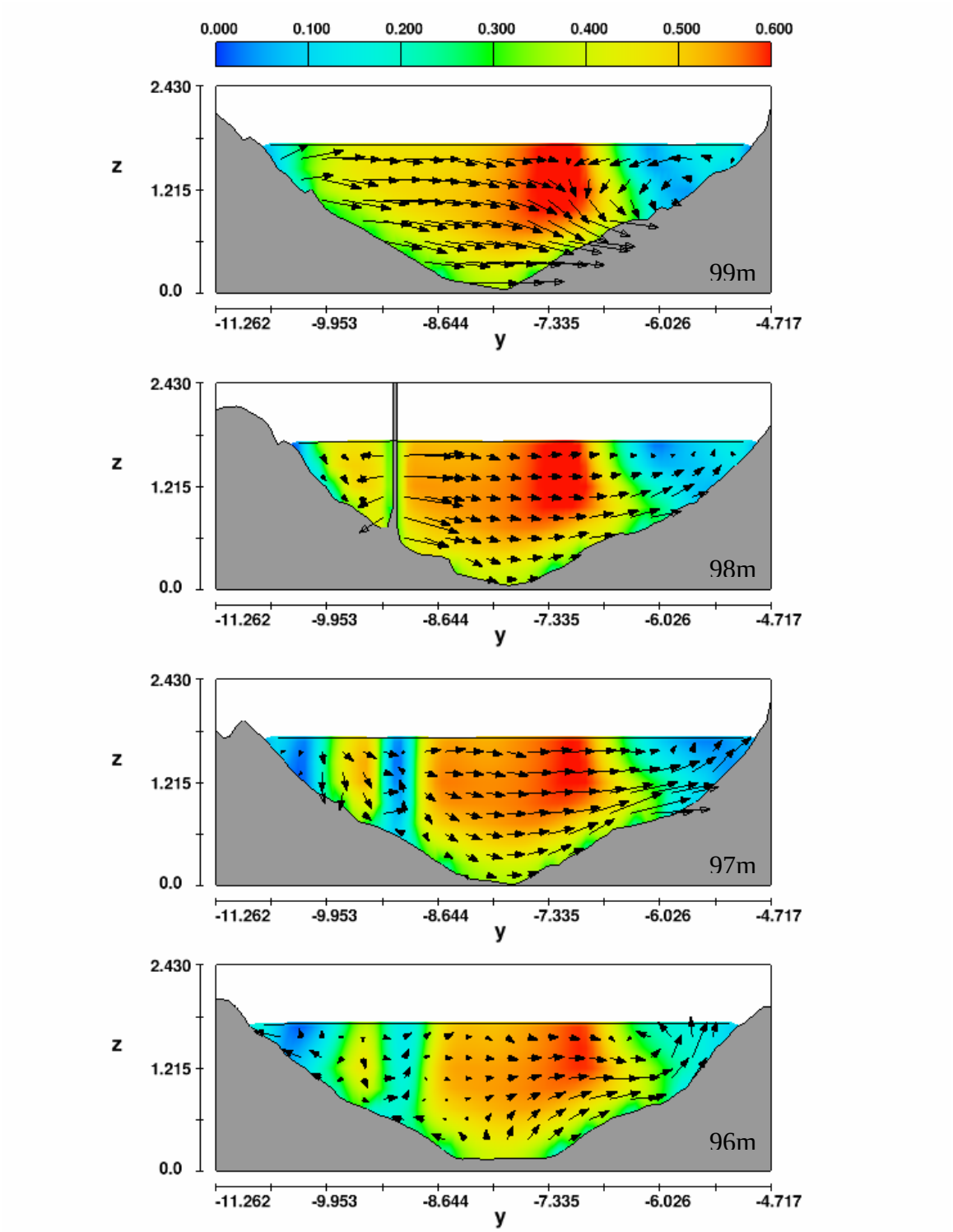

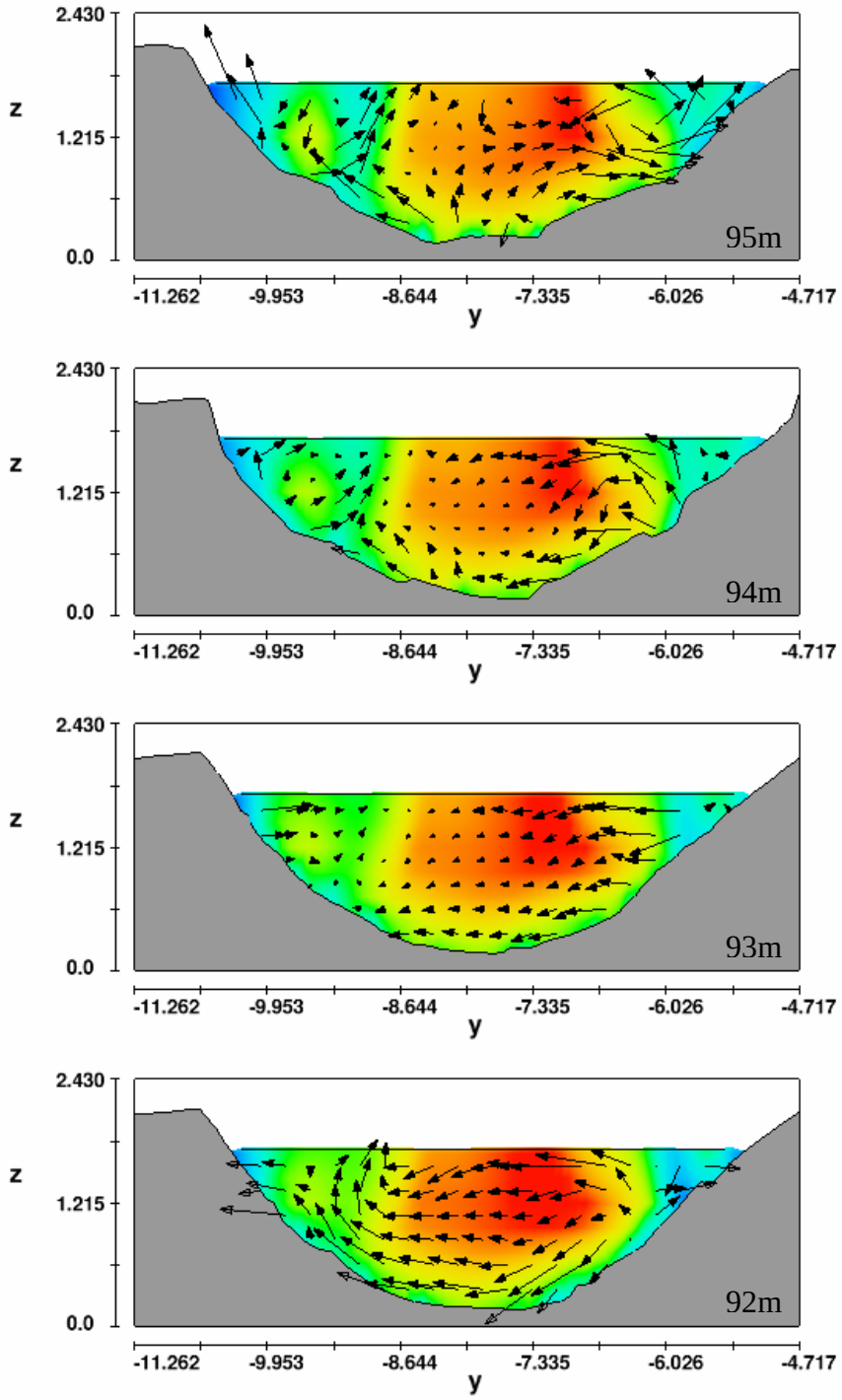
2.430
z
1.215
0.0
95m
-11.262
-9.953
-8.644
-7.335
-6.026
-4.717
y
2.430
z
1.215
0.0
94m
-11.262
-9.953
-8.644
-7.335
-6.026
-4.717
y
2.430
z
1.215
0.0
93m
-11.262
-9.953
-8.644
-7.335
-6.026
-4.717
y
2.430
z
1.215
0.0
92m
-11.262
-9.953
-8.644
-7.335
-6.026
-4.717
y

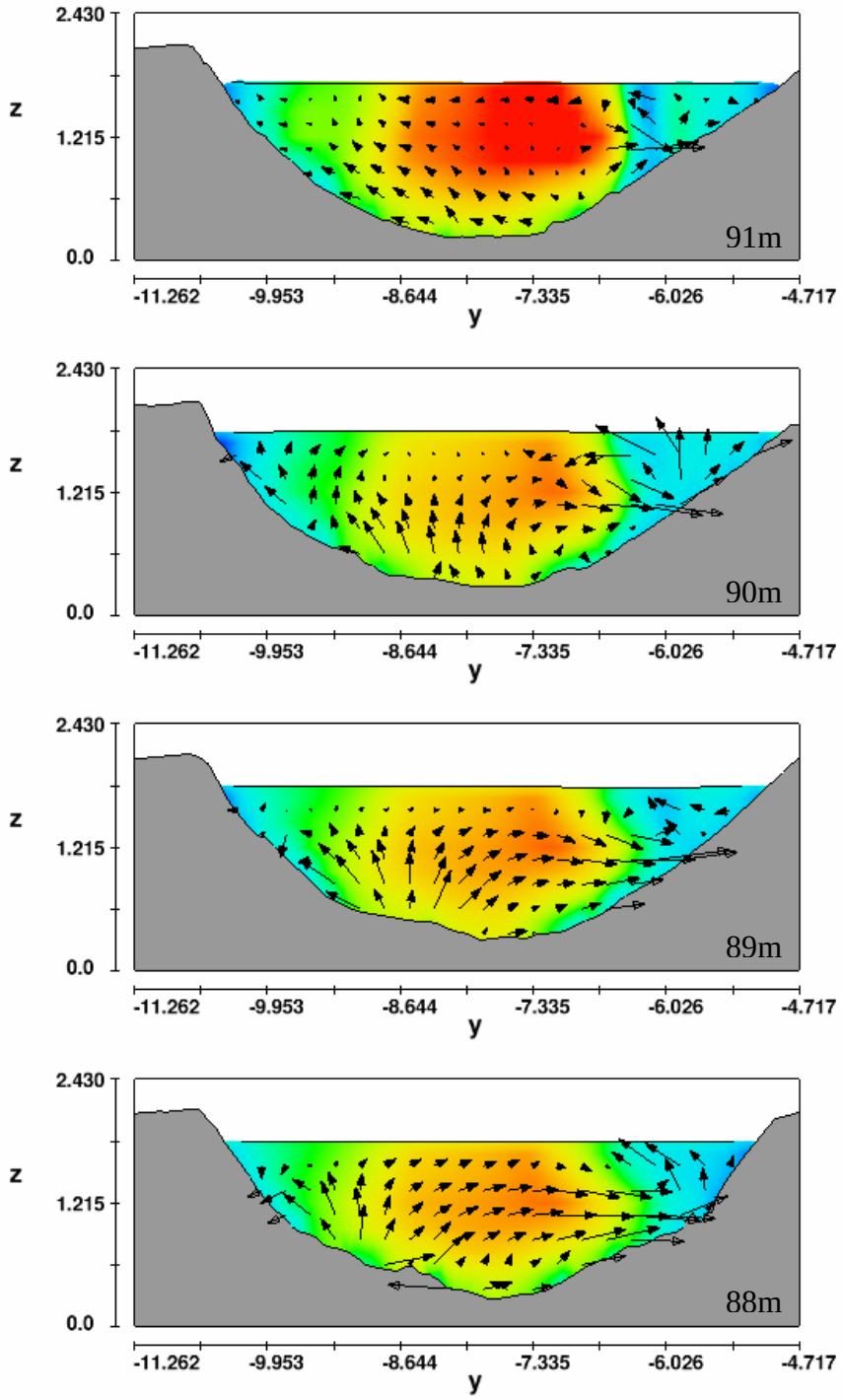
2.430
z
1.215
0.0
91m
-11.262
-9.953
-8.644
-7.335
-6.026
-4.717
y
2.430
z
1.215
0.0
90m
-11.262
-9.953
-8.644
-7.335
-6.026
-4.717
y
2.430
z
1.215
0.0
89m
-11.262
-9.953
-8.644
-7.335
-6.026
-4.717
y
2.430
z
1.215
0.0
88m
-11.262
-9.953
-8.644
-7.335
-6.026
-4.717
y

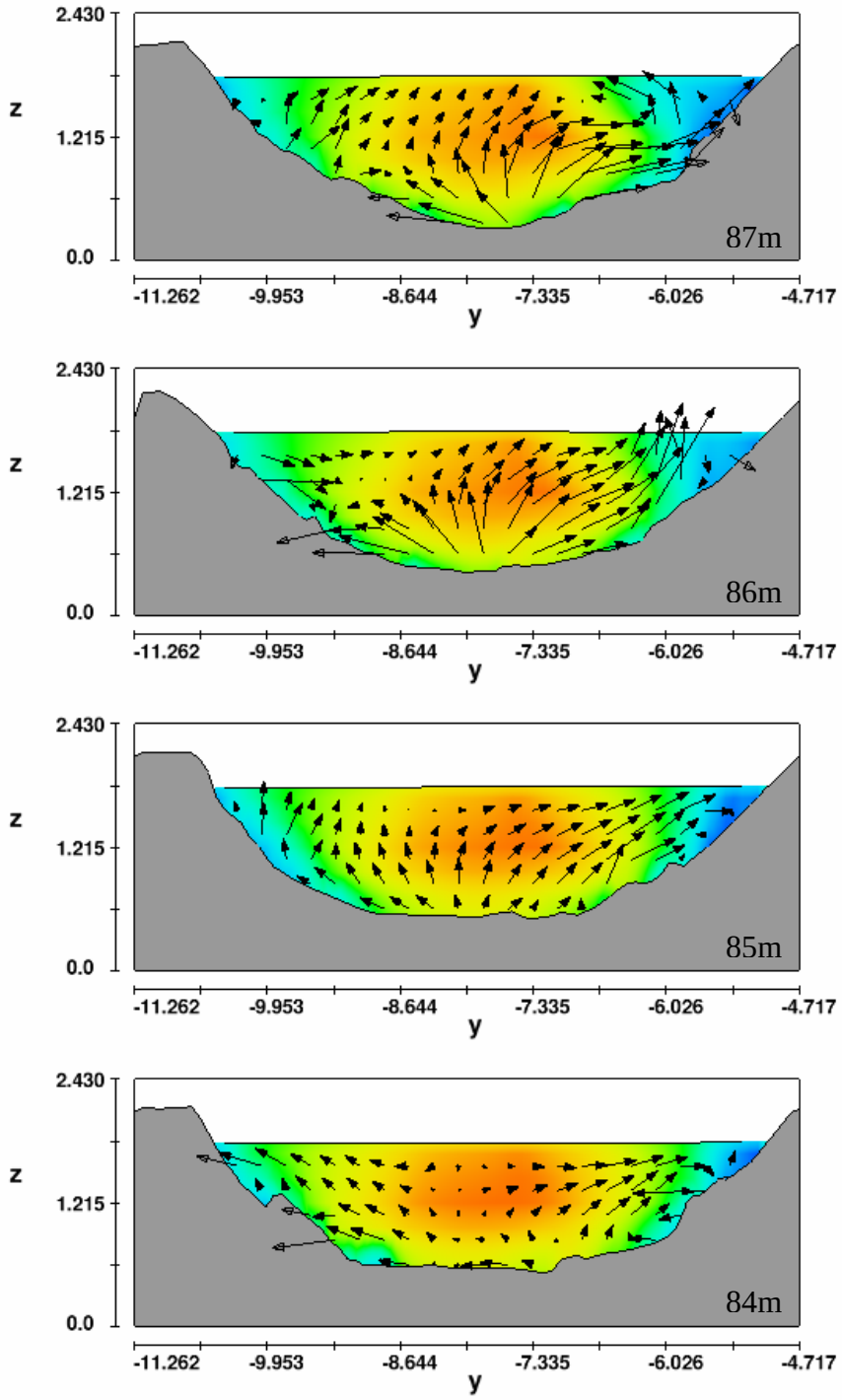
2.430
z
1.215
0.0
87m
-11.262
-9.953
-8.644
-7.335
-6.026
-4.717
y
2.430
z
1.215
0.0
86m
-11.262
-9.953
-8.644
-7.335
-6.026
-4.717
y
2.430
z
1.215
0.0
85m
-11.262
-9.953
-8.644
-7.335
-6.026
-4.717
y
2.430
z
1.215
0.0
84m
-11.262
-9.953
-8.644
-7.335
-6.026
-4.717
y

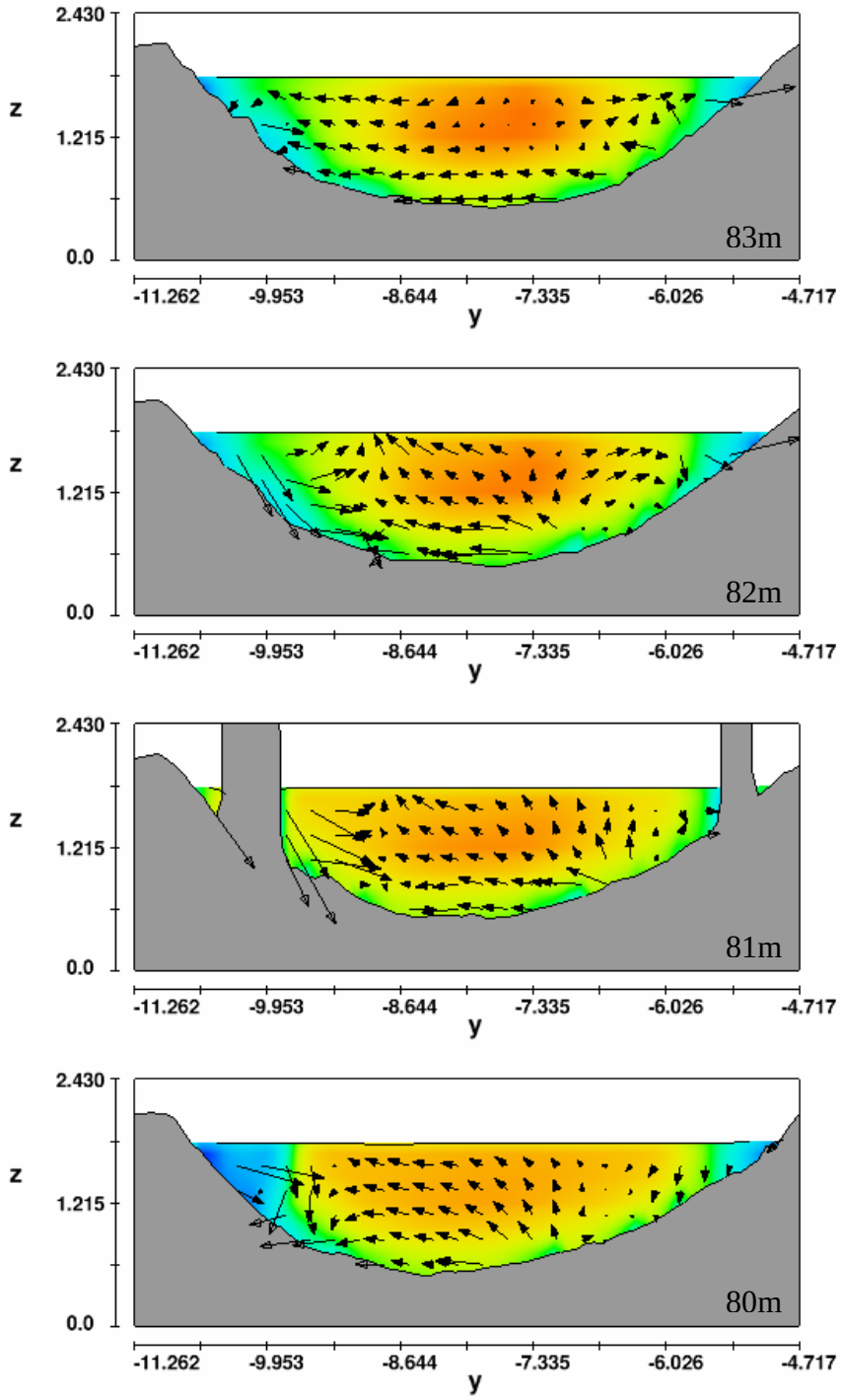
2.430
z
1.215
0.0
83m
-11.262
-9.953
-8.644
-7.335
-6.026
-4.717
y
2.430
z
1.215
0.0
82m
-11.262
-9.953
-8.644
-7.335
-6.026
-4.717
y
2.430
z
1.215
0.0
81m
-11.262
-9.953
-8.644
-7.335
-6.026
-4.717
y
2.430
z
1.215
0.0
80m
-11.262
-9.953
-8.644
-7.335
-6.026
-4.717
y

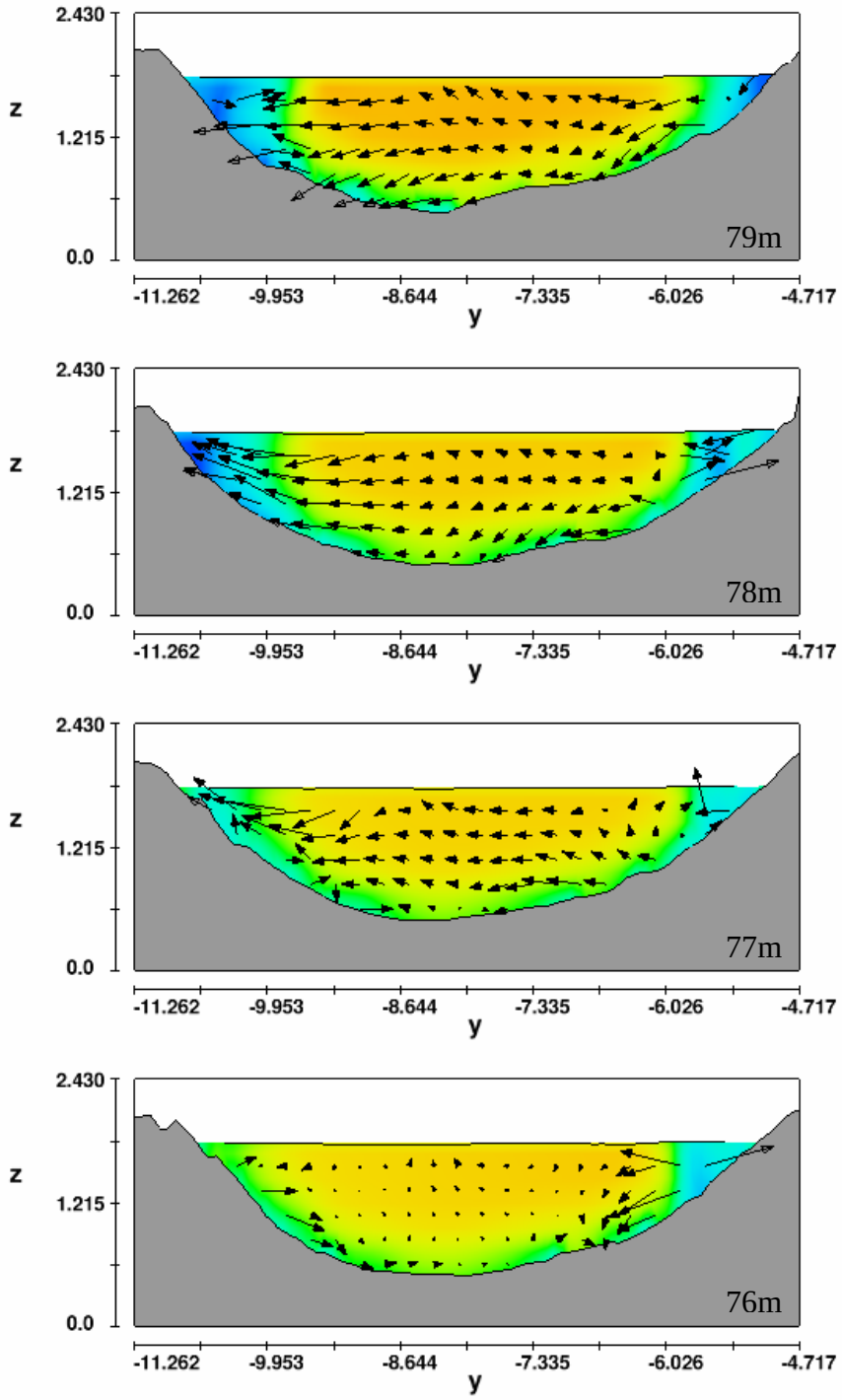
2.430
z
1.215
0.0
79m
-11.262
-9.953
-8.644
-7.335
-6.026
-4.717
y
2.430
z
1.215
0.0
78m
-11.262
-9.953
-8.644
-7.335
-6.026
-4.717
y
2.430
z
1.215
0.0
77m
-11.262
-9.953
-8.644
-7.335
-6.026
-4.717
y
2.430
z
1.215
0.0
76m
-11.262
-9.953
-8.644
-7.335
-6.026
-4.717
y

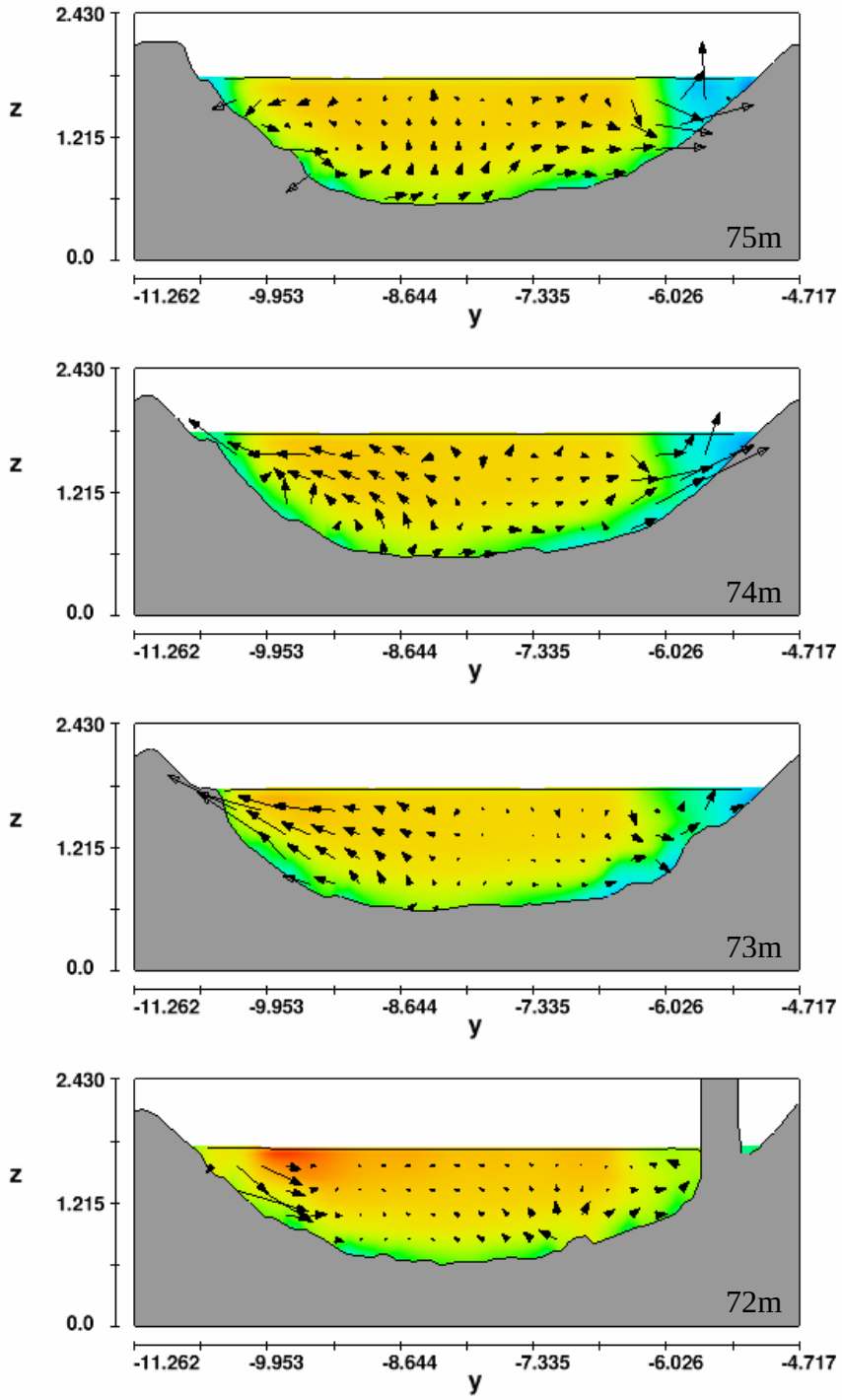
2.430
z
1.215
0.0
75m
-11.262
-9.953
-8.644
-7.335
-6.026
-4.717
y
2.430
z
1.215
0.0
74m
-11.262
-9.953
-8.644
-7.335
-6.026
-4.717
y
2.430
z
1.215
0.0
73m
-11.262
-9.953
-8.644
-7.335
-6.026
-4.717
y
2.430
z
1.215
0.0
72m
-11.262
-9.953
-8.644
-7.335
-6.026
-4.717
y

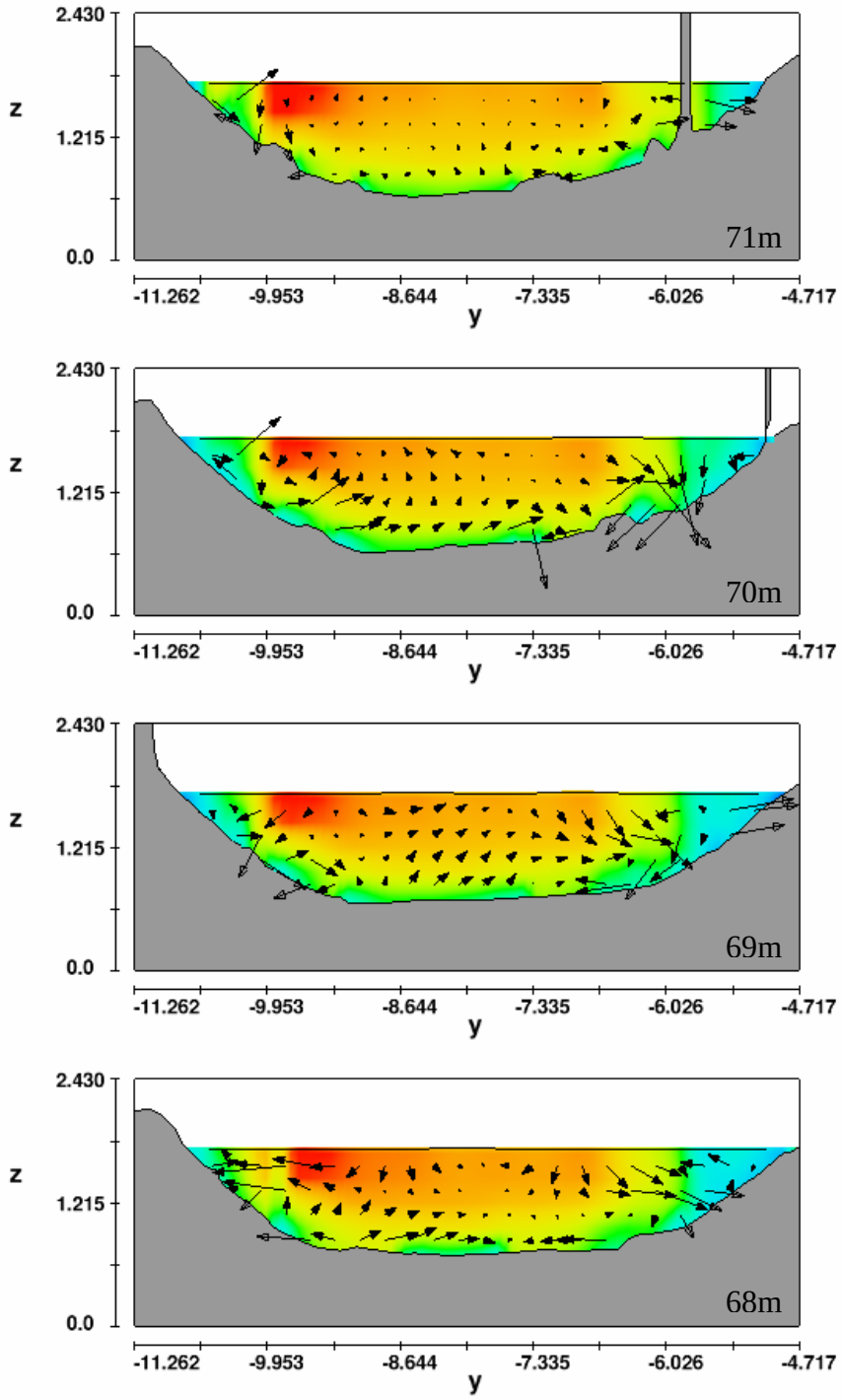
2.430
z
1.215
0.0
71m
-11.262
-9.953
-8.644
-7.335
-6.026
-4.717
y
2.430
z
1.215
0.0
70m
-11.262
-9.953
-8.644
-7.335
-6.026
-4.717
y
2.430
z
1.215
0.0
69m
-11.262
-9.953
-8.644
-7.335
-6.026
-4.717
y
2.430
z
1.215
0.0
68m
-11.262
-9.953
-8.644
-7.335
-6.026
-4.717
y

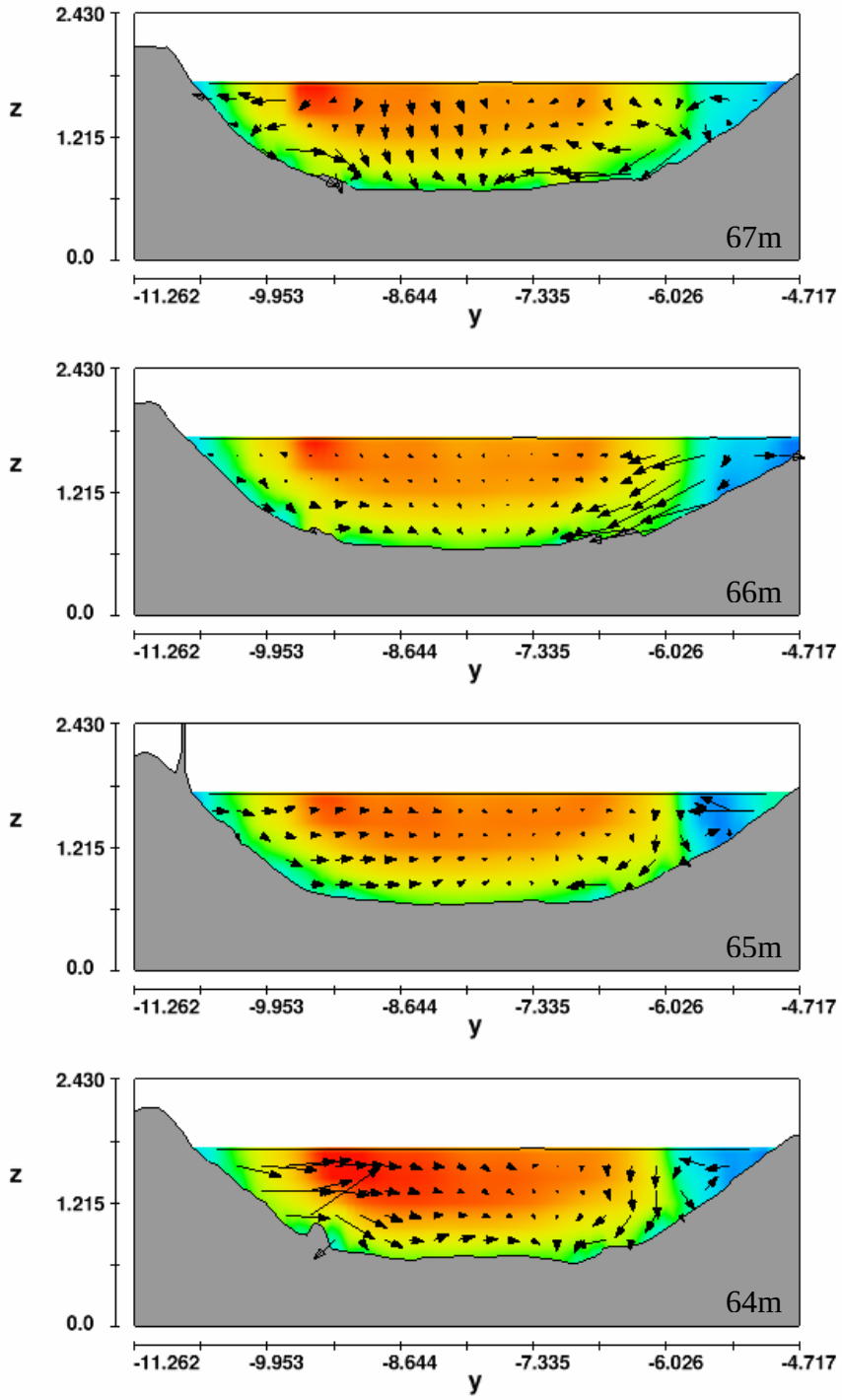
2.430
z
1.215
0.0
67m
-11.262
-9.953
-8.644
-7.335
-6.026
-4.717
y
2.430
z
1.215
0.0
66m
-11.262
-9.953
-8.644
-7.335
-6.026
-4.717
y
2.430
z
1.215
0.0
65m
-11.262
-9.953
-8.644
-7.335
-6.026
-4.717
y
2.430
z
1.215
0.0
64m
-11.262
-9.953
-8.644
-7.335
-6.026
-4.717
y

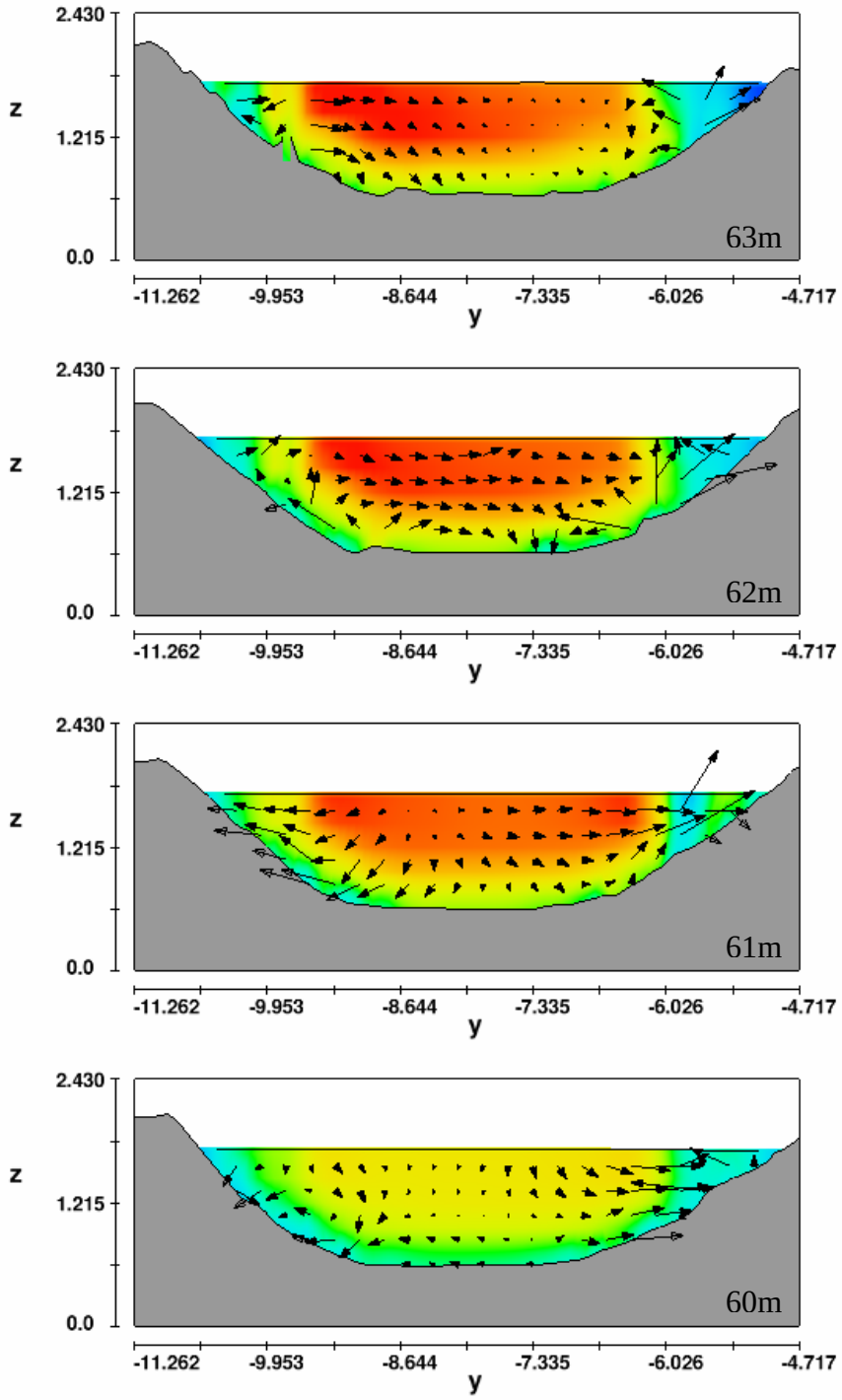
2.430
z
1.215
0.0
63m
-11.262
-9.953
-8.644
-7.335
-6.026
-4.717
y
2.430
z
1.215
0.0
62m
-11.262
-9.953
-8.644
-7.335
-6.026
-4.717
y
2.430
z
1.215
0.0
61m
-11.262
-9.953
-8.644
-7.335
-6.026
-4.717
y
2.430
z
1.215
0.0
60m
-11.262
-9.953
-8.644
-7.335
-6.026
-4.717
y

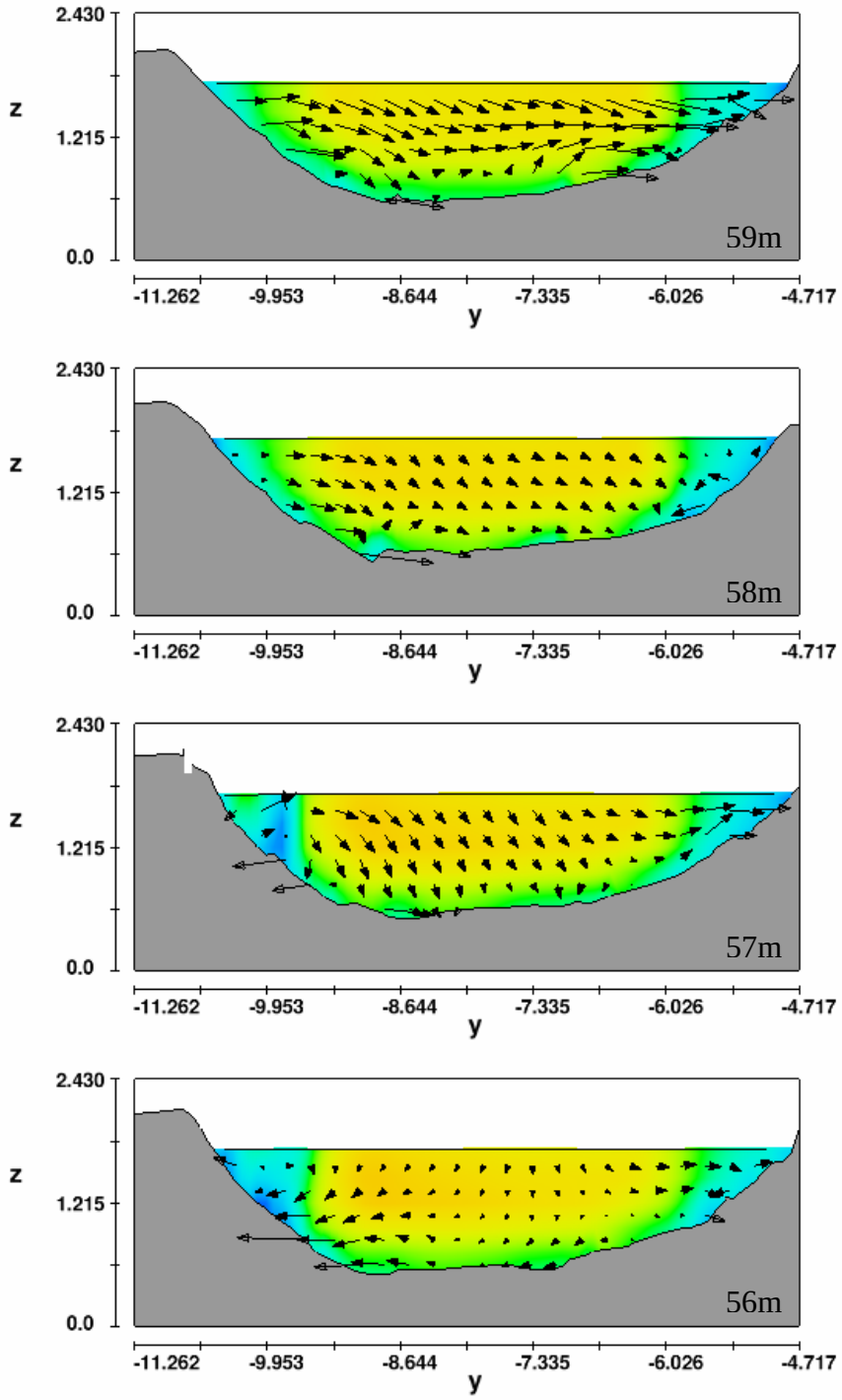
2.430
z
1.215
0.0
59m
-11.262
-9.953
-8.644
-7.335
-6.026
-4.717
y
2.430
z
1.215
0.0
58m
-11.262
-9.953
-8.644
-7.335
-6.026
-4.717
y
2.430
z
1.215
0.0
57m
-11.262
-9.953
-8.644
-7.335
-6.026
-4.717
y
2.430
z
1.215
0.0
56m
-11.262
-9.953
-8.644
-7.335
-6.026
-4.717
y

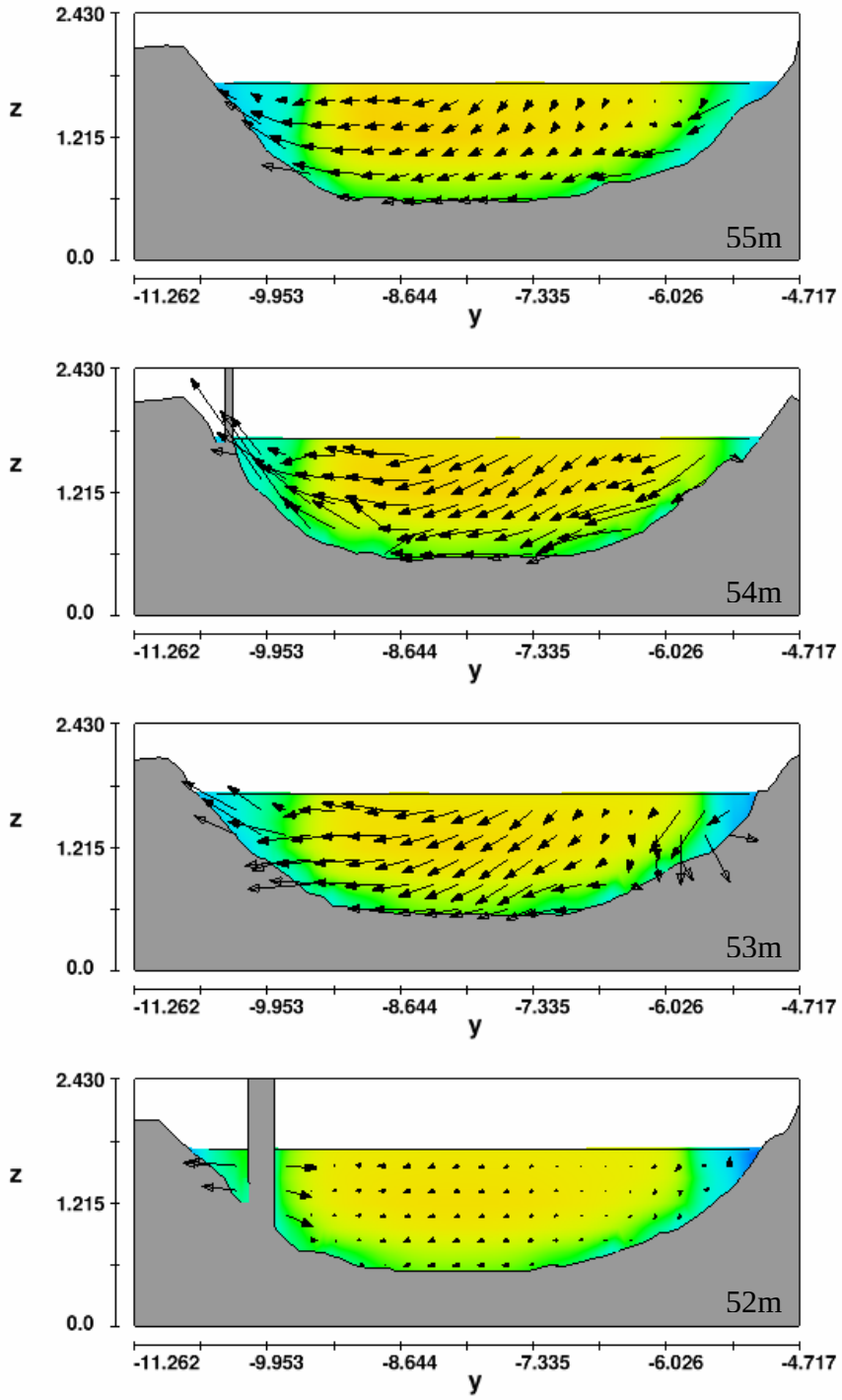
2.430
z
1.215
0.0
55m
-11.262
-9.953
-8.644
-7.335
-6.026
-4.717
y
2.430
z
1.215
0.0
54m
-11.262
-9.953
-8.644
-7.335
-6.026
-4.717
y
2.430
z
1.215
0.0
53m
-11.262
-9.953
-8.644
-7.335
-6.026
-4.717
y
2.430
z
1.215
0.0
52m
-11.262
-9.953
-8.644
-7.335
-6.026
-4.717
y

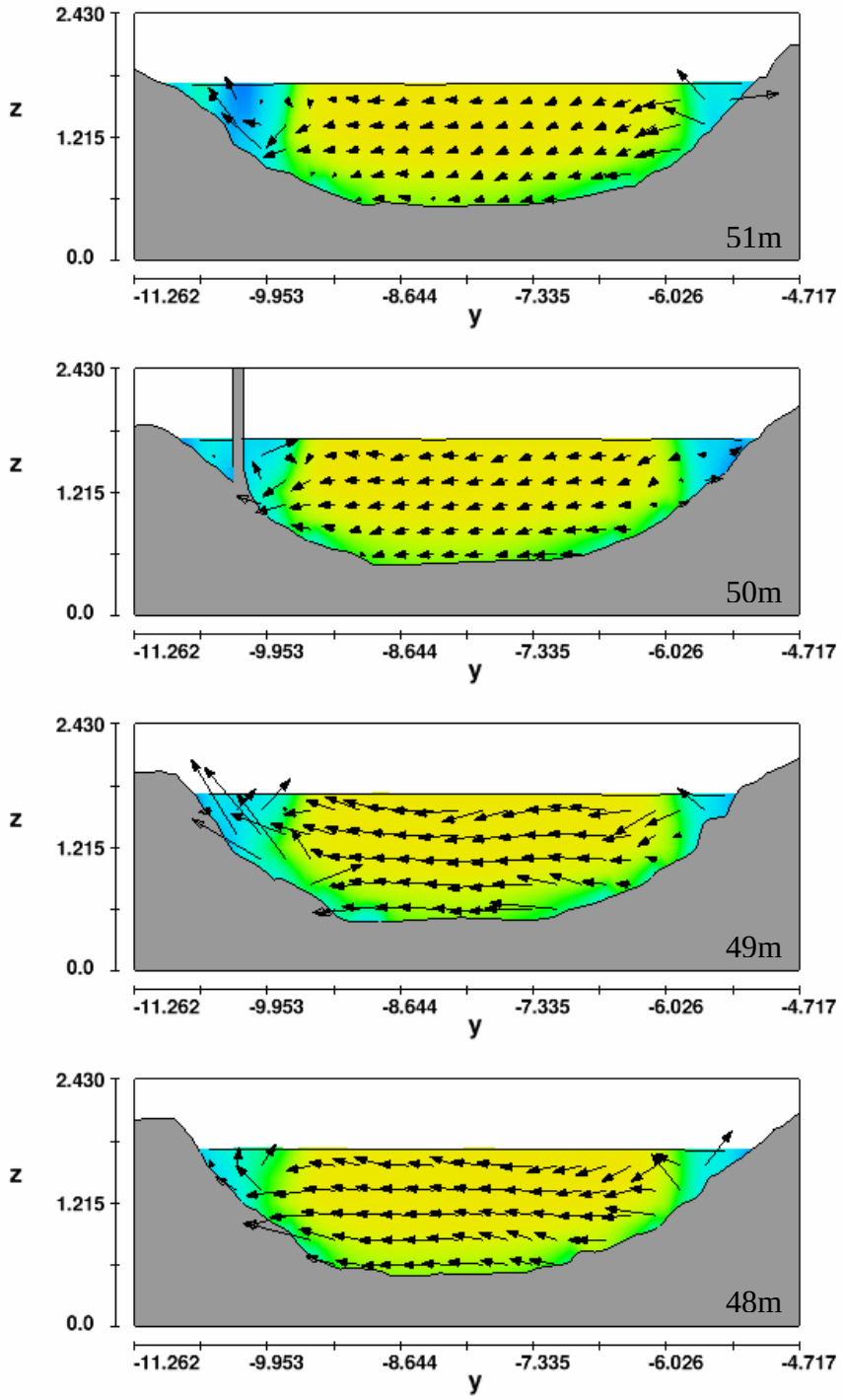
2.430
z
1.215
0.0
51m
-11.262
-9.953
-8.644
-7.335
-6.026
-4.717
y
2.430
z
1.215
0.0
50m
-11.262
-9.953
-8.644
-7.335
-6.026
-4.717
y
2.430
z
1.215
0.0
49m
-11.262
-9.953
-8.644
-7.335
-6.026
-4.717
y
2.430
z
1.215
0.0
48m
-11.262
-9.953
-8.644
-7.335
-6.026
-4.717
y

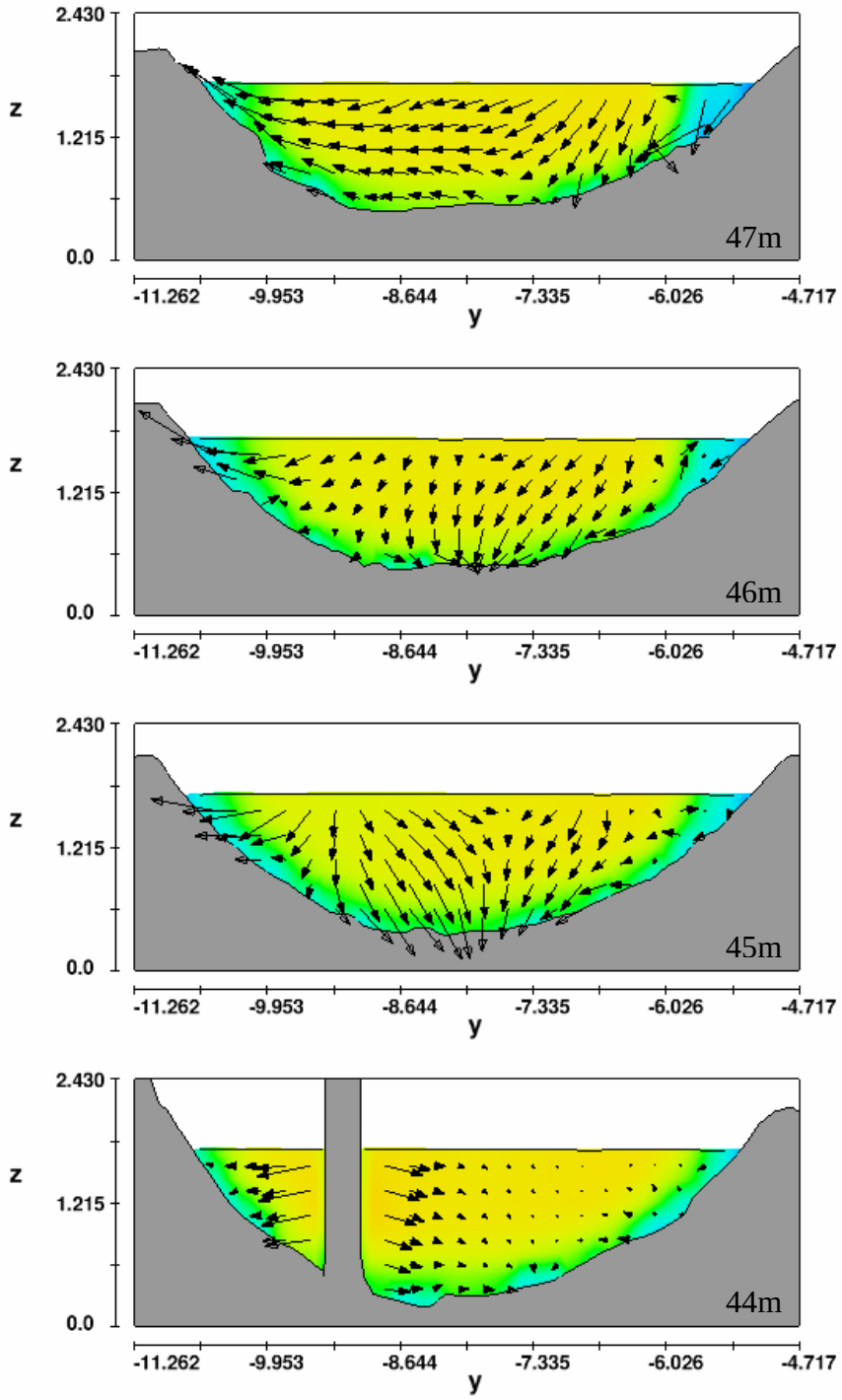
2.430
z
1.215
0.0
47m
-11.262
-9.953
-8.644
-7.335
-6.026
-4.717
y
2.430
z
1.215
0.0
46m
-11.262
-9.953
-8.644
-7.335
-6.026
-4.717
y
2.430
z
1.215
0.0
45m
-11.262
-9.953
-8.644
-7.335
-6.026
-4.717
y
2.430
z
1.215
0.0
44m
-11.262
-9.953
-8.644
-7.335
-6.026
-4.717
y

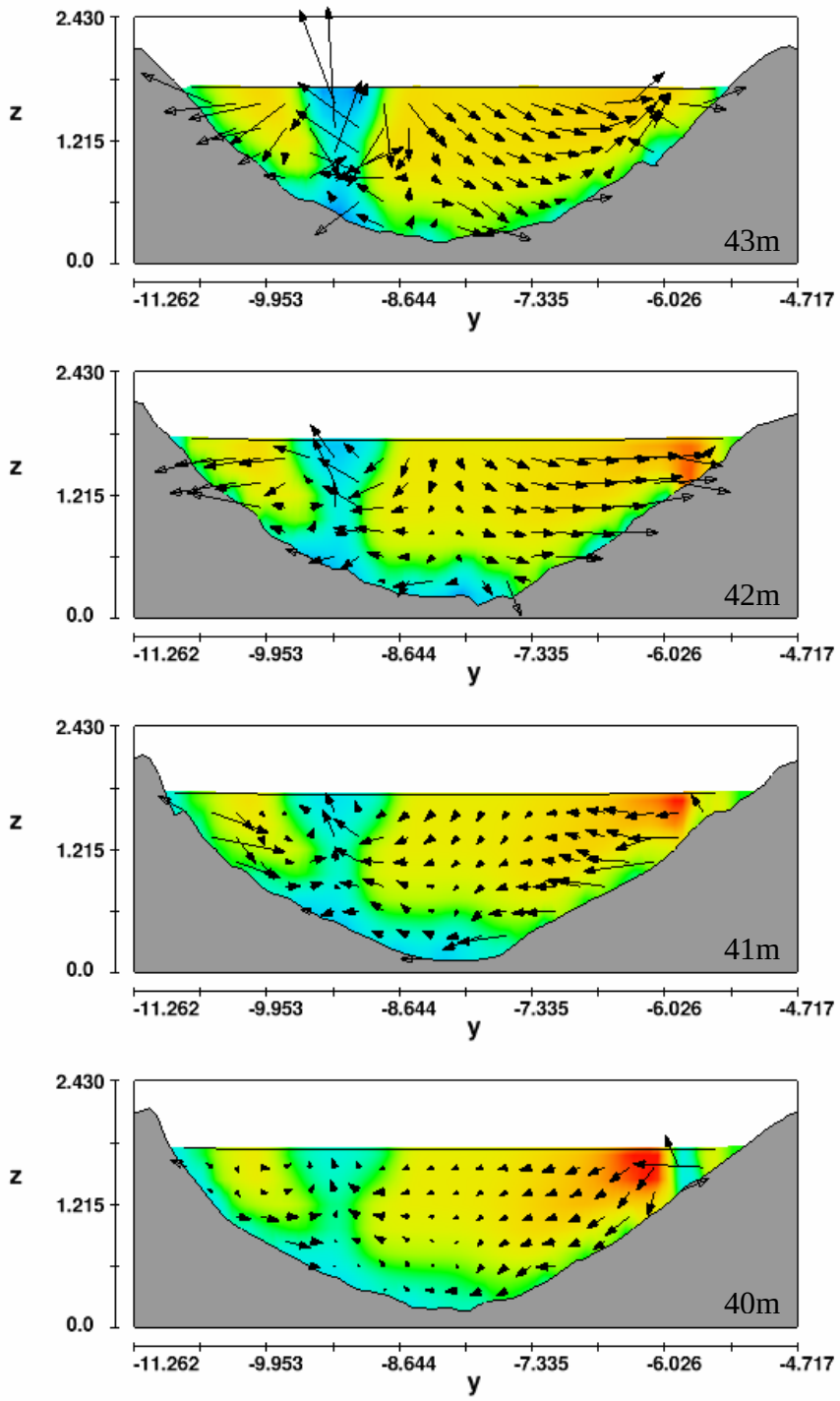
2.430
z
1.215
0.0
43m
-11.262
-9.953
-8.644
-7.335
-6.026
-4.717
y
2.430
z
1.215
0.0
42m
-11.262
-9.953
-8.644
-7.335
-6.026
-4.717
y
2.430
z
1.215
0.0
41m
-11.262
-9.953
-8.644
-7.335
-6.026
-4.717
y
2.430
z
1.215
0.0
40m
-11.262
-9.953
-8.644
-7.335
-6.026
-4.717
y

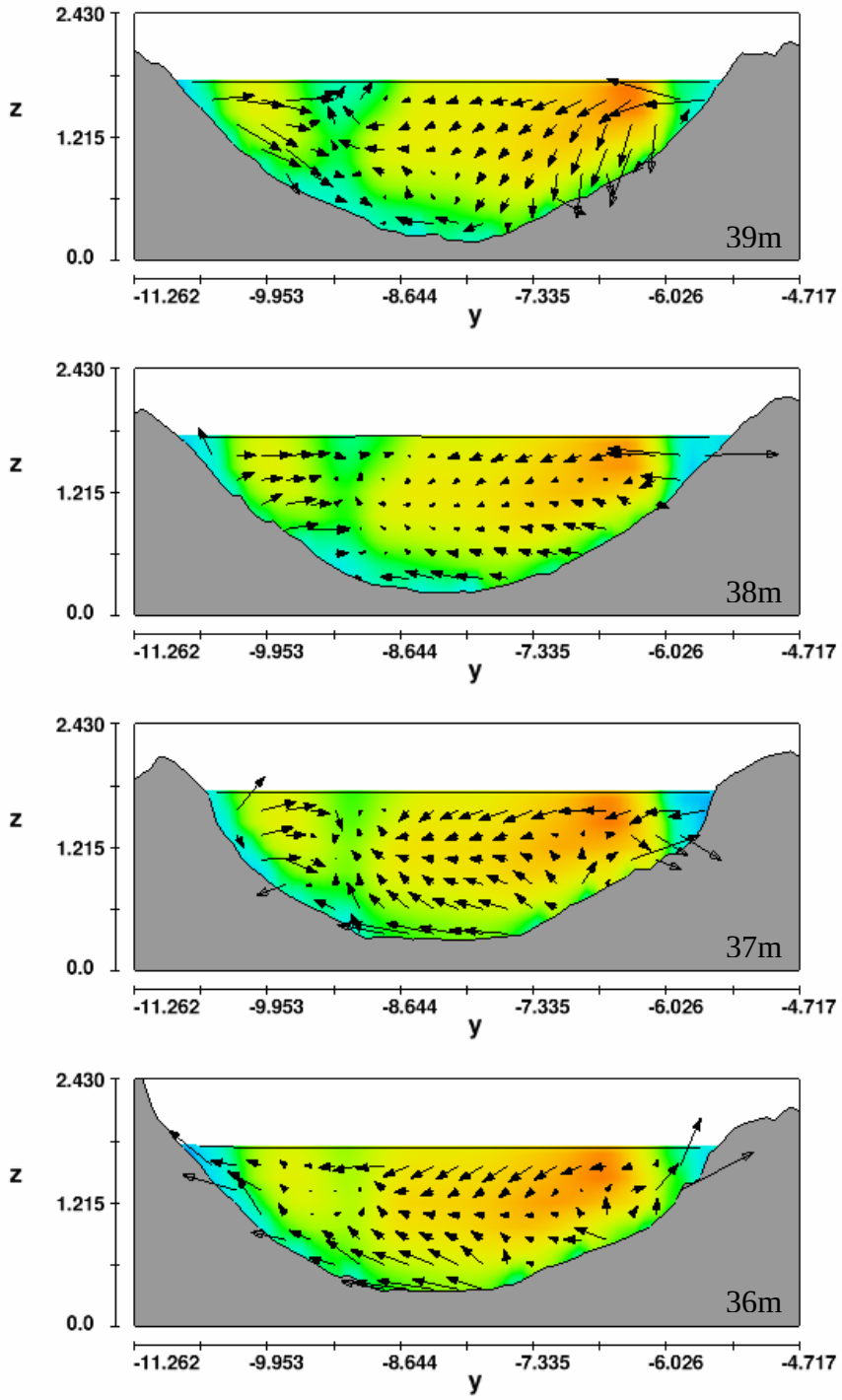
2.430
z
1.215
0.0
39m
-11.262
-9.953
-8.644
-7.335
-6.026
-4.717
y
2.430
z
1.215
0.0
38m
-11.262
-9.953
-8.644
-7.335
-6.026
-4.717
y
2.430
z
1.215
0.0
37m
-11.262
-9.953
-8.644
-7.335
-6.026
-4.717
y
2.430
z
1.215
0.0
36m
-11.262
-9.953
-8.644
-7.335
-6.026
-4.717
y

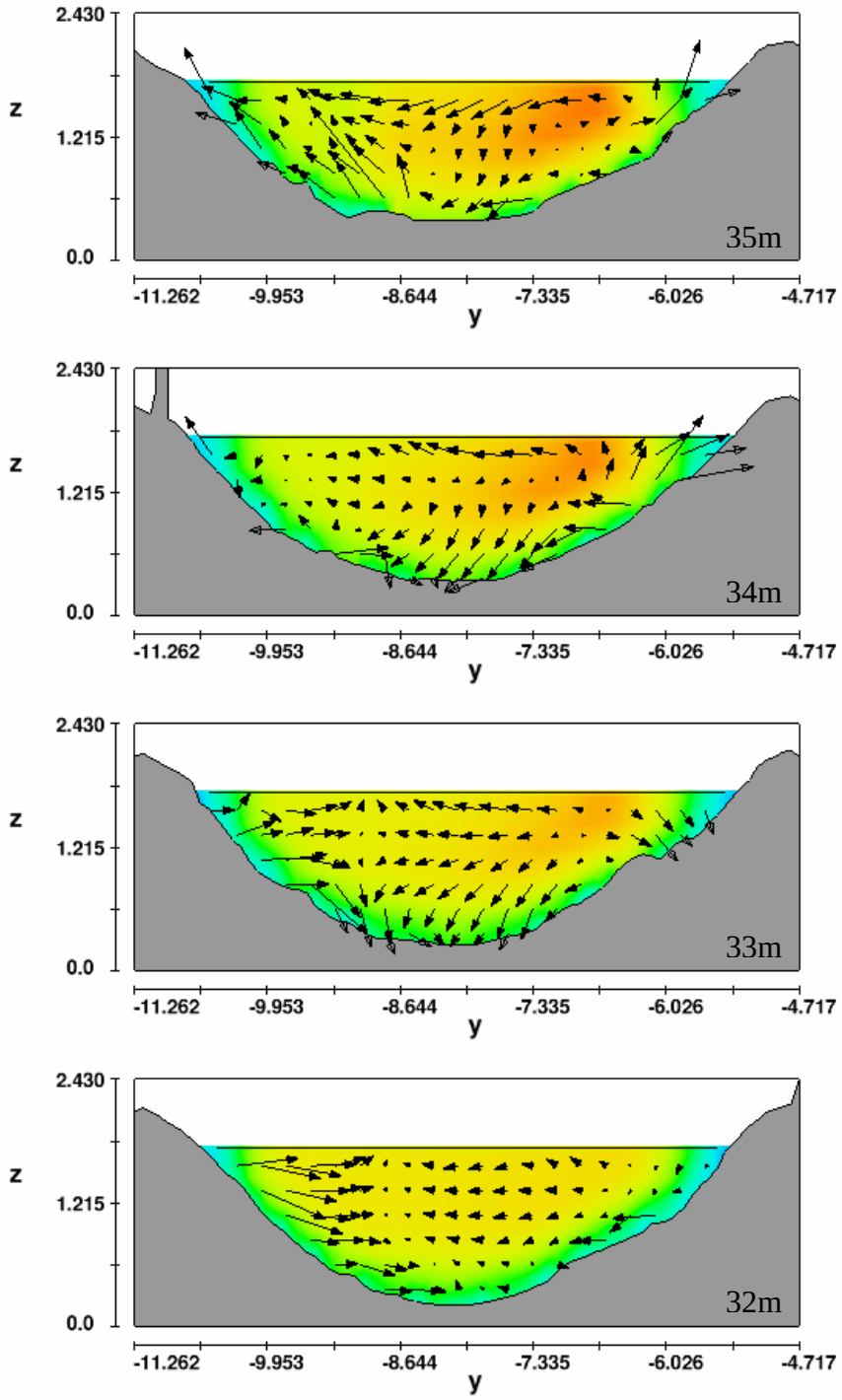
2.430
z
1.215
0.0
35m
-11.262
-9.953
-8.644
-7.335
-6.026
-4.717
y
2.430
z
1.215
0.0
34m
-11.262
-9.953
-8.644
-7.335
-6.026
-4.717
y
2.430
z
1.215
0.0
33m
-11.262
-9.953
-8.644
-7.335
-6.026
-4.717
y
2.430
z
1.215
0.0
32m
-11.262
-9.953
-8.644
-7.335
-6.026
-4.717
y

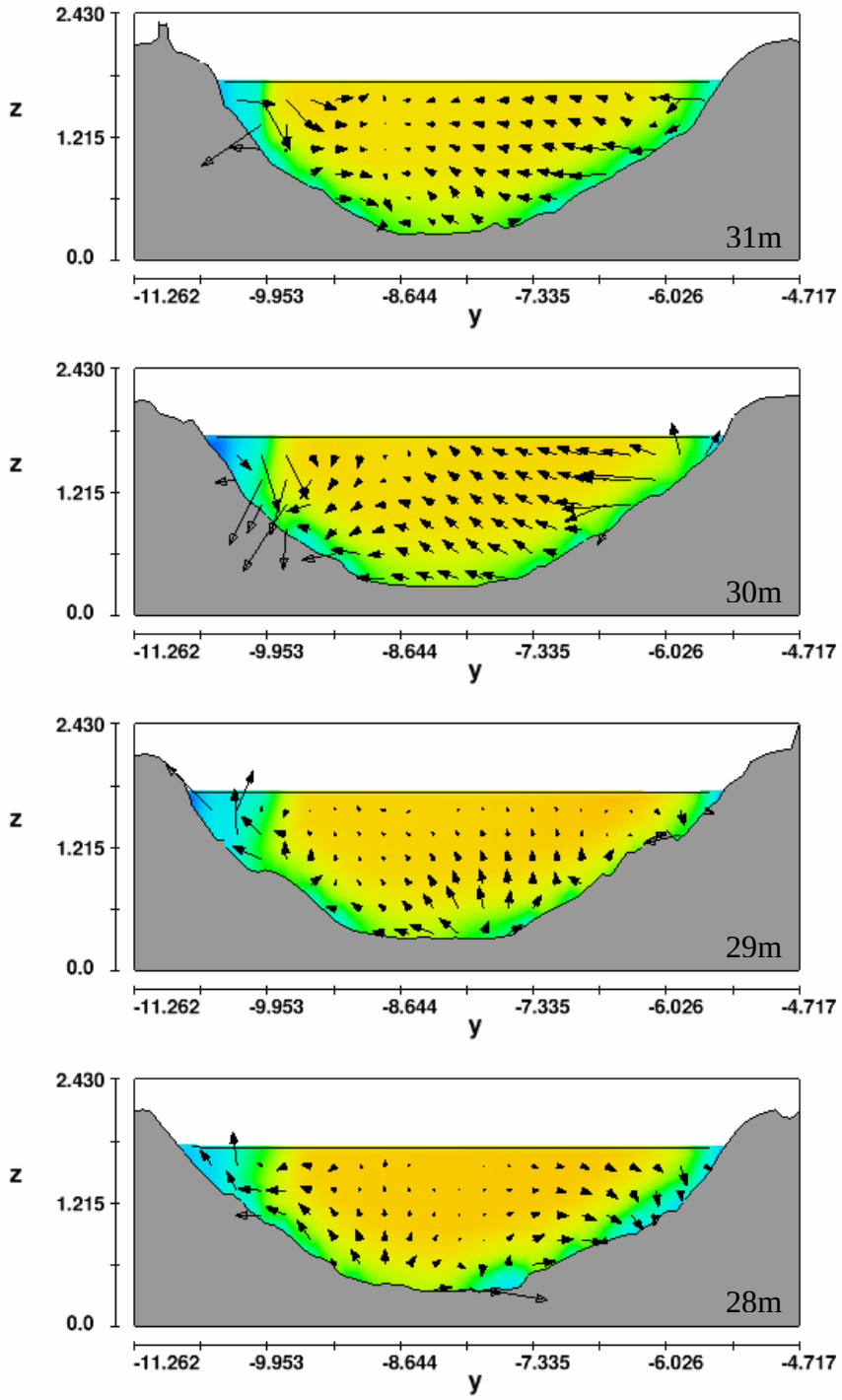
2.430
z
1.215
0.0
31m
-11.262
-9.953
-8.644
-7.335
-6.026
-4.717
y
2.430
z
1.215
0.0
30m
-11.262
-9.953
-8.644
-7.335
-6.026
-4.717
y
2.430
z
1.215
0.0
29m
-11.262
-9.953
-8.644
-7.335
-6.026
-4.717
y
2.430
z
1.215
0.0
28m
-11.262
-9.953
-8.644
-7.335
-6.026
-4.717
y

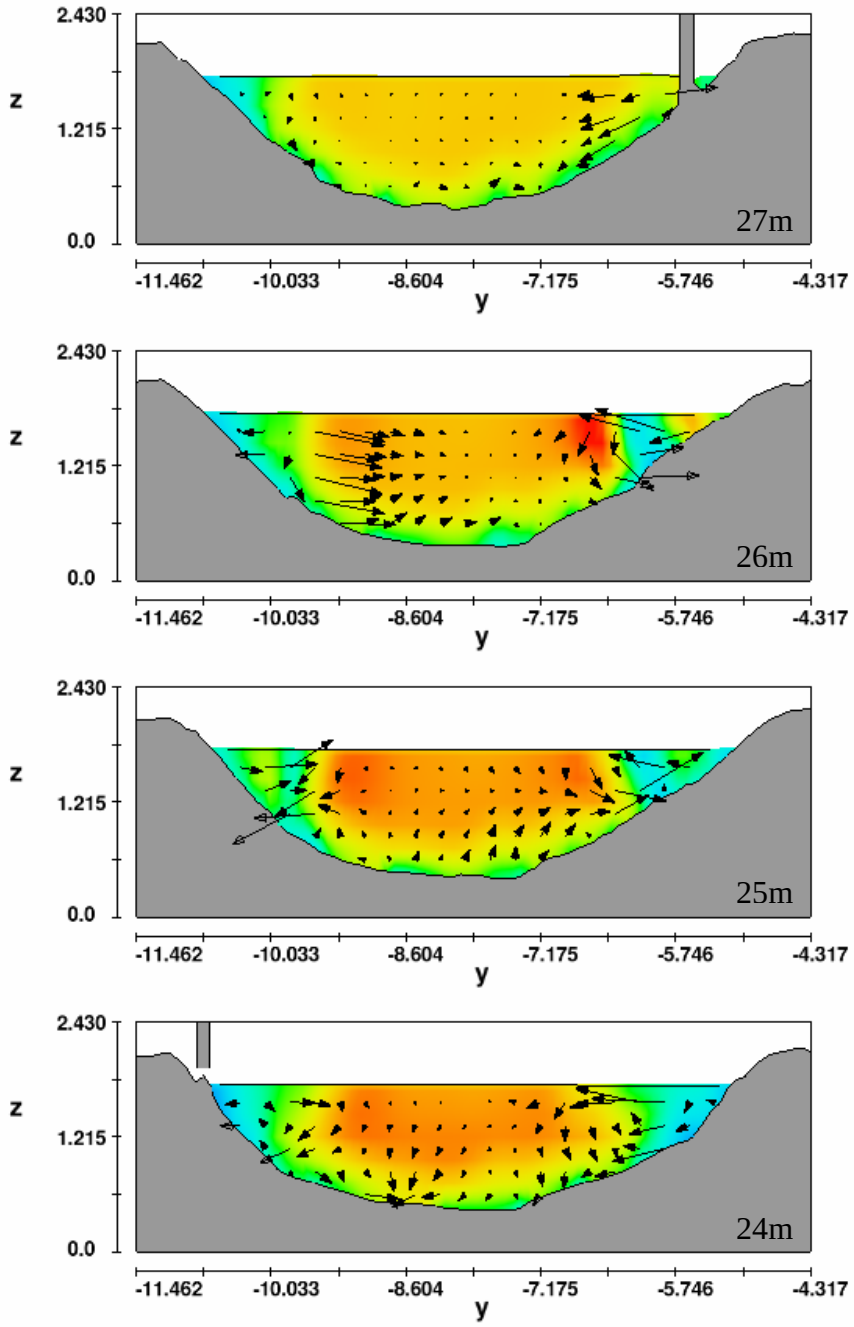
2.430
z
1.215
0.0
27m
-11.462
-10.033
-8.604
-7.175
-5.746
-4.317
y
2.430
z
1.215
0.0
26m
-11.462
-10.033
-8.604
-7.175
-5.746
-4.317
y
2.430
z
1.215
0.0
25m
-11.462
-10.033
-8.604
-7.175
-5.746
-4.317
y
2.430
z
1.215
0.0
24m
-11.462
-10.033
-8.604
-7.175
-5.746
-4.317
y

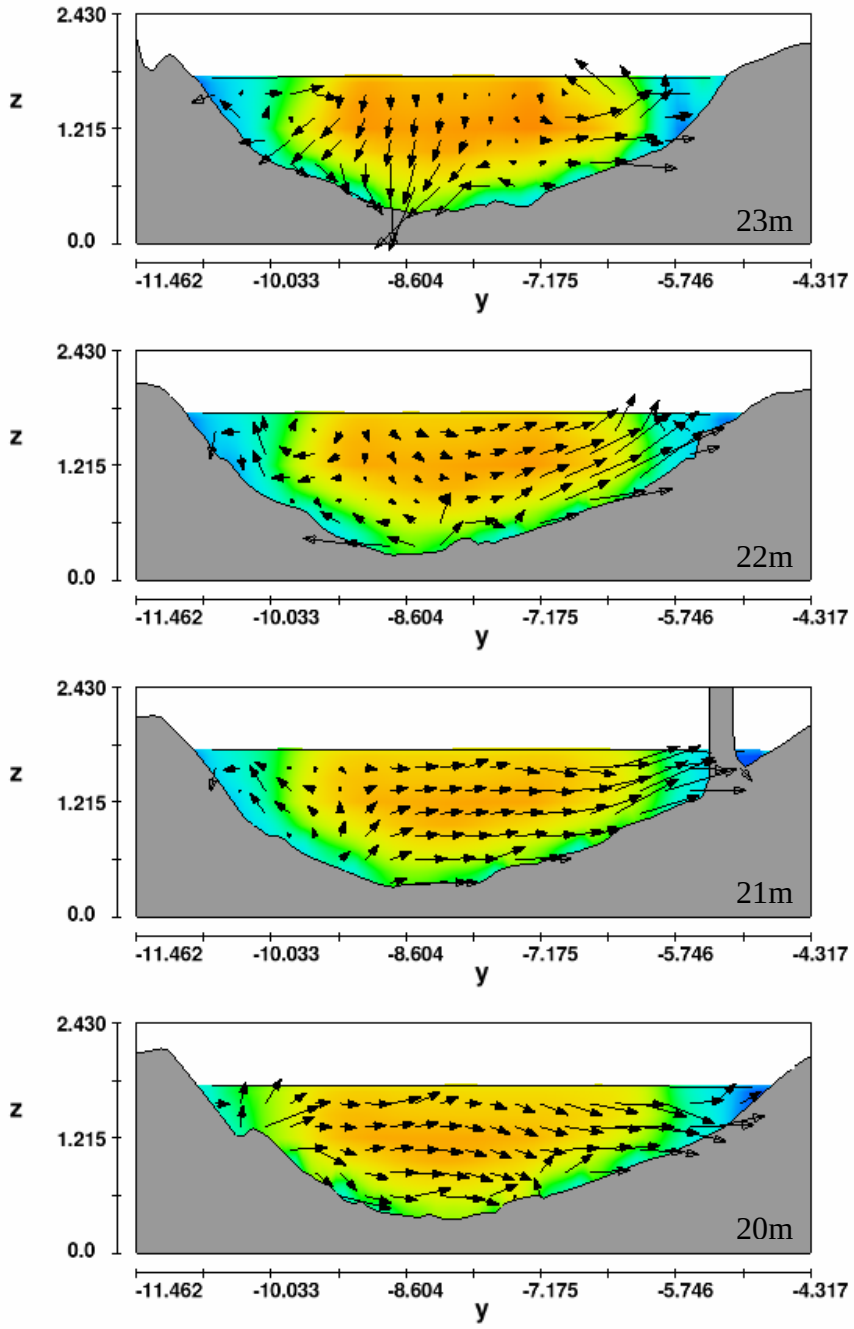
2.430
z
1.215
0.0
23m
-11.462
-10.033
-8.604
-7.175
-5.746
-4.317
y
2.430
z
1.215
0.0
22m
-11.462
-10.033
-8.604
-7.175
-5.746
-4.317
y
2.430
z
1.215
0.0
21m
-11.462
-10.033
-8.604
-7.175
-5.746
-4.317
y
2.430
z
1.215
0.0
20m
-11.462
-10.033
-8.604
-7.175
-5.746
-4.317
y

Appendix B

With No Trees

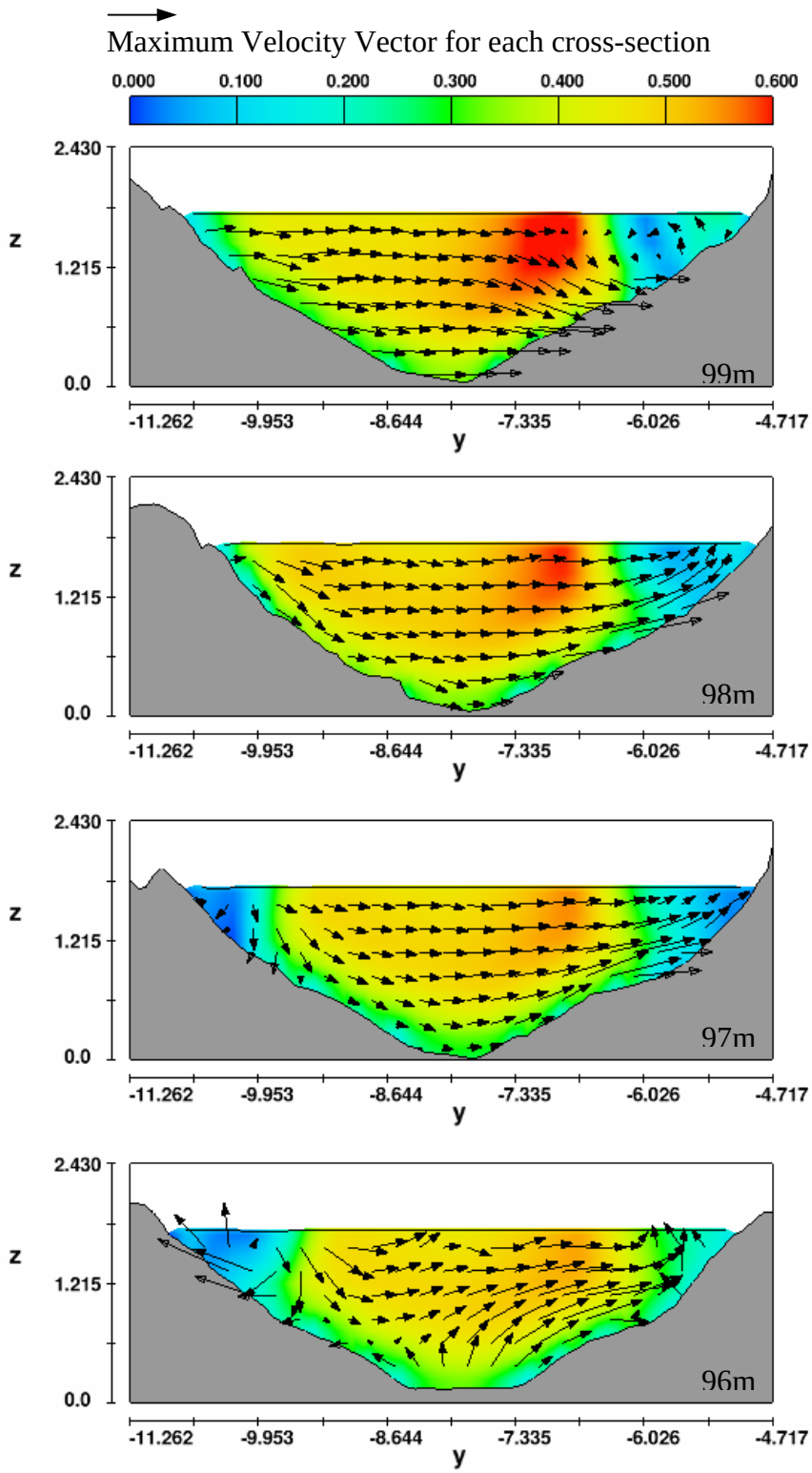

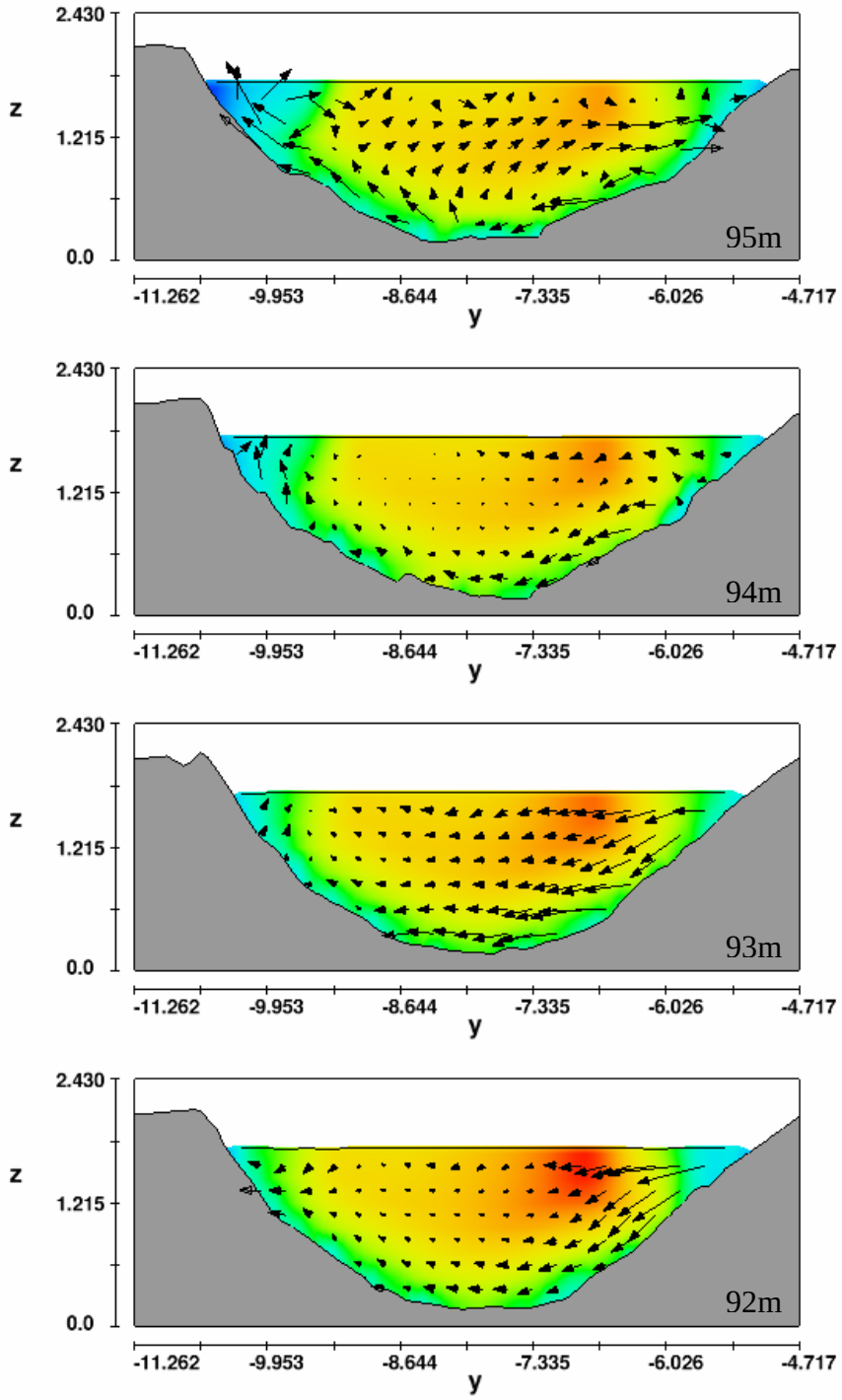
2.430
z
1.215
0.0
95m
-11.262
-9.953
-8.644
-7.335
-6.026
-4.717
y
2.430
z
1.215
0.0
94m
-11.262
-9.953
-8.644
-7.335
-6.026
-4.717
y
2.430
z
1.215
0.0
93m
-11.262
-9.953
-8.644
-7.335
-6.026
-4.717
y
2.430
z
1.215
0.0
92m
-11.262
-9.953
-8.644
-7.335
-6.026
-4.717
y

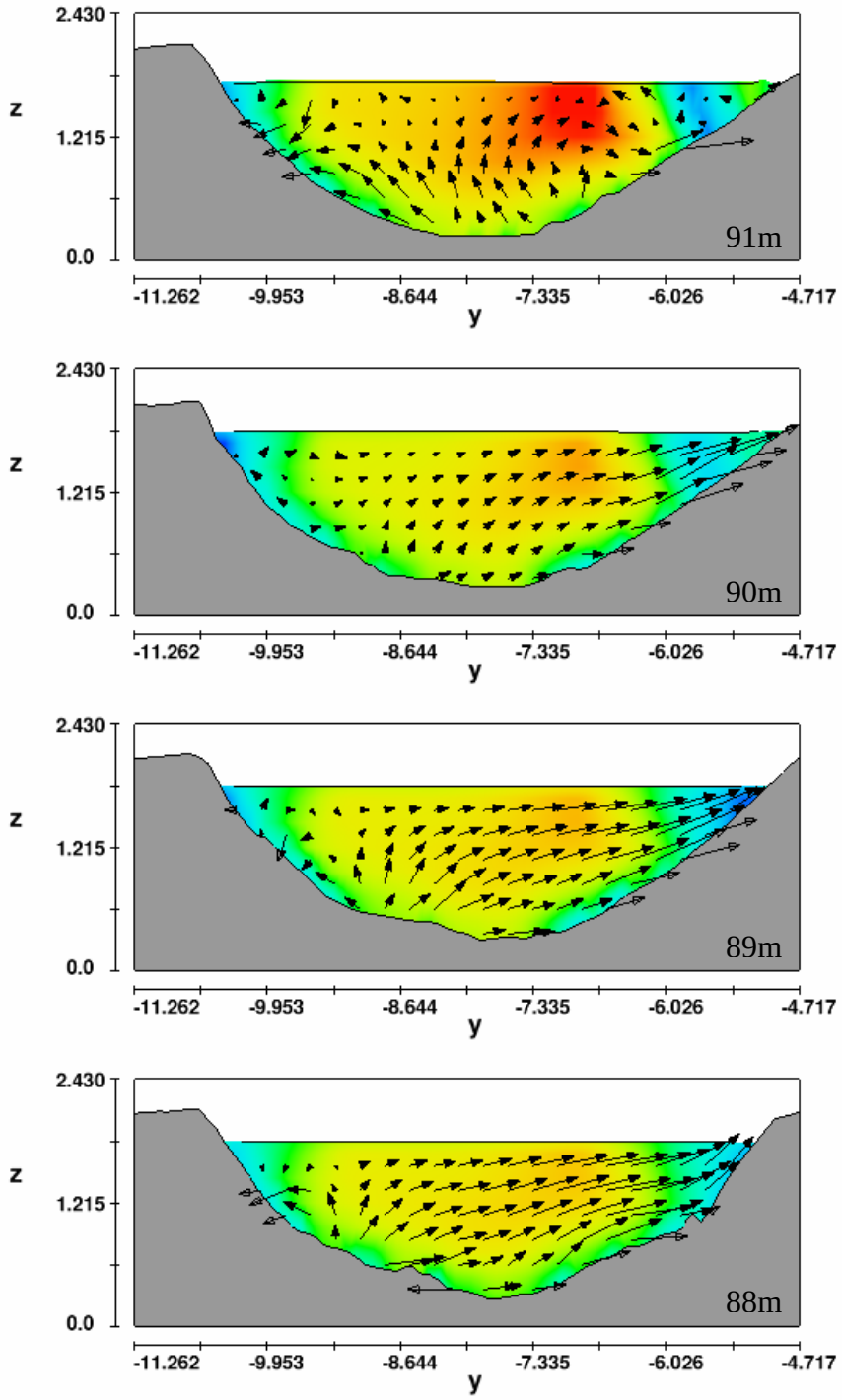
2.430
z
1.215
0.0
91m
-11.262
-9.953
-8.644
-7.335
-6.026
-4.717
y
2.430
z
1.215
0.0
90m
-11.262
-9.953
-8.644
-7.335
-6.026
-4.717
y
2.430
z
1.215
0.0
89m
-11.262
-9.953
-8.644
-7.335
-6.026
-4.717
y
2.430
z
1.215
0.0
88m
-11.262
-9.953
-8.644
-7.335
-6.026
-4.717
y

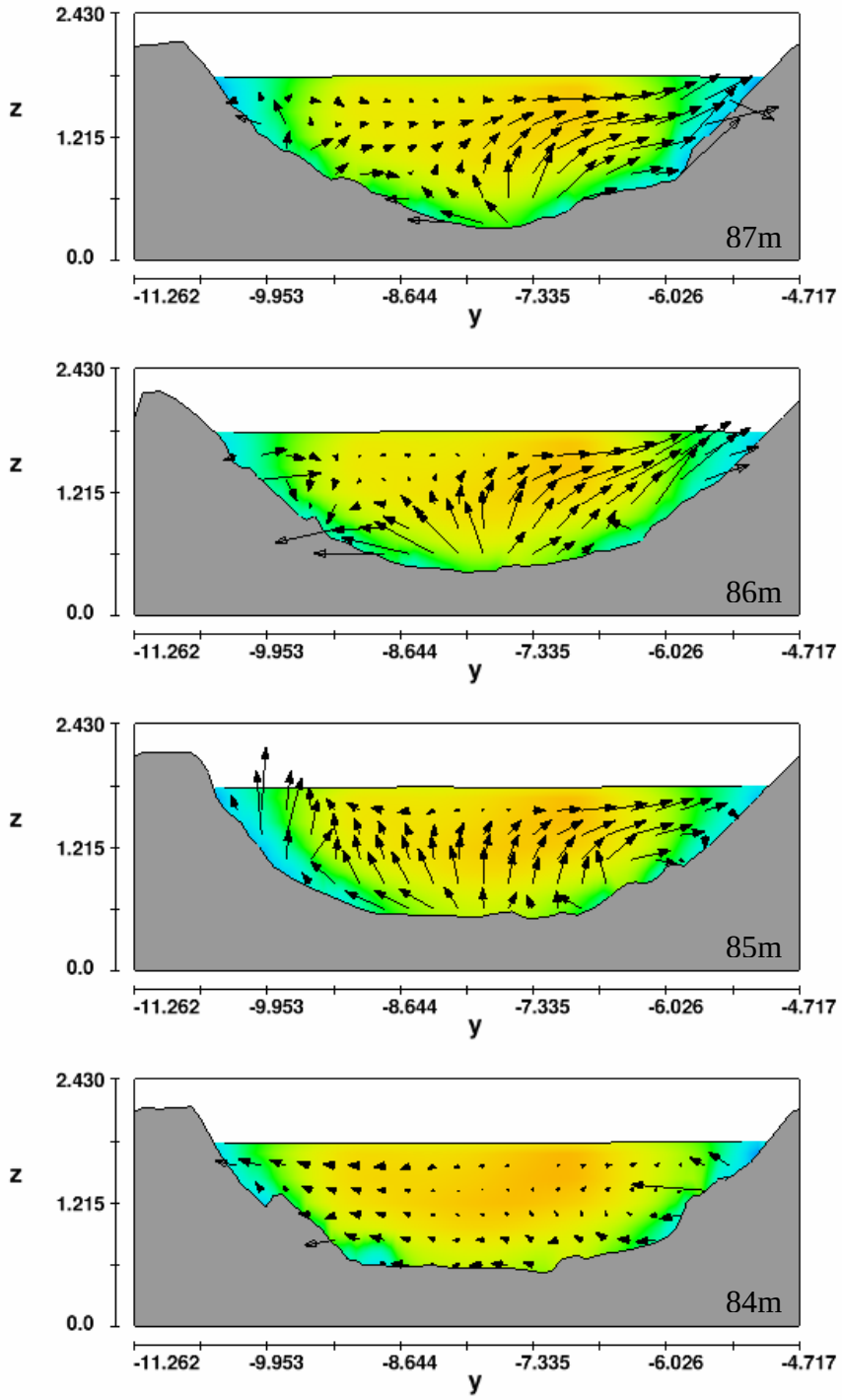
2.430
z
1.215
0.0
87m
-11.262
-9.953
-8.644
-7.335
-6.026
-4.717
y
2.430
z
1.215
0.0
86m
-11.262
-9.953
-8.644
-7.335
-6.026
-4.717
y
2.430
z
1.215
0.0
85m
-11.262
-9.953
-8.644
-7.335
-6.026
-4.717
y
2.430
z
1.215
0.0
84m
-11.262
-9.953
-8.644
-7.335
-6.026
-4.717
y

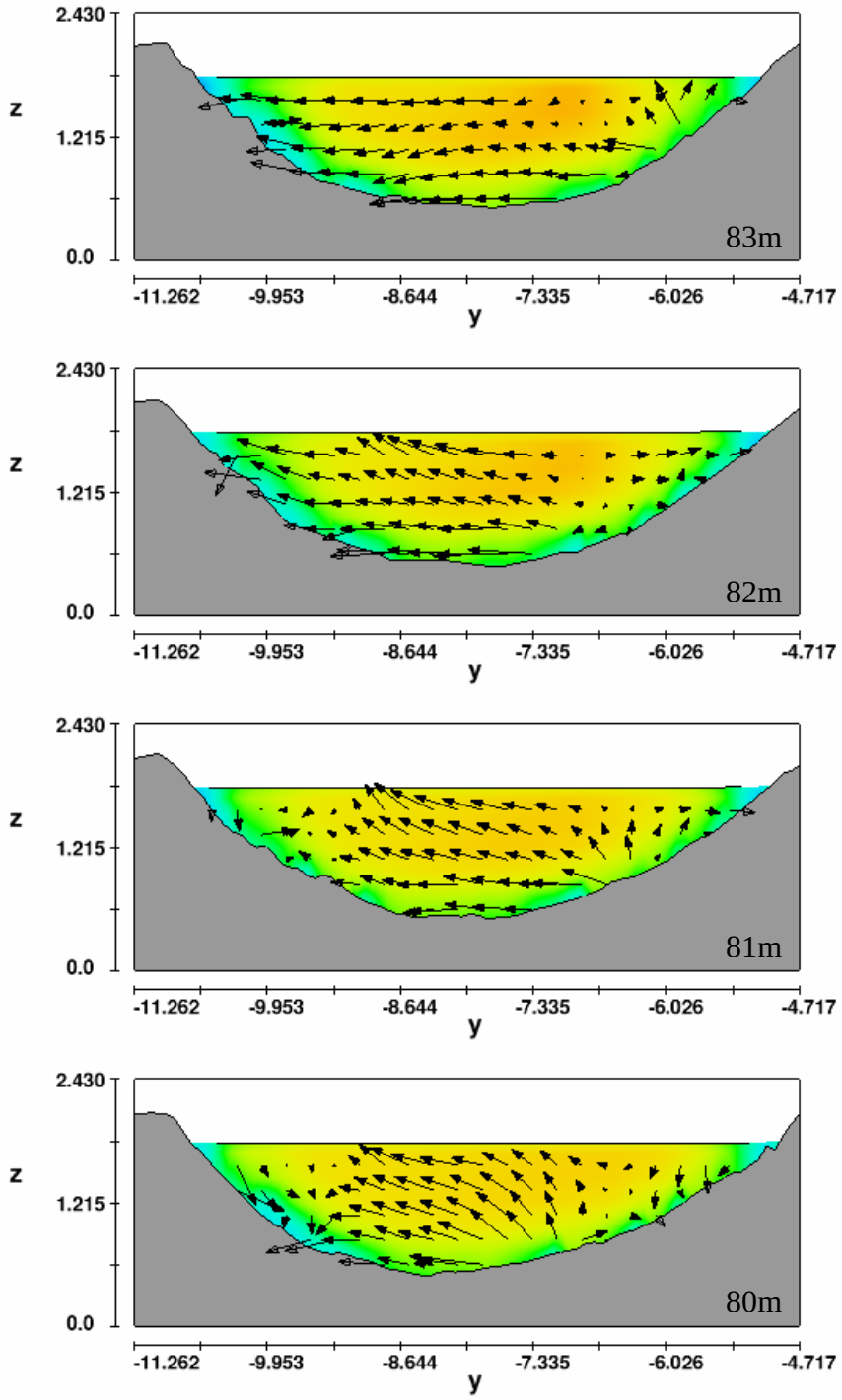
2.430
z
1.215
0.0
83m
-11.262
-9.953
-8.644
-7.335
-6.026
-4.717
y
2.430
z
1.215
0.0
82m
-11.262
-9.953
-8.644
-7.335
-6.026
-4.717
y
2.430
z
1.215
0.0
81m
-11.262
-9.953
-8.644
-7.335
-6.026
-4.717
y
2.430
z
1.215
0.0
80m
-11.262
-9.953
-8.644
-7.335
-6.026
-4.717
y

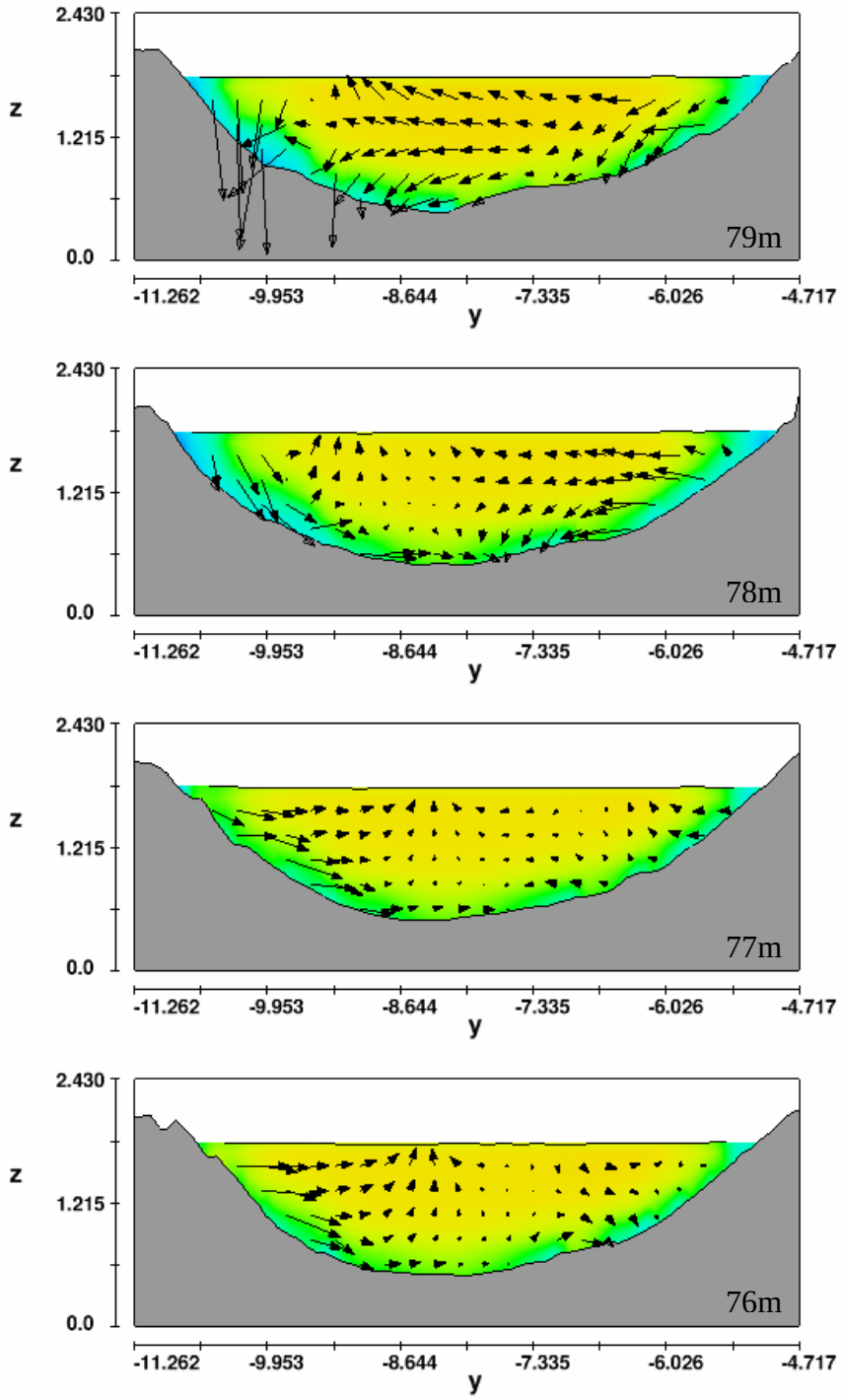
2.430
z
1.215
0.0
79m
-11.262
-9.953
-8.644
-7.335
-6.026
-4.717
y
2.430
z
1.215
0.0
78m
-11.262
-9.953
-8.644
-7.335
-6.026
-4.717
y
2.430
z
1.215
0.0
77m
-11.262
-9.953
-8.644
-7.335
-6.026
-4.717
y
2.430
z
1.215
0.0
76m
-11.262
-9.953
-8.644
-7.335
-6.026
-4.717
y

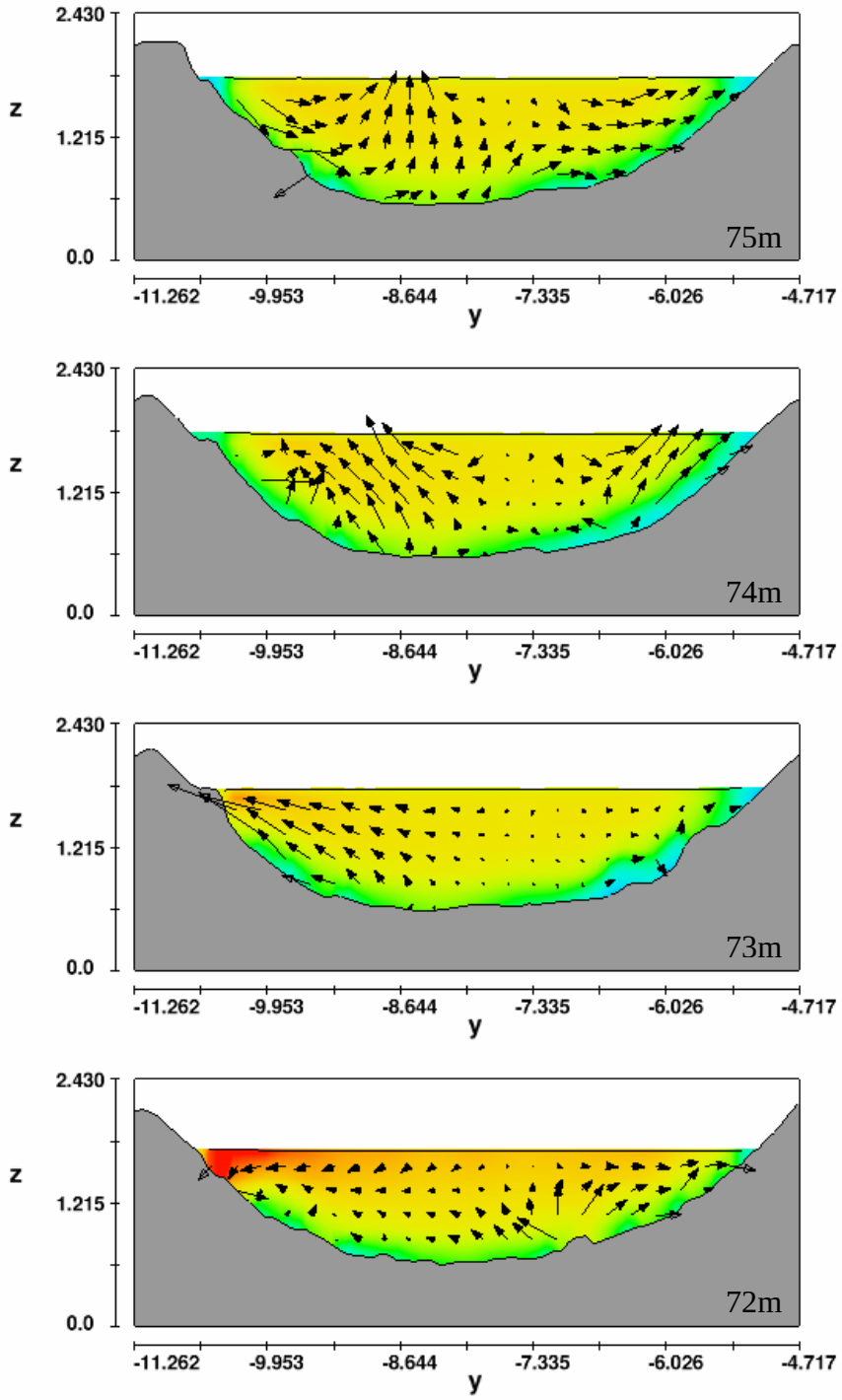
2.430
z
1.215
0.0
75m
-11.262
-9.953
-8.644
-7.335
-6.026
-4.717
y
2.430
z
1.215
0.0
74m
-11.262
-9.953
-8.644
-7.335
-6.026
-4.717
y
2.430
z
1.215
0.0
73m
-11.262
-9.953
-8.644
-7.335
-6.026
-4.717
y
2.430
z
1.215
0.0
72m
-11.262
-9.953
-8.644
-7.335
-6.026
-4.717
y

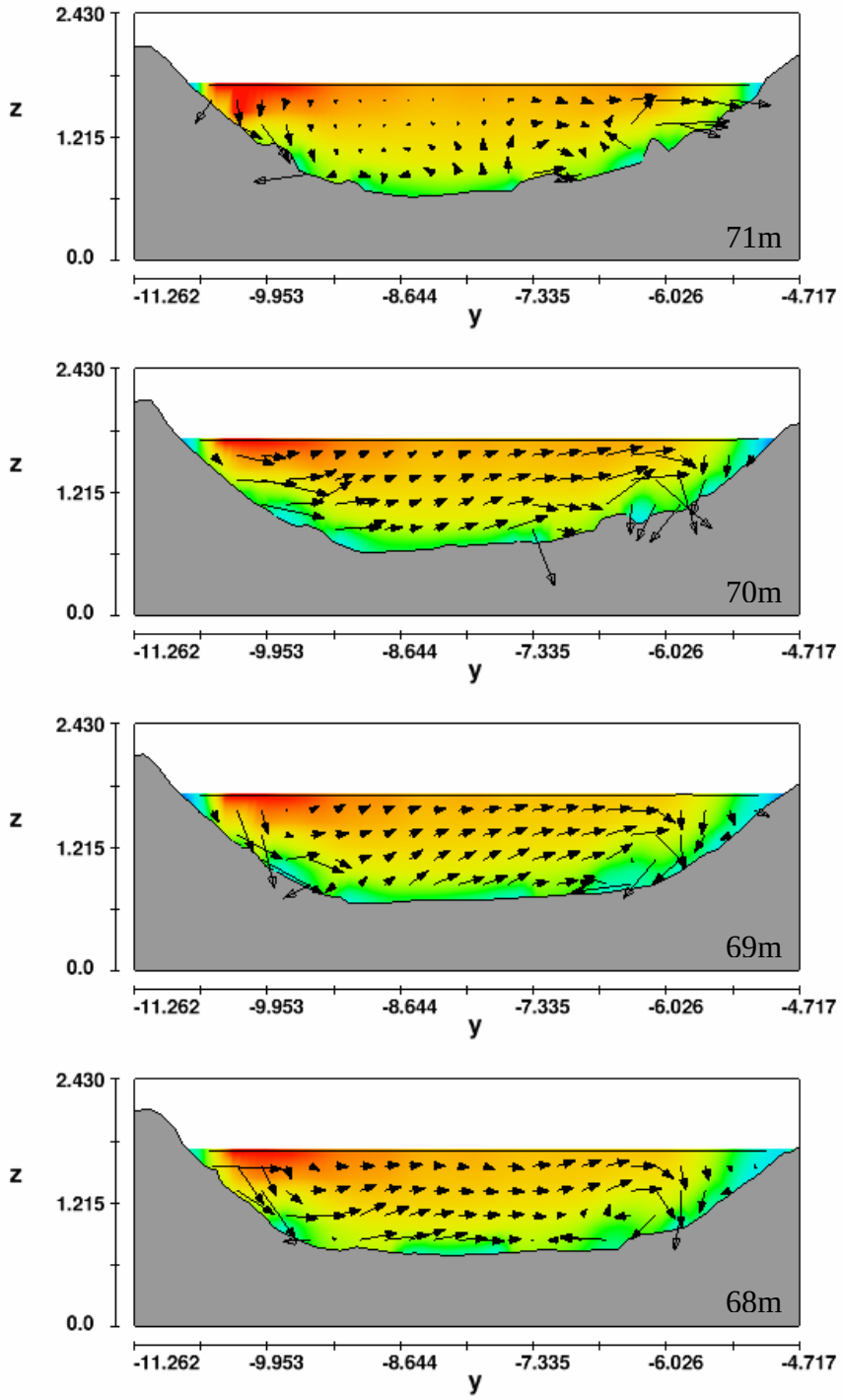
2.430
z
1.215
0.0
71m
-11.262
-9.953
-8.644
-7.335
-6.026
-4.717
y
2.430
z
1.215
0.0
70m
-11.262
-9.953
-8.644
-7.335
-6.026
-4.717
y
2.430
z
1.215
0.0
69m
-11.262
-9.953
-8.644
-7.335
-6.026
-4.717
y
2.430
z
1.215
0.0
68m
-11.262
-9.953
-8.644
-7.335
-6.026
-4.717
y

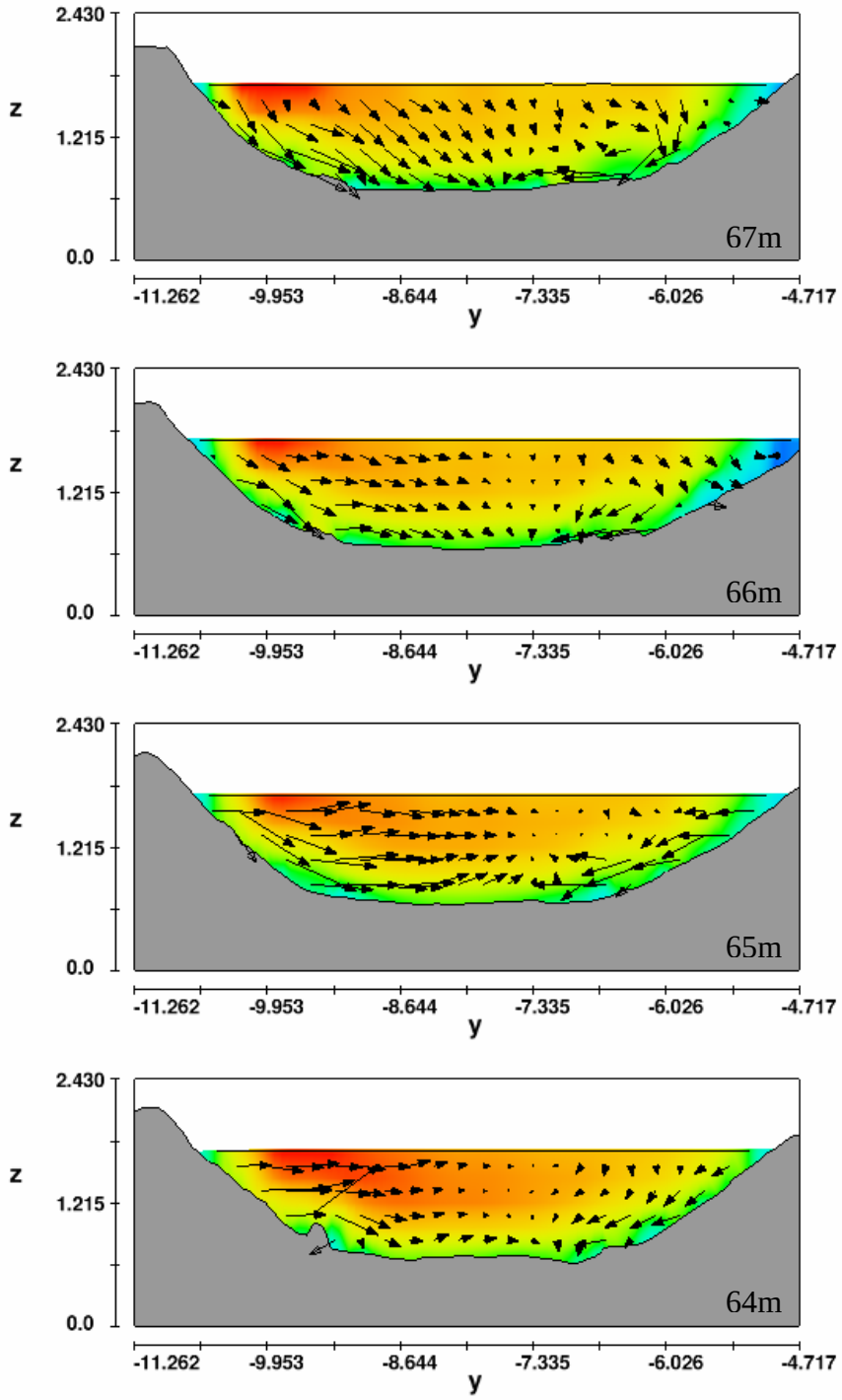
2.430
z
1.215
0.0
67m
-11.262
-9.953
-8.644
-7.335
-6.026
-4.717
y
2.430
z
1.215
0.0
66m
-11.262
-9.953
-8.644
-7.335
-6.026
-4.717
y
2.430
z
1.215
0.0
65m
-11.262
-9.953
-8.644
-7.335
-6.026
-4.717
y
2.430
z
1.215
0.0
64m
-11.262
-9.953
-8.644
-7.335
-6.026
-4.717
y

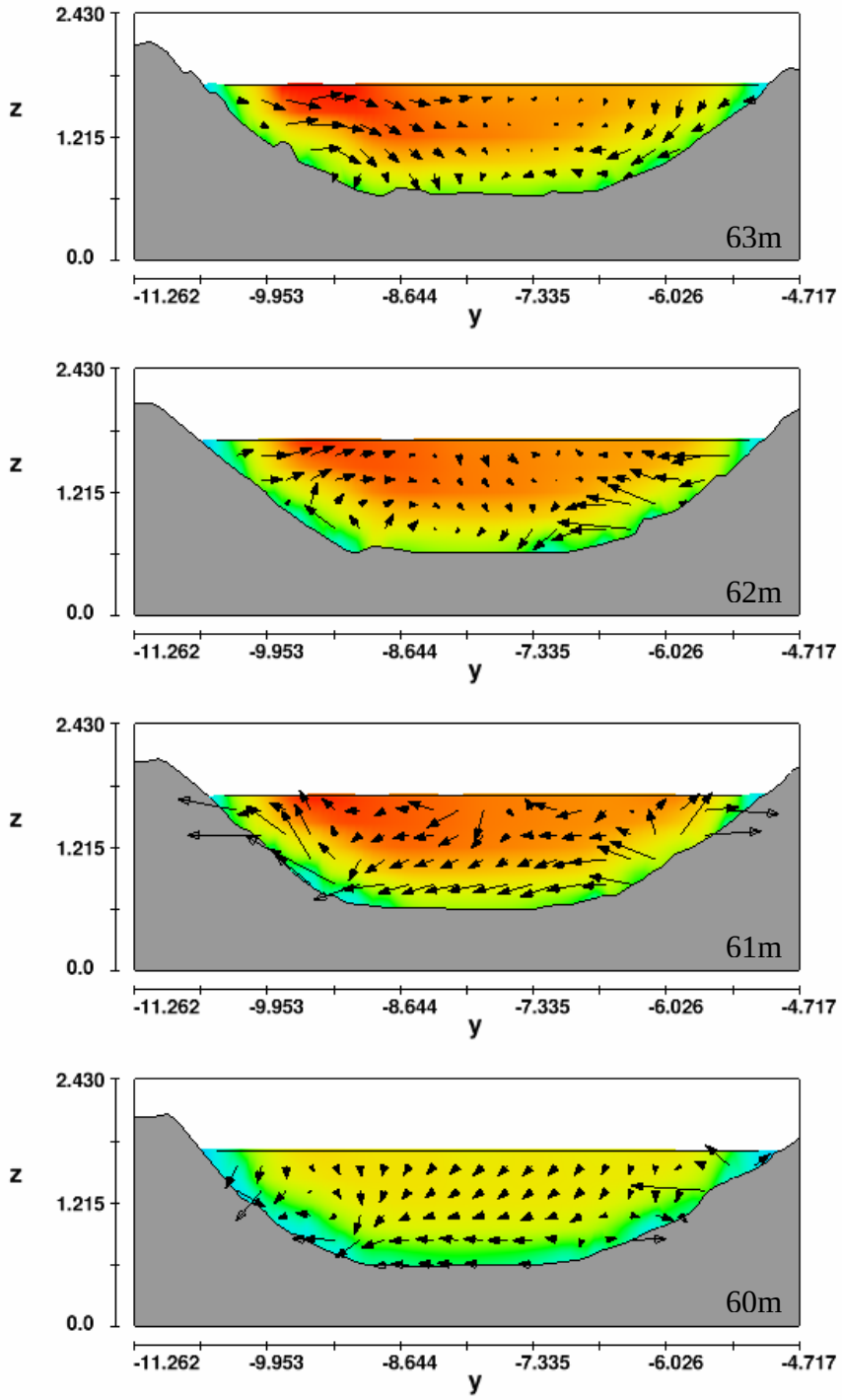
2.430
z
1.215
0.0
63m
-11.262
-9.953
-8.644
-7.335
-6.026
-4.717
y
2.430
z
1.215
0.0
62m
-11.262
-9.953
-8.644
-7.335
-6.026
-4.717
y
2.430
z
1.215
0.0
61m
-11.262
-9.953
-8.644
-7.335
-6.026
-4.717
y
2.430
z
1.215
0.0
60m
-11.262
-9.953
-8.644
-7.335
-6.026
-4.717
y

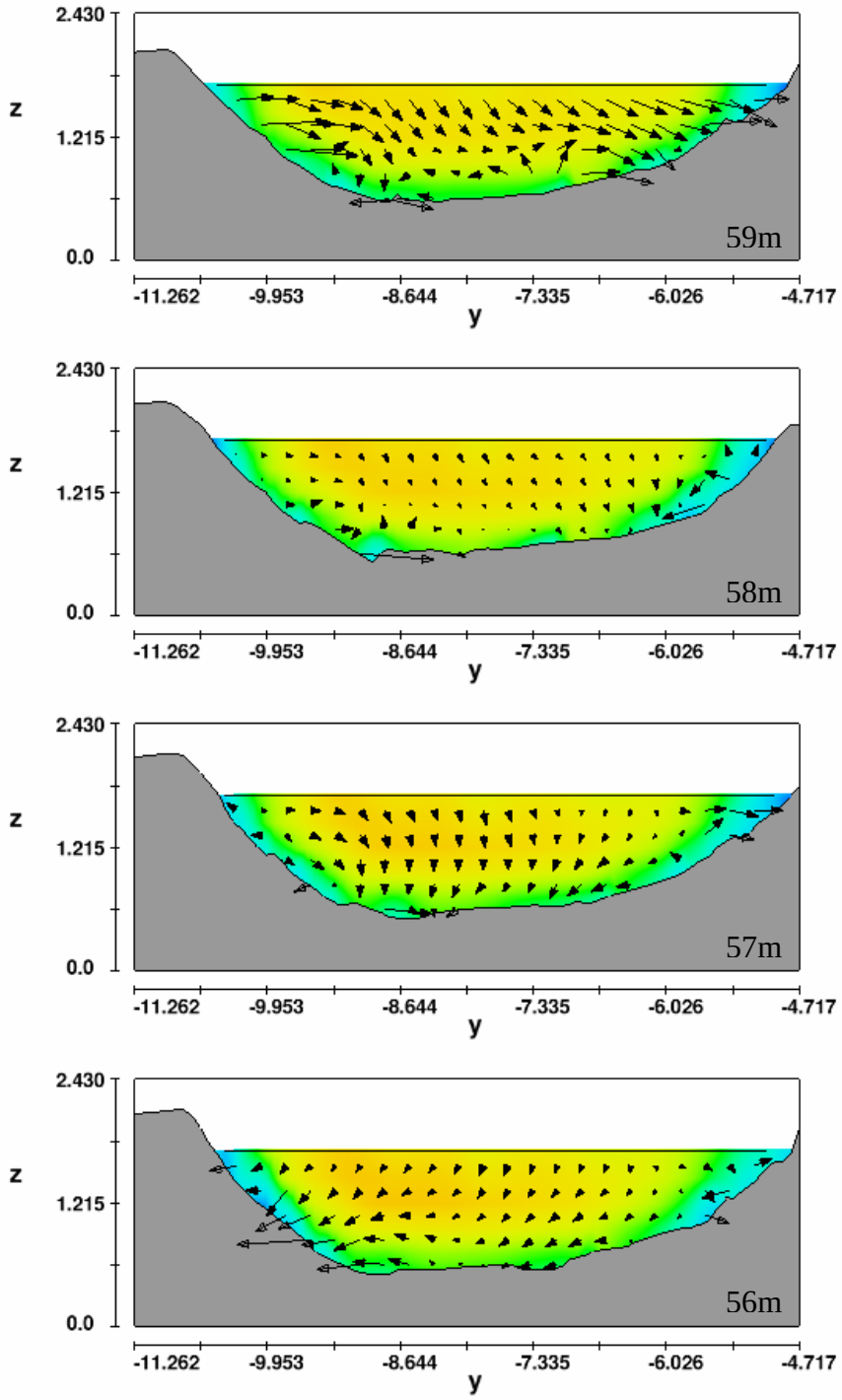
2.430
z
1.215
0.0
59m
-11.262
-9.953
-8.644
-7.335
-6.026
-4.717
y
2.430
z
1.215
0.0
58m
-11.262
-9.953
-8.644
-7.335
-6.026
-4.717
y
2.430
z
1.215
0.0
57m
-11.262
-9.953
-8.644
-7.335
-6.026
-4.717
y
2.430
z
1.215
0.0
56m
-11.262
-9.953
-8.644
-7.335
-6.026
-4.717
y

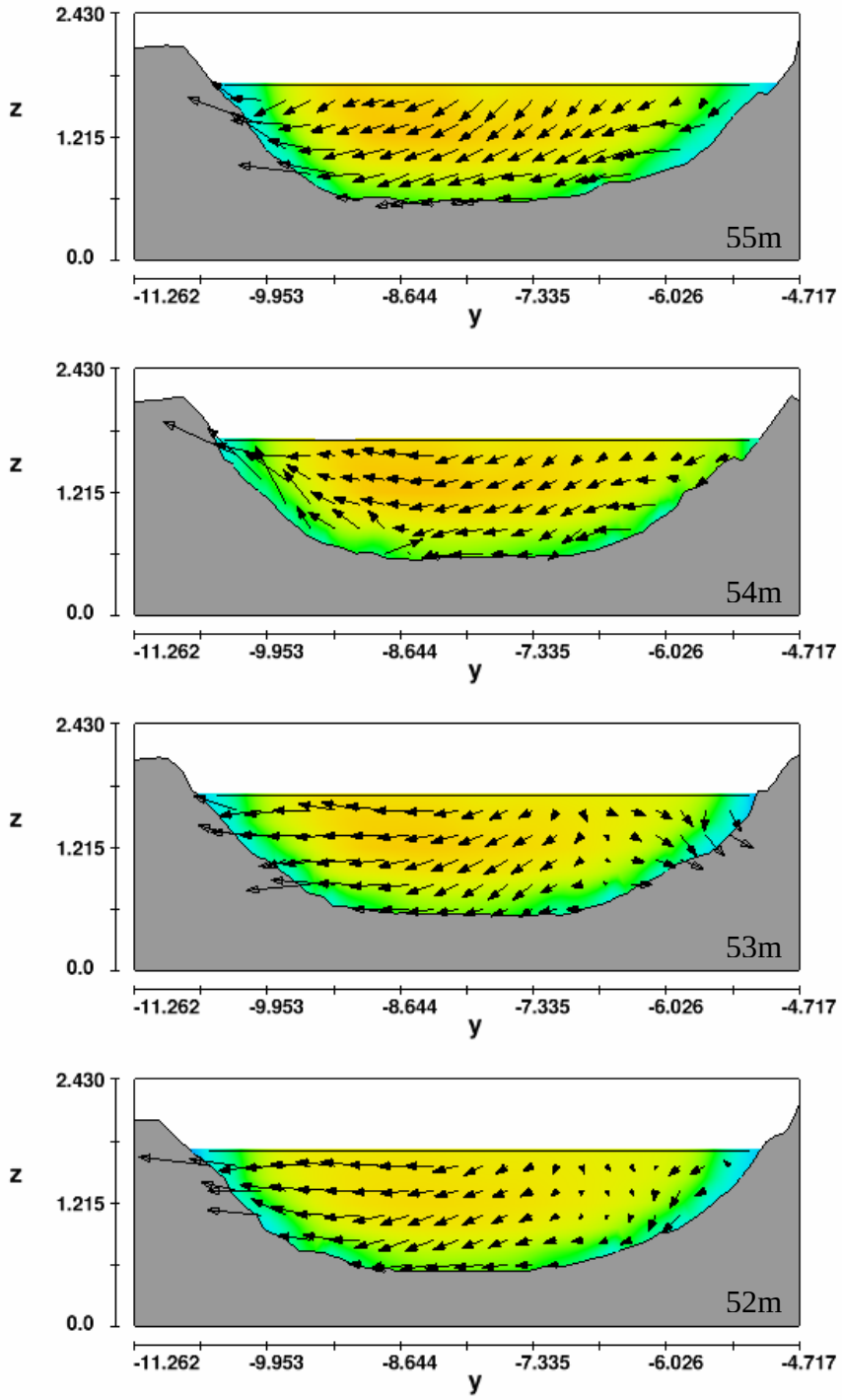
2.430
z
1.215
0.0
55m
-11.262
-9.953
-8.644
-7.335
-6.026
-4.717
y
2.430
z
1.215
0.0
54m
-11.262
-9.953
-8.644
-7.335
-6.026
-4.717
y
2.430
z
1.215
0.0
53m
-11.262
-9.953
-8.644
-7.335
-6.026
-4.717
y
2.430
z
1.215
0.0
52m
-11.262
-9.953
-8.644
-7.335
-6.026
-4.717
y

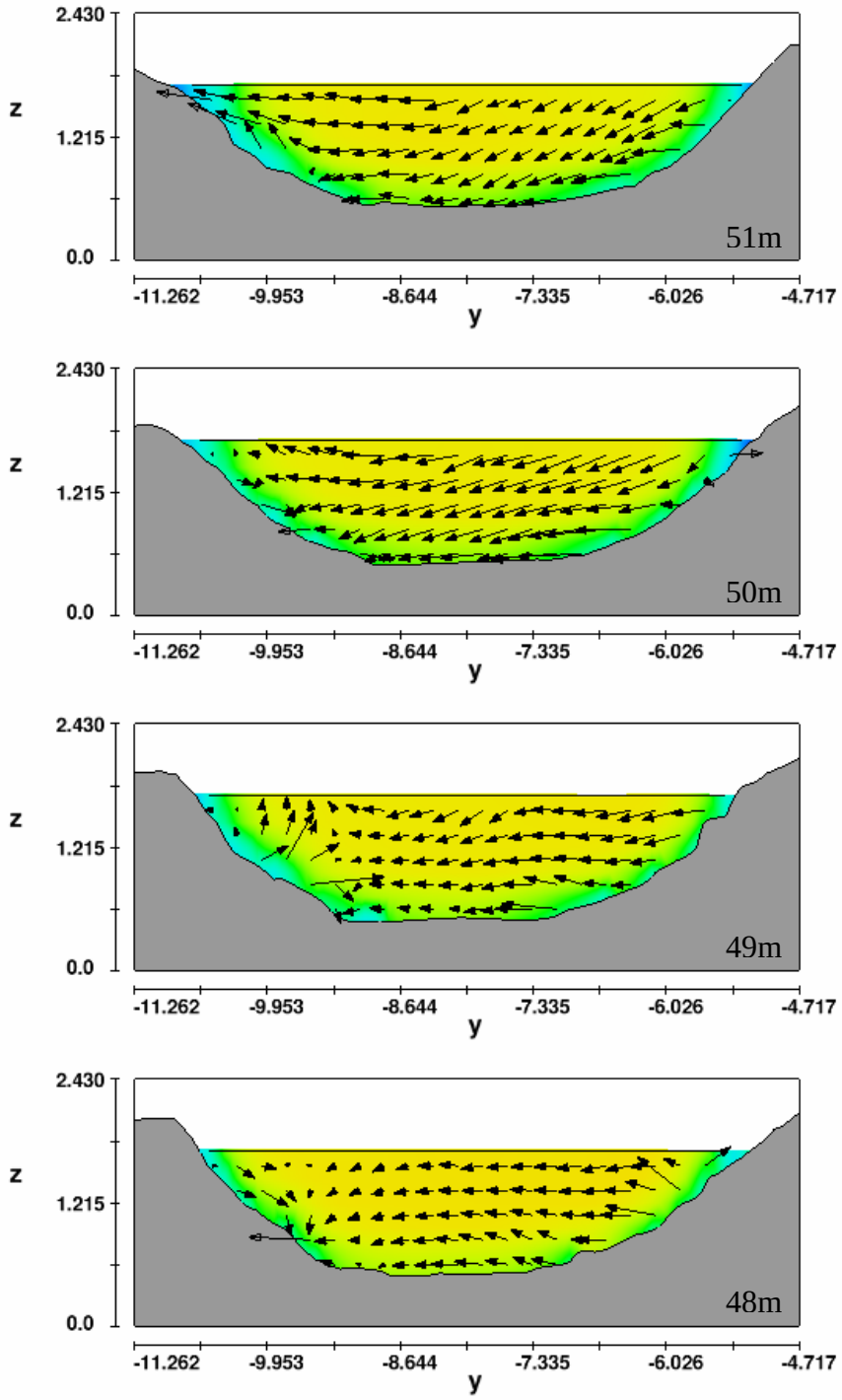
2.430
z
1.215
0.0
51m
-11.262
-9.953
-8.644
-7.335
-6.026
-4.717
y
2.430
z
1.215
0.0
50m
-11.262
-9.953
-8.644
-7.335
-6.026
-4.717
y
2.430
z
1.215
0.0
49m
-11.262
-9.953
-8.644
-7.335
-6.026
-4.717
y
2.430
z
1.215
0.0
48m
-11.262
-9.953
-8.644
-7.335
-6.026
-4.717
y

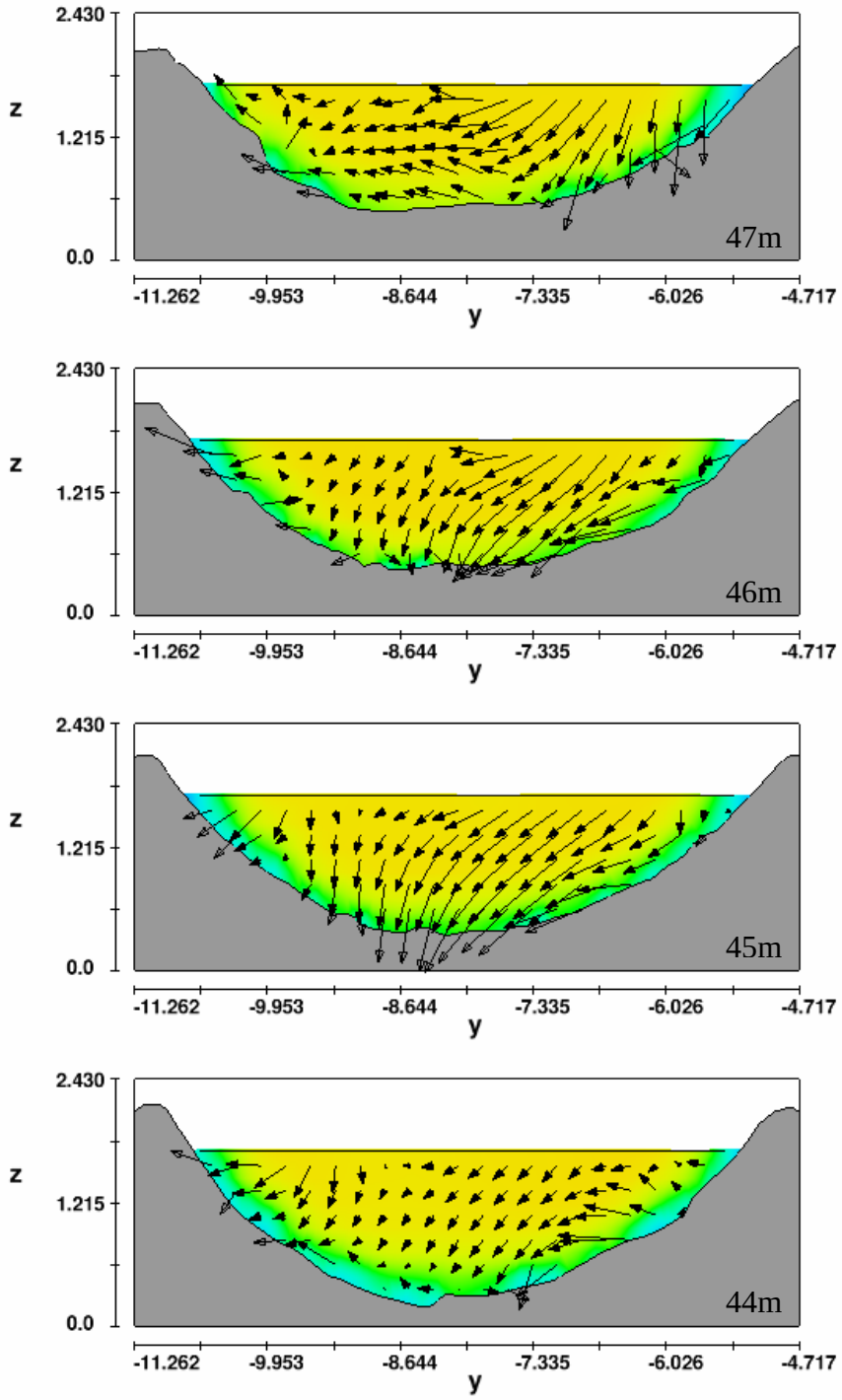
2.430
z
1.215
0.0
47m
-11.262
-9.953
-8.644
-7.335
-6.026
-4.717
y
2.430
z
1.215
0.0
46m
-11.262
-9.953
-8.644
-7.335
-6.026
-4.717
y
2.430
z
1.215
0.0
45m
-11.262
-9.953
-8.644
-7.335
-6.026
-4.717
y
2.430
z
1.215
0.0
44m
-11.262
-9.953
-8.644
-7.335
-6.026
-4.717
y

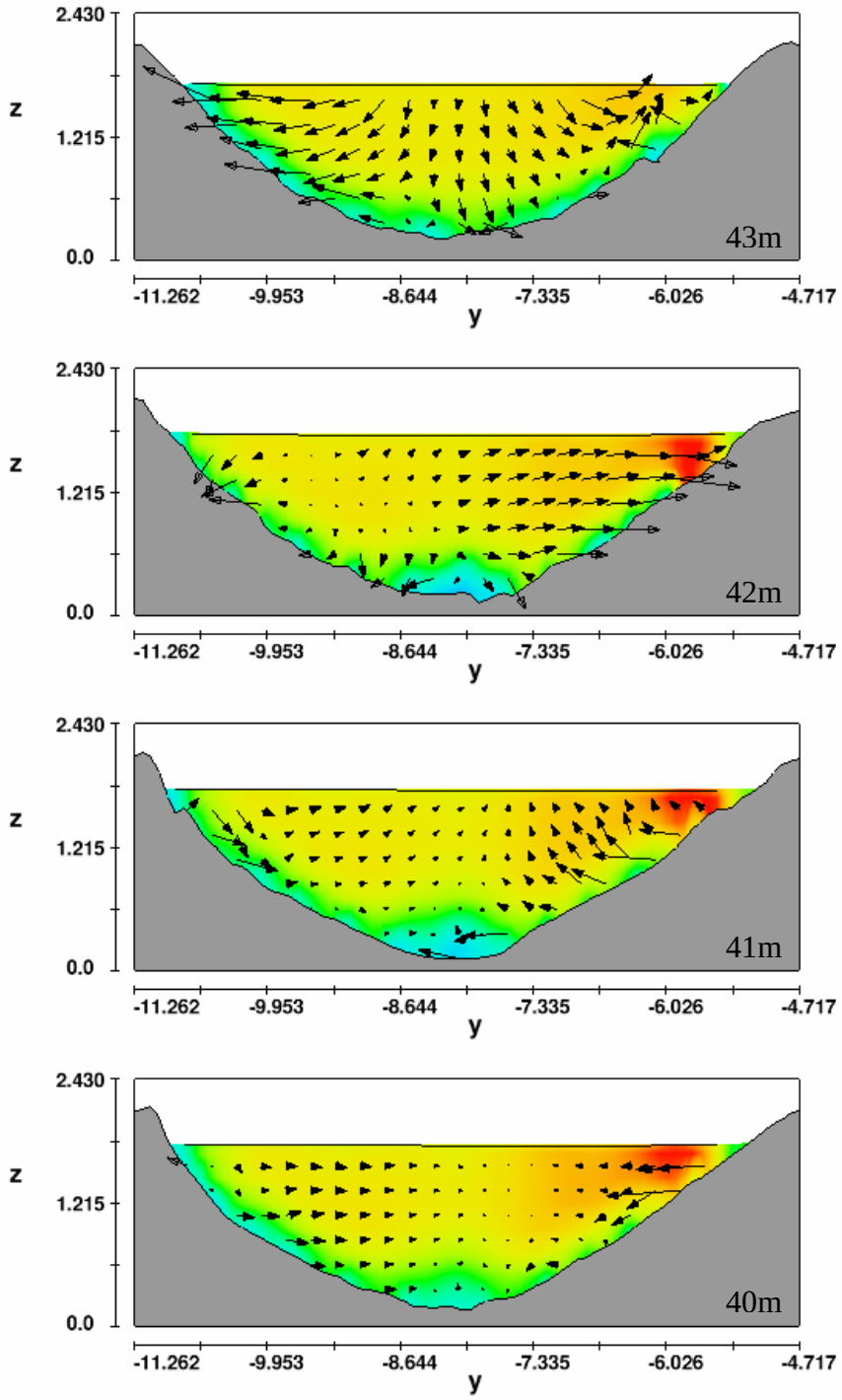
2.430
z
1.215
0.0
43m
-11.262
-9.953
-8.644
-7.335
-6.026
-4.717
y
2.430
z
1.215
0.0
42m
-11.262
-9.953
-8.644
-7.335
-6.026
-4.717
y
2.430
z
1.215
0.0
41m
-11.262
-9.953
-8.644
-7.335
-6.026
-4.717
y
2.430
z
1.215
0.0
40m
-11.262
-9.953
-8.644
-7.335
-6.026
-4.717
y

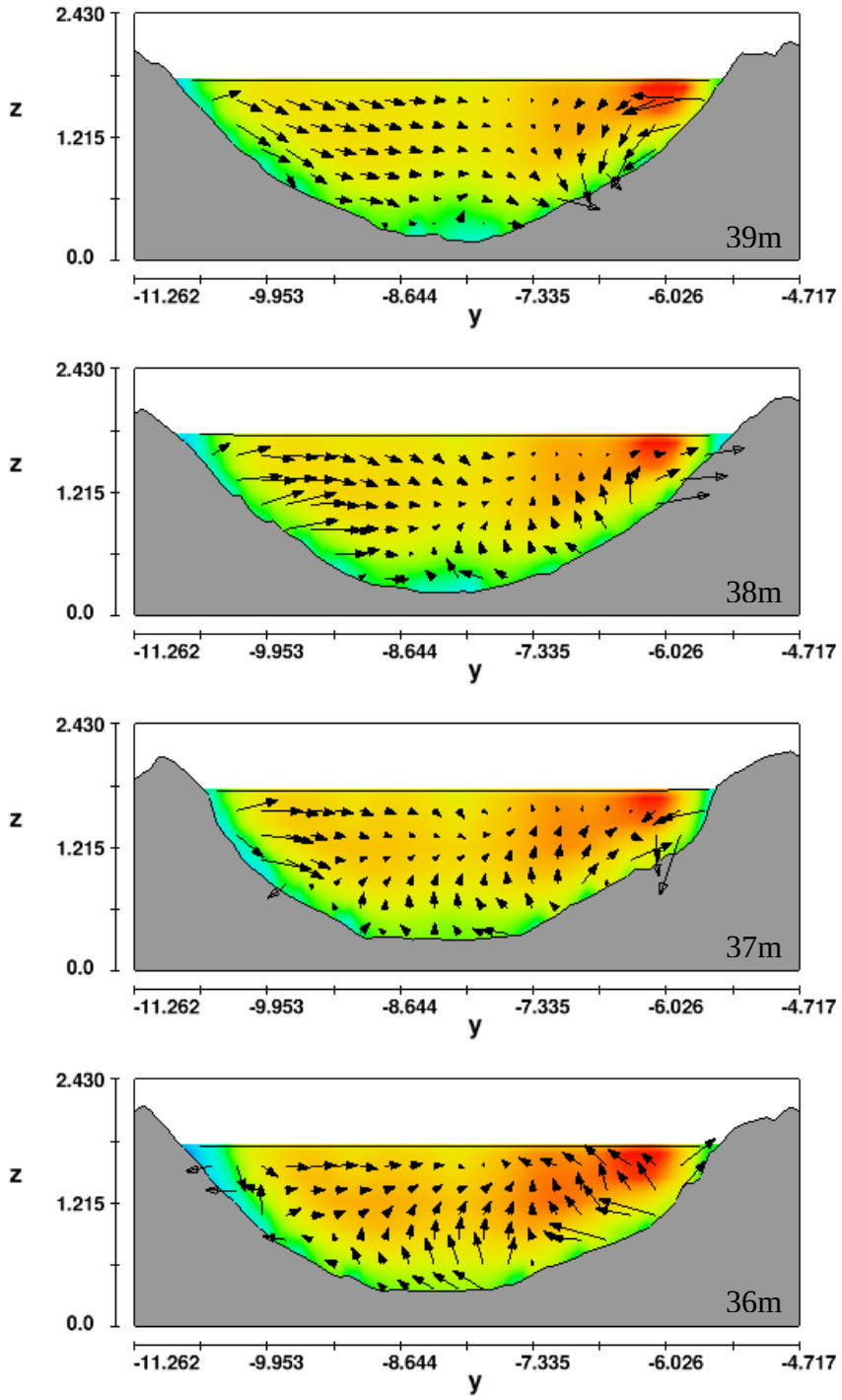
2.430
z
1.215
0.0
39m
-11.262
-9.953
-8.644
-7.335
-6.026
-4.717
y
2.430
z
1.215
0.0
38m
-11.262
-9.953
-8.644
-7.335
-6.026
-4.717
y
2.430
z
1.215
0.0
37m
-11.262
-9.953
-8.644
-7.335
-6.026
-4.717
y
2.430
z
1.215
0.0
36m
-11.262
-9.953
-8.644
-7.335
-6.026
-4.717
y

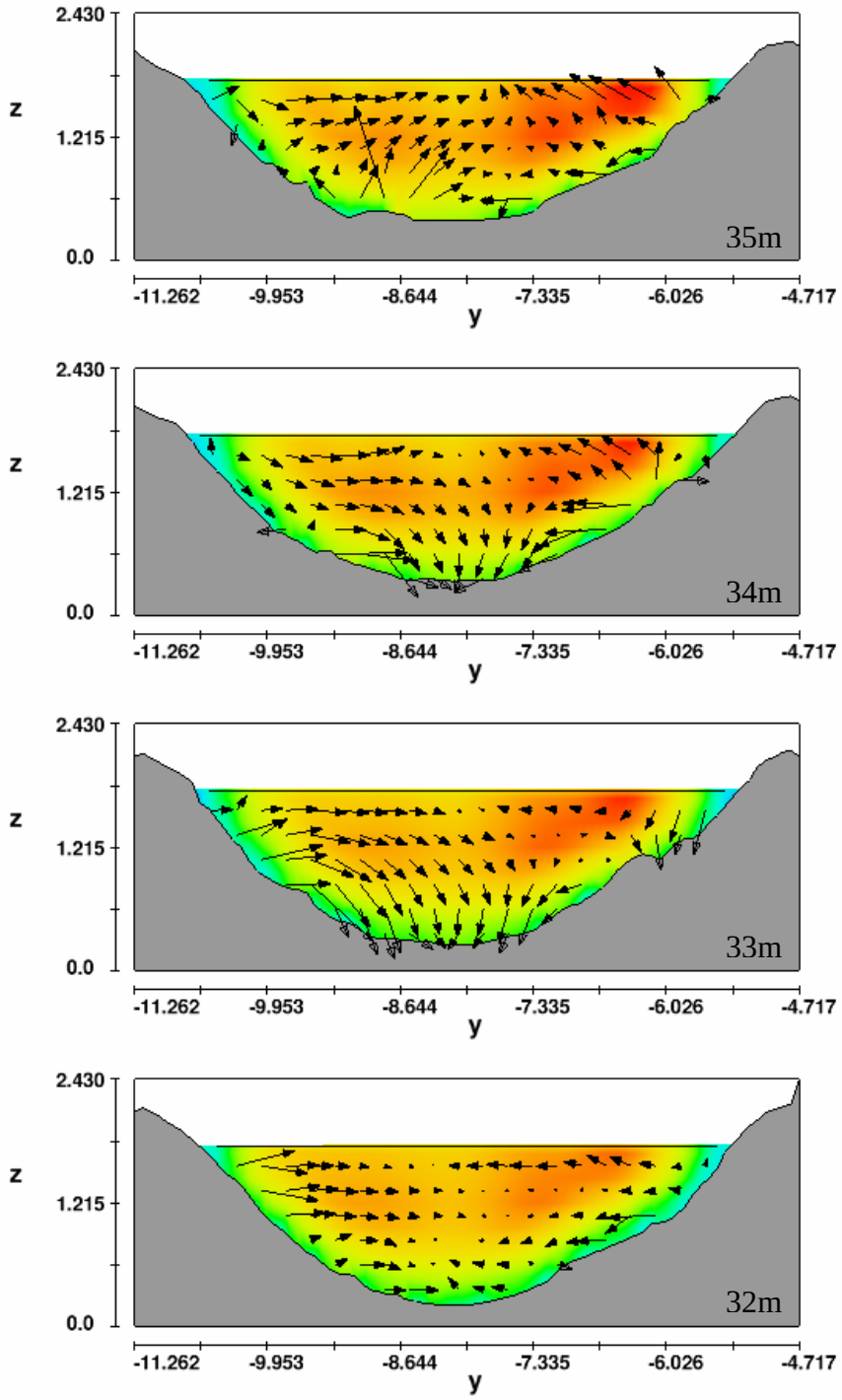
2.430
z
1.215
0.0
35m
-11.262
-9.953
-8.644
-7.335
-6.026
-4.717
y
2.430
z
1.215
0.0
34m
-11.262
-9.953
-8.644
-7.335
-6.026
-4.717
y
2.430
z
1.215
0.0
33m
-11.262
-9.953
-8.644
-7.335
-6.026
-4.717
y
2.430
z
1.215
0.0
32m
-11.262
-9.953
-8.644
-7.335
-6.026
-4.717
y

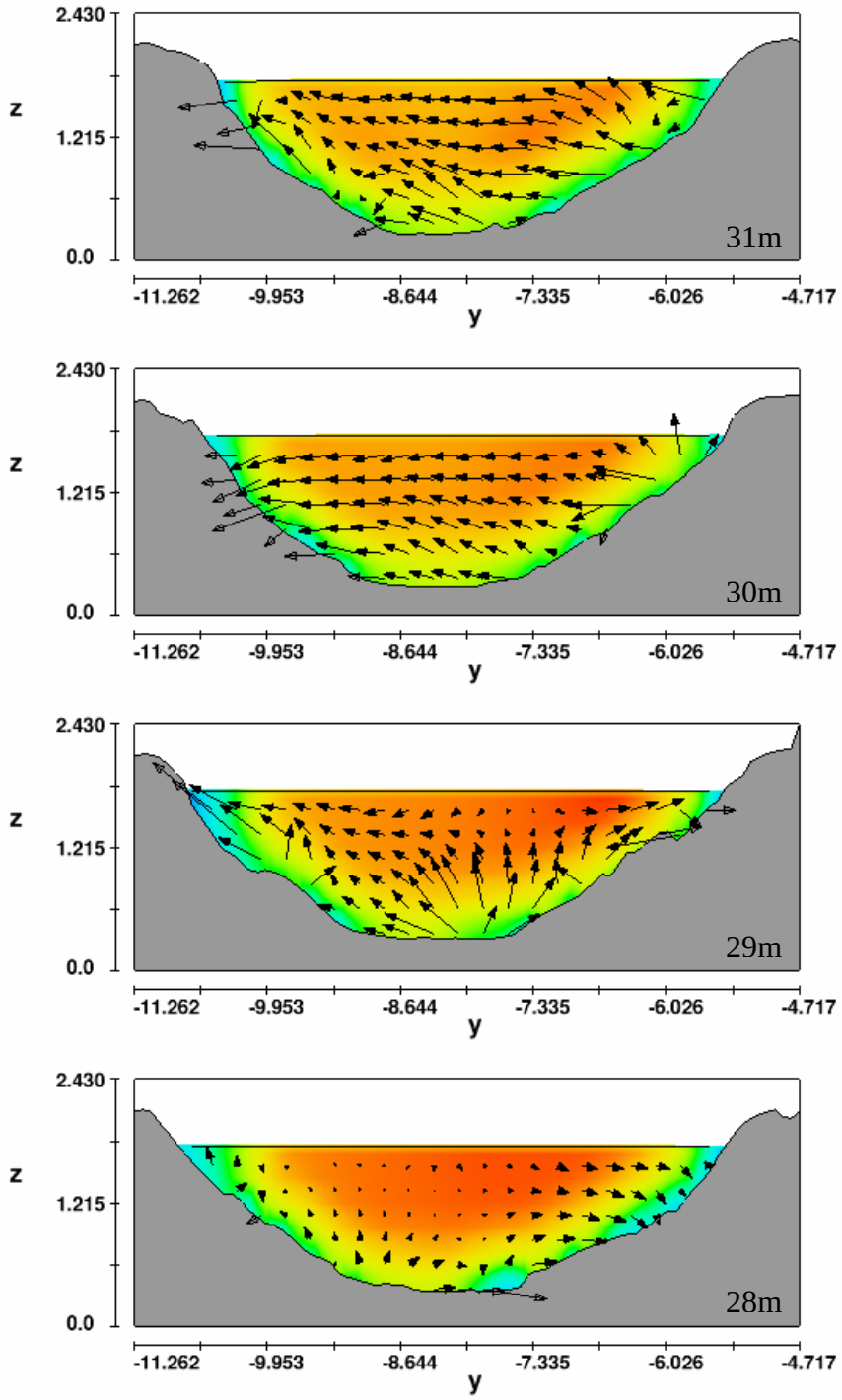
2.430
z
1.215
0.0
31m
-11.262
-9.953
-8.644
-7.335
-6.026
-4.717
y
2.430
z
1.215
0.0
30m
-11.262
-9.953
-8.644
-7.335
-6.026
-4.717
y
2.430
z
1.215
0.0
29m
-11.262
-9.953
-8.644
-7.335
-6.026
-4.717
y
2.430
z
1.215
0.0
28m
-11.262
-9.953
-8.644
-7.335
-6.026
-4.717
y

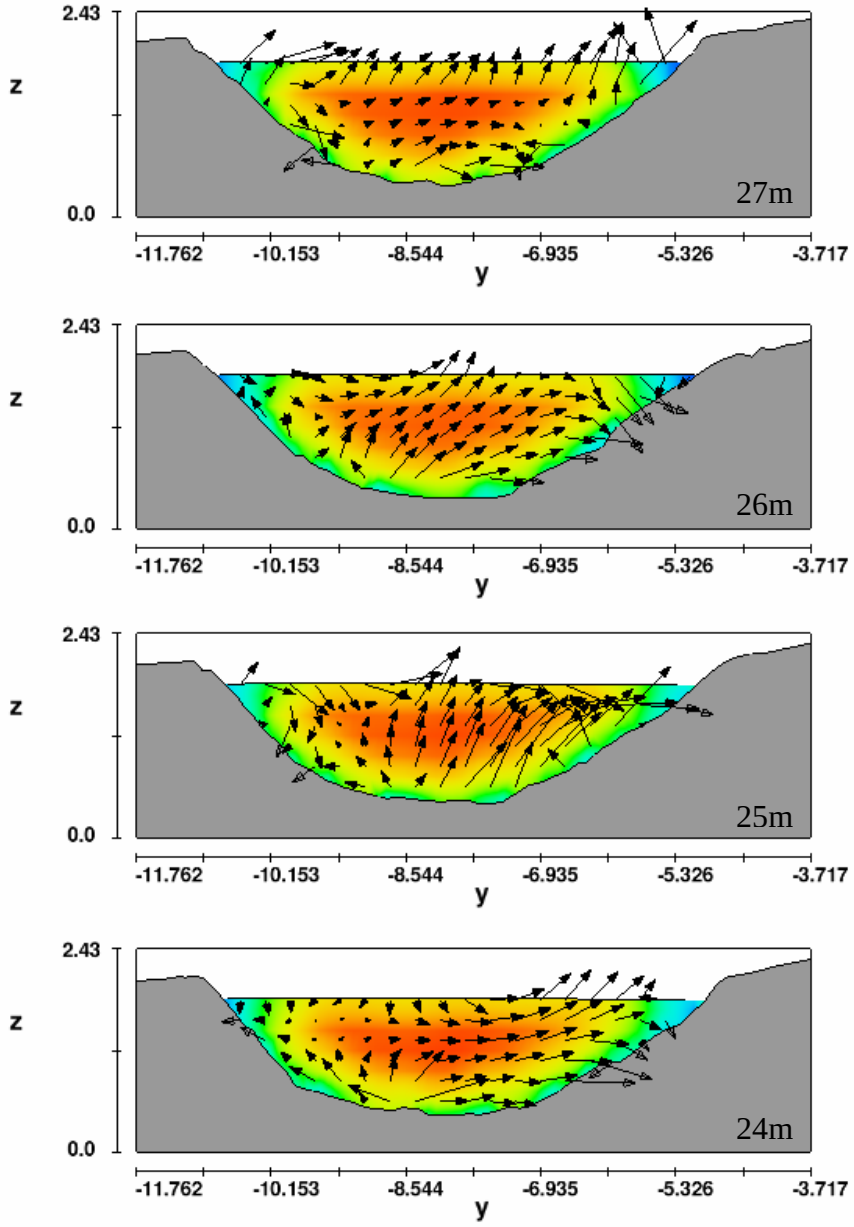
2.43
z
0.0
27m
-11.762
-10.153
-8.544
-6.935
-5.326
-3.717
y
2.43
z
0.0
26m
-11.762
-10.153
-8.544
-6.935
-5.326
-3.717
y
2.43
z
0.0
25m
-11.762
-10.153
-8.544
-6.935
-5.326
-3.717
y
2.43
z
0.0
24m
-11.762
-10.153
-8.544
-6.935
-5.326
-3.717
y

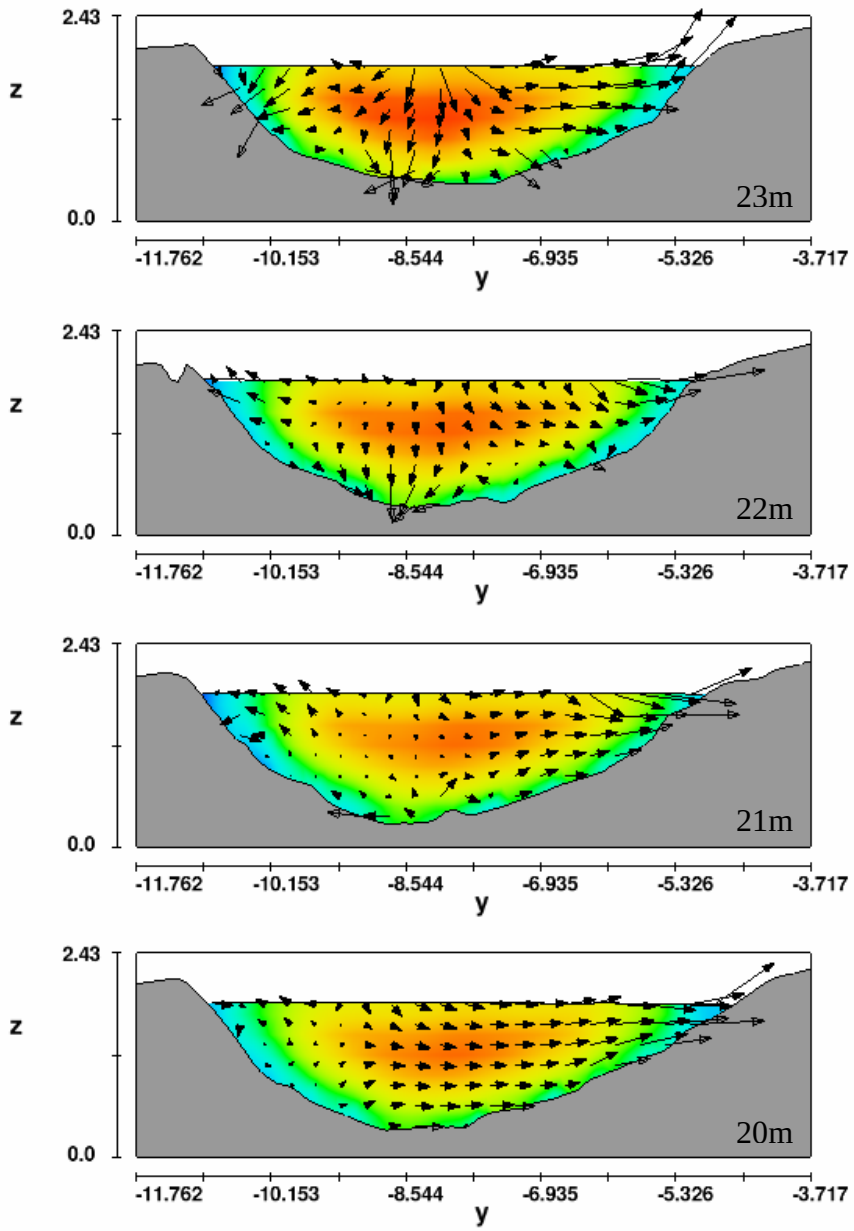
2.43
z
0.0
23m
-11.762
-10.153
-8.544
-6.935
-5.326
-3.717
y
2.43
z
0.0
22m
-11.762
-10.153
-8.544
-6.935
-5.326
-3.717
y
2.43
z
0.0
21m
-11.762
-10.153
-8.544
-6.935
-5.326
-3.717
y
2.43
z
0.0
20m
-11.762
-10.153
-8.544
-6.935
-5.326
-3.717
y

Appendix C

Restoration Design

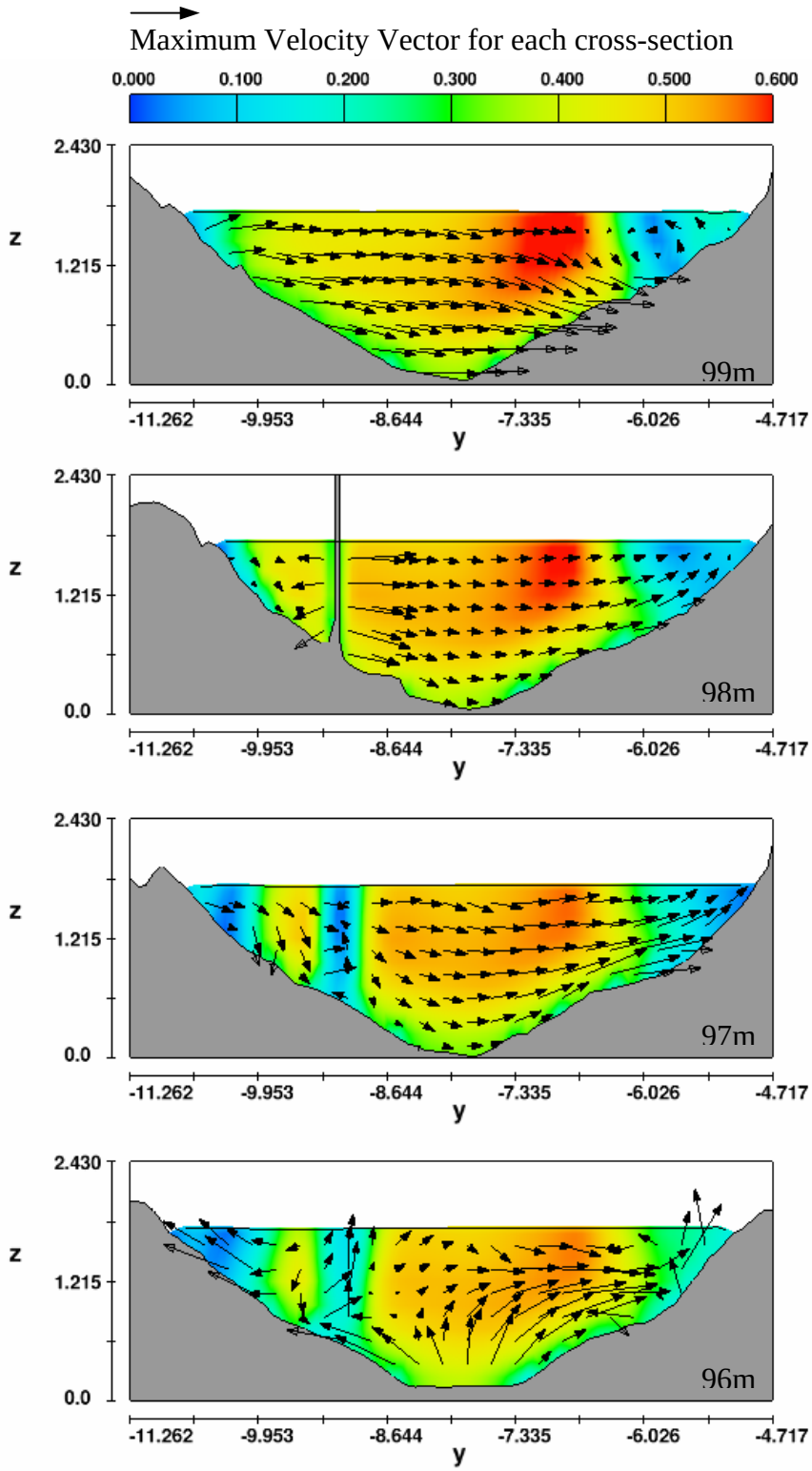

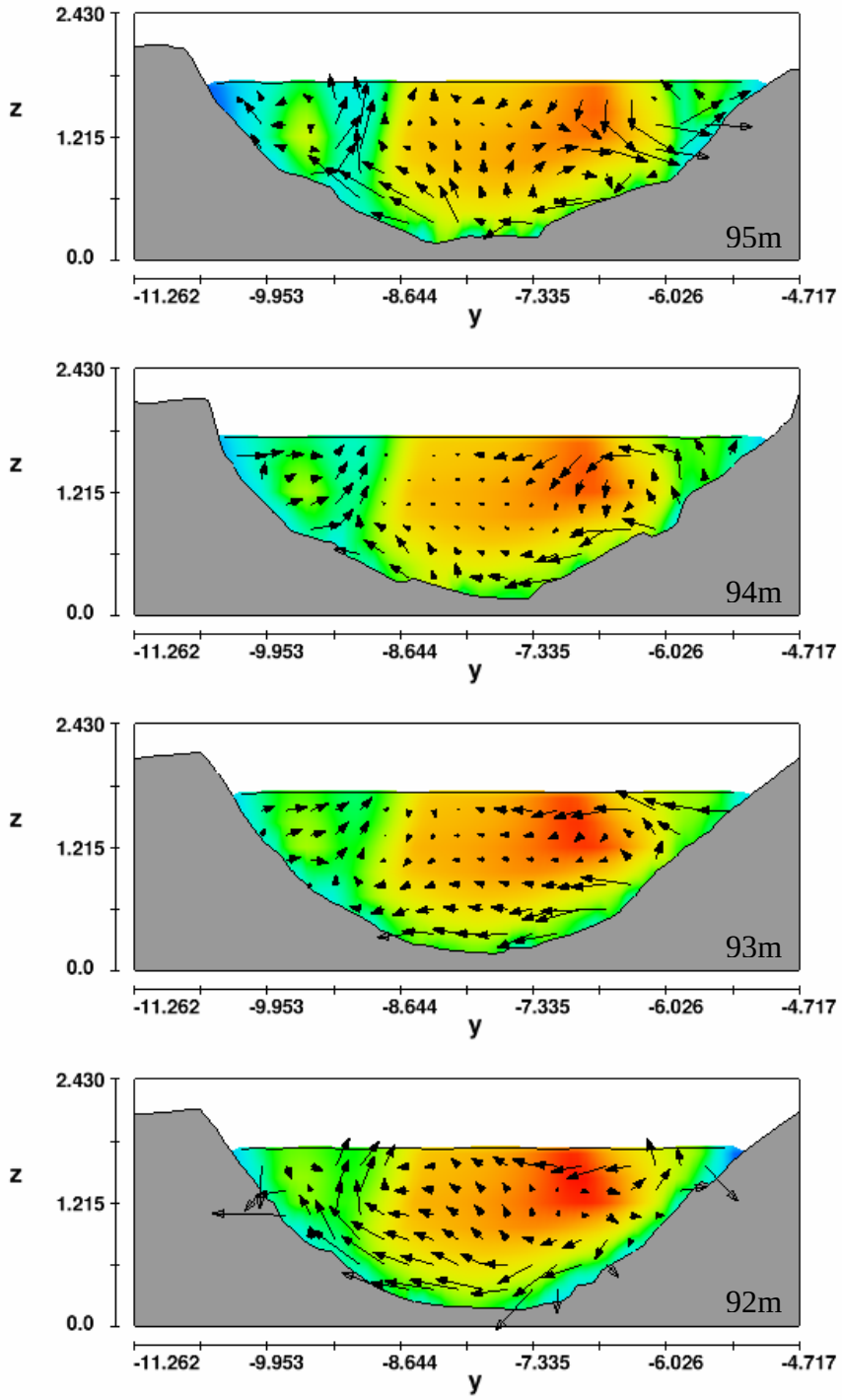
2.430
z
1.215
0.0
95m
-11.262
-9.953
-8.644
-7.335
-6.026
-4.717
y
2.430
z
1.215
0.0
94m
-11.262
-9.953
-8.644
-7.335
-6.026
-4.717
y
2.430
z
1.215
0.0
93m
-11.262
-9.953
-8.644
-7.335
-6.026
-4.717
y
2.430
z
1.215
0.0
92m
-11.262
-9.953
-8.644
-7.335
-6.026
-4.717
y

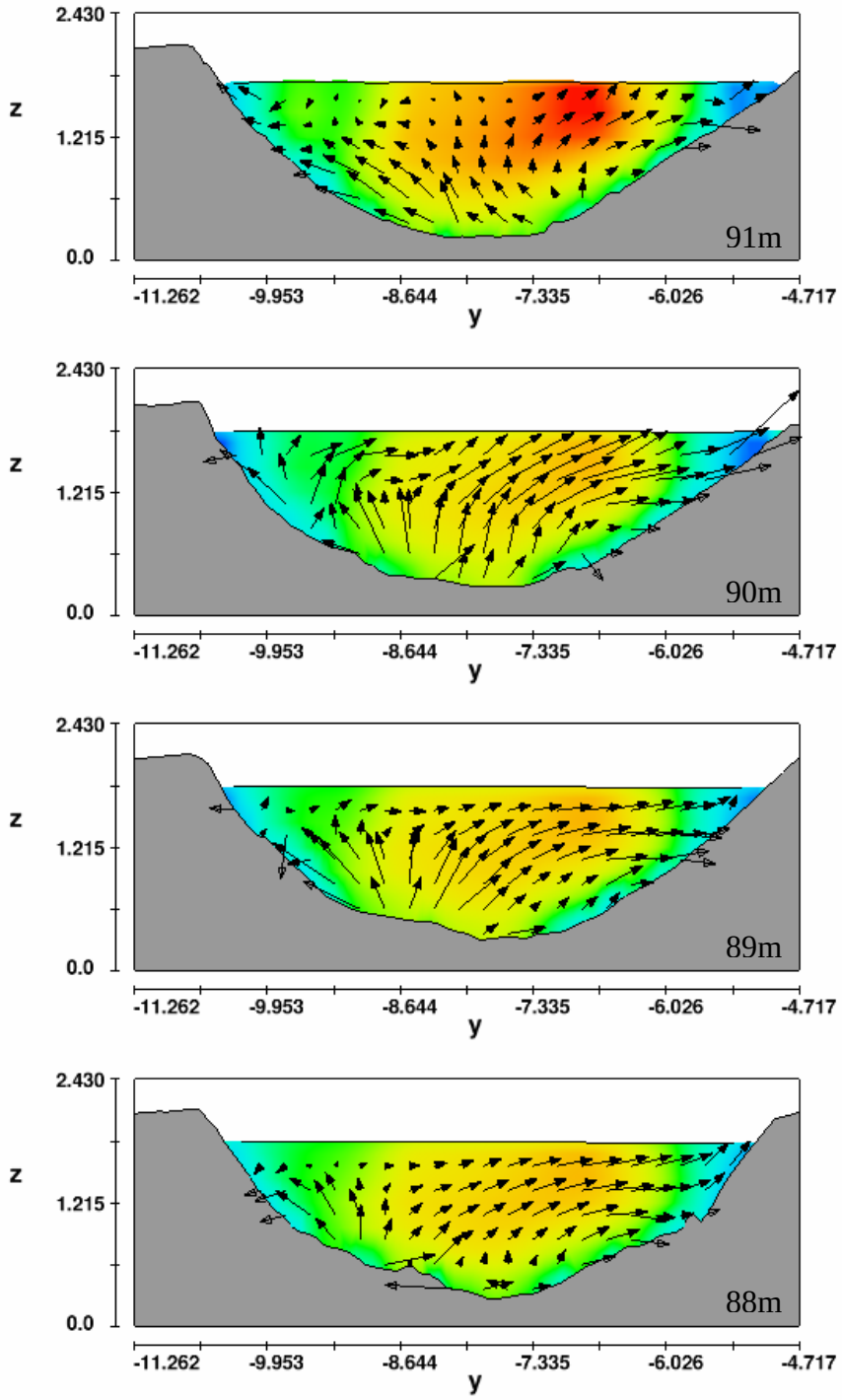
2.430
z
1.215
0.0
91m
-11.262
-9.953
-8.644
-7.335
-6.026
-4.717
y
2.430
z
1.215
0.0
90m
-11.262
-9.953
-8.644
-7.335
-6.026
-4.717
y
2.430
z
1.215
0.0
89m
-11.262
-9.953
-8.644
-7.335
-6.026
-4.717
y
2.430
z
1.215
0.0
88m
-11.262
-9.953
-8.644
-7.335
-6.026
-4.717
y

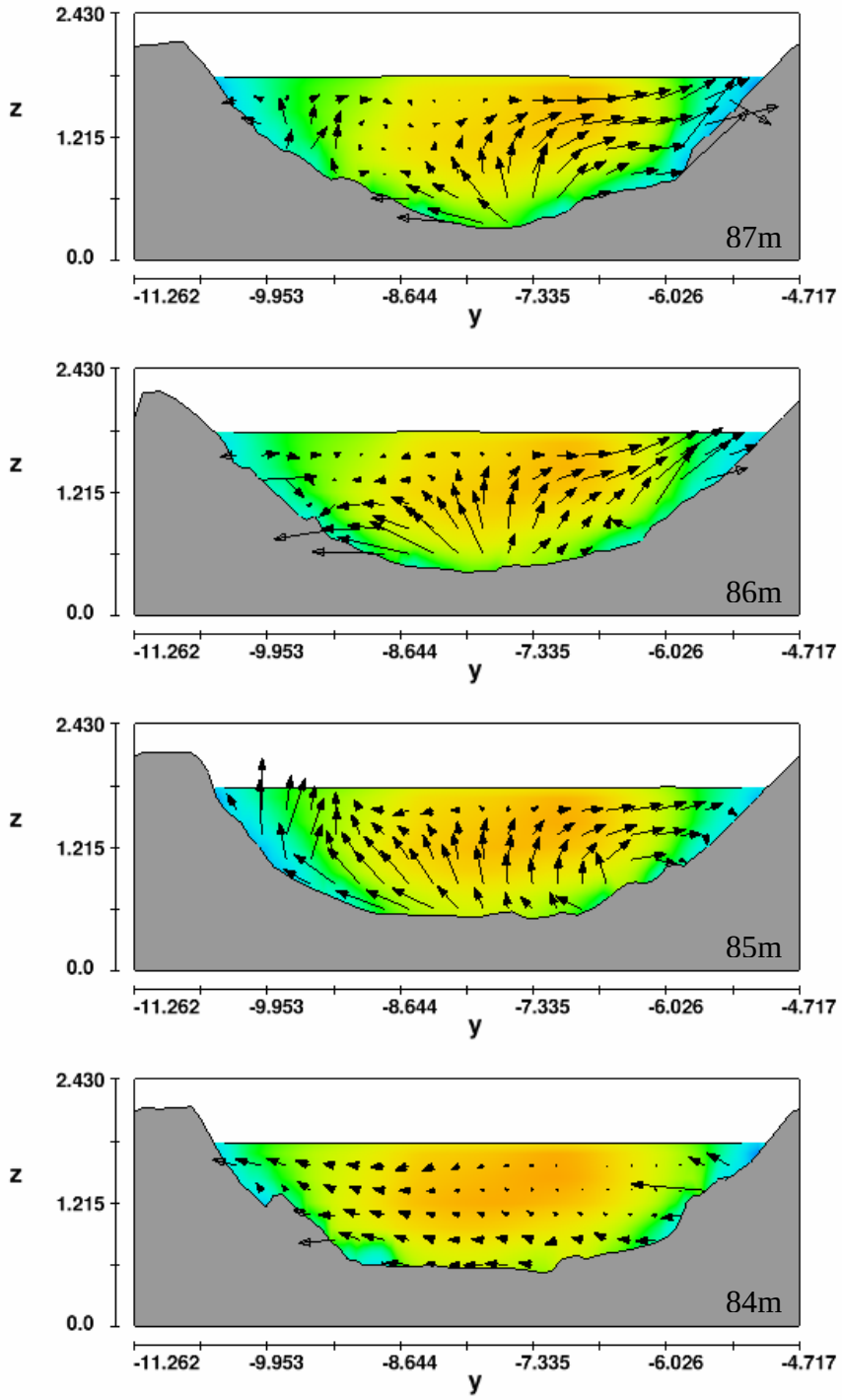
2.430
z
1.215
0.0
87m
-11.262
-9.953
-8.644
-7.335
-6.026
-4.717
y
2.430
z
1.215
0.0
86m
-11.262
-9.953
-8.644
-7.335
-6.026
-4.717
y
2.430
z
1.215
0.0
85m
-11.262
-9.953
-8.644
-7.335
-6.026
-4.717
y
2.430
z
1.215
0.0
84m
-11.262
-9.953
-8.644
-7.335
-6.026
-4.717
y

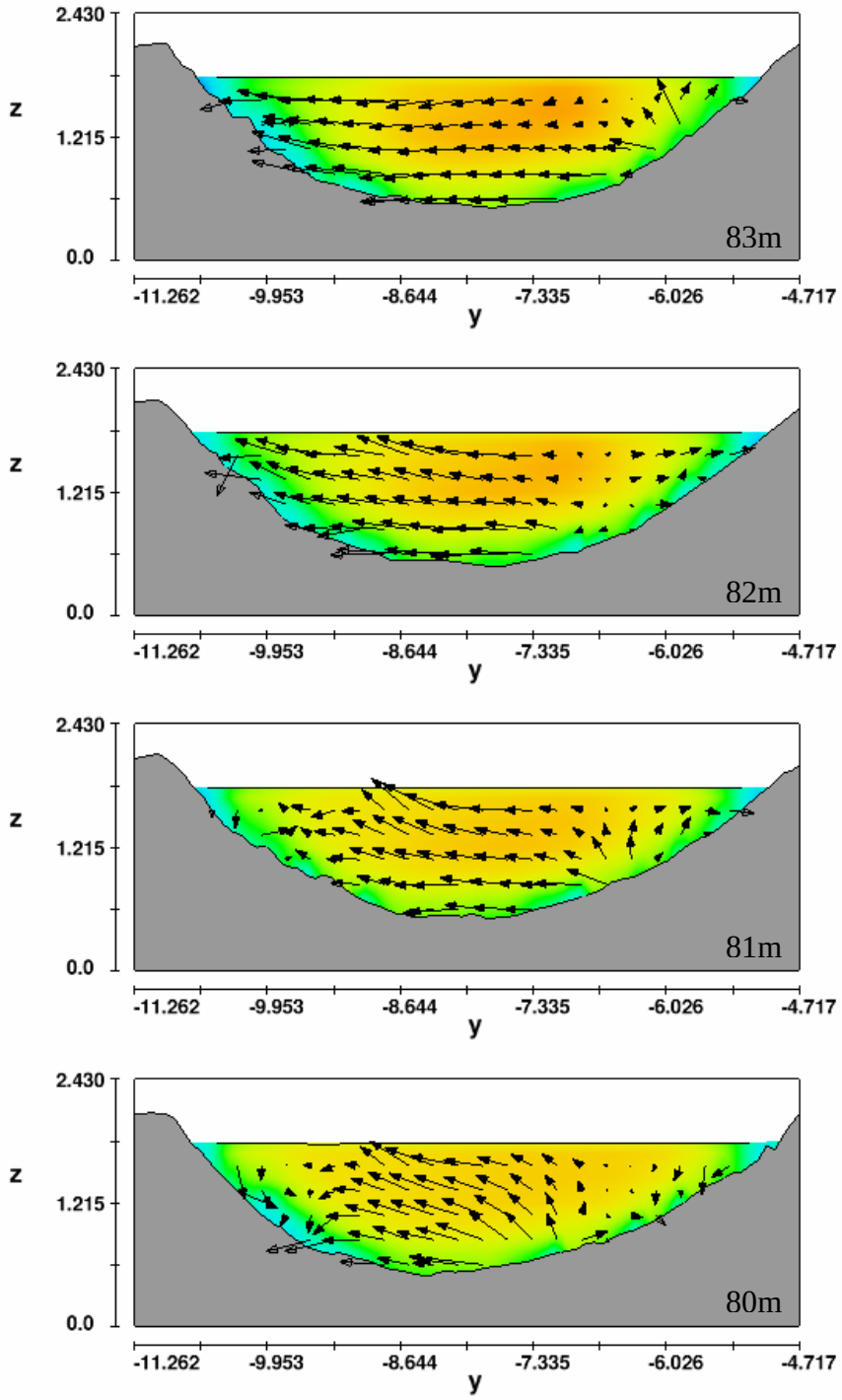
2.430
z
1.215
0.0
83m
-11.262
-9.953
-8.644
-7.335
-6.026
-4.717
y
2.430
z
1.215
0.0
82m
-11.262
-9.953
-8.644
-7.335
-6.026
-4.717
y
2.430
z
1.215
0.0
81m
-11.262
-9.953
-8.644
-7.335
-6.026
-4.717
y
2.430
z
1.215
0.0
80m
-11.262
-9.953
-8.644
-7.335
-6.026
-4.717
y

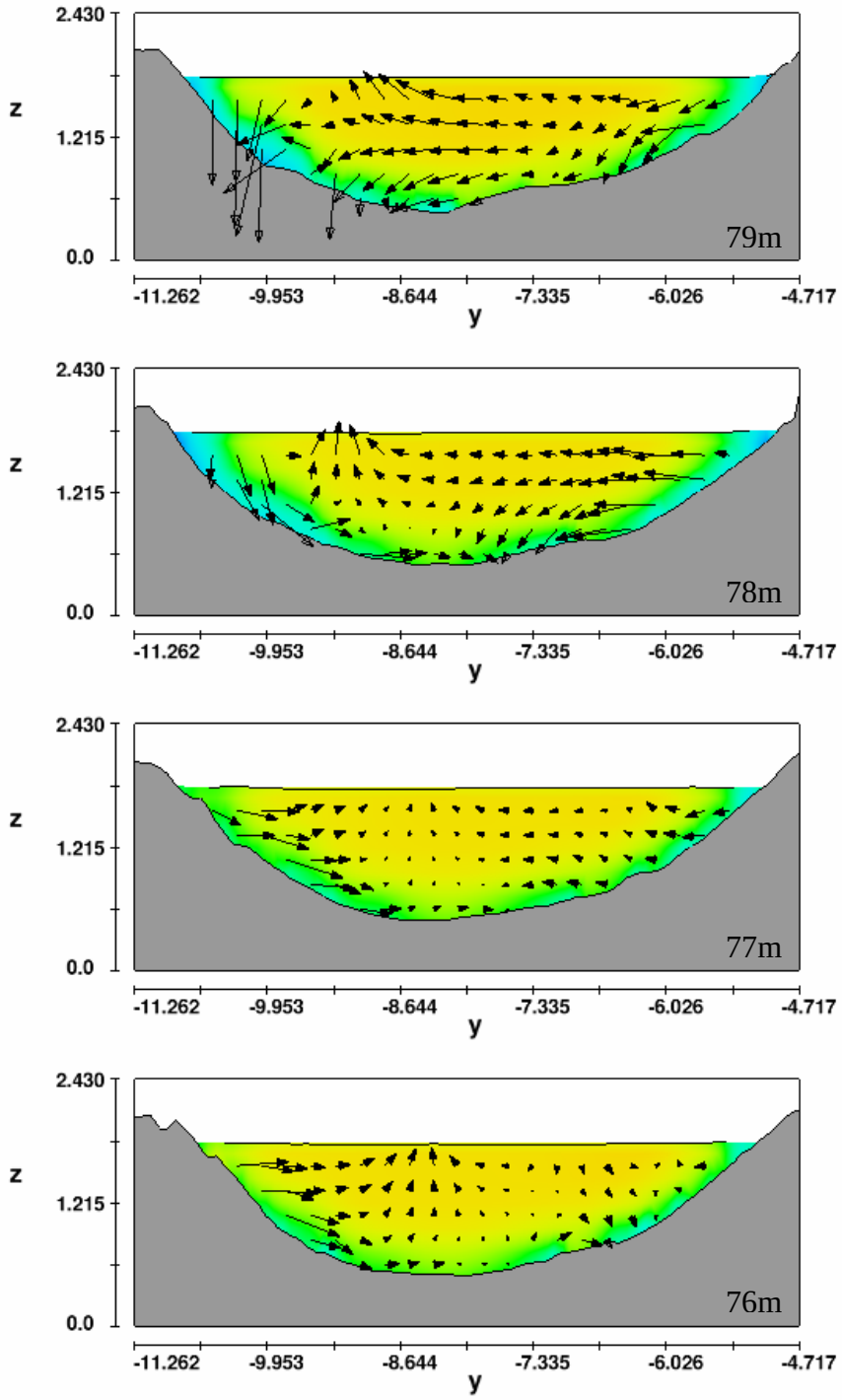
2.430
z
1.215
0.0
79m
-11.262
-9.953
-8.644
-7.335
-6.026
-4.717
y
2.430
z
1.215
0.0
78m
-11.262
-9.953
-8.644
-7.335
-6.026
-4.717
y
2.430
z
1.215
0.0
77m
-11.262
-9.953
-8.644
-7.335
-6.026
-4.717
y
2.430
z
1.215
0.0
76m
-11.262
-9.953
-8.644
-7.335
-6.026
-4.717
y

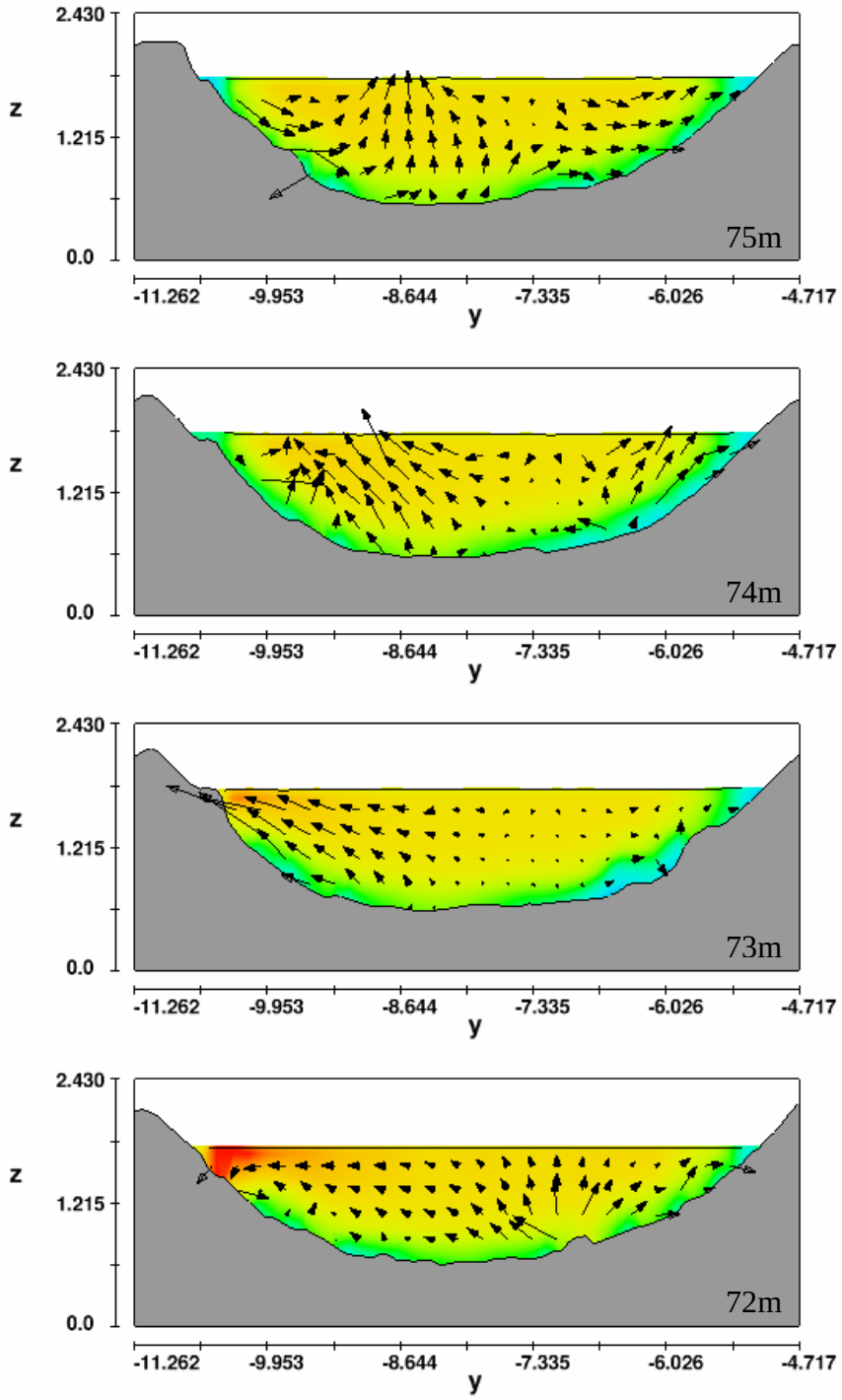
2.430
z
1.215
0.0
75m
-11.262
-9.953
-8.644
-7.335
-6.026
-4.717
y
2.430
z
1.215
0.0
74m
-11.262
-9.953
-8.644
-7.335
-6.026
-4.717
y
2.430
z
1.215
0.0
73m
-11.262
-9.953
-8.644
-7.335
-6.026
-4.717
y
2.430
z
1.215
0.0
72m
-11.262
-9.953
-8.644
-7.335
-6.026
-4.717
y

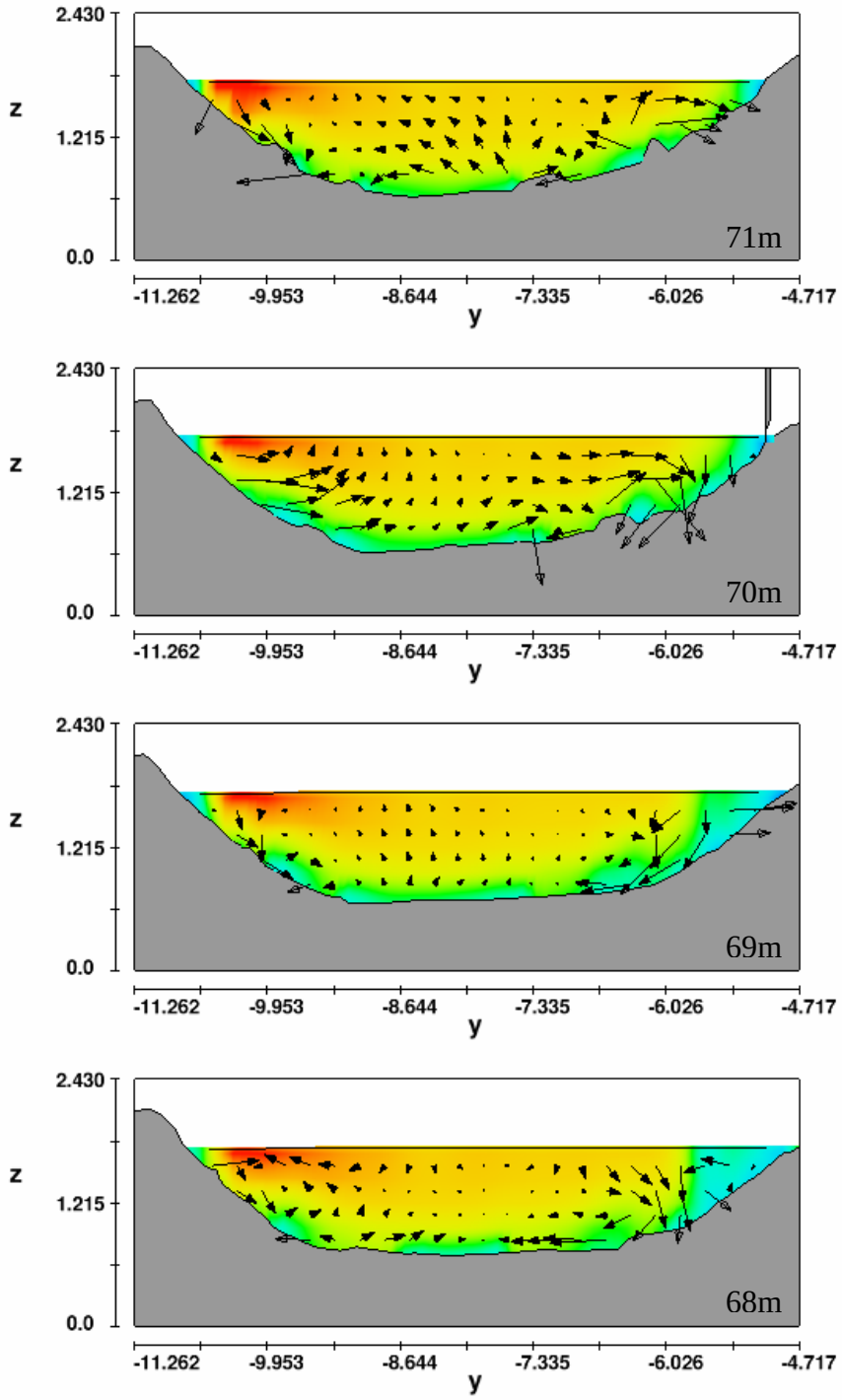
2.430
z
1.215
0.0
71m
-11.262
-9.953
-8.644
-7.335
-6.026
-4.717
y
2.430
z
1.215
0.0
70m
-11.262
-9.953
-8.644
-7.335
-6.026
-4.717
y
2.430
z
1.215
0.0
69m
-11.262
-9.953
-8.644
-7.335
-6.026
-4.717
y
2.430
z
1.215
0.0
68m
-11.262
-9.953
-8.644
-7.335
-6.026
-4.717
y

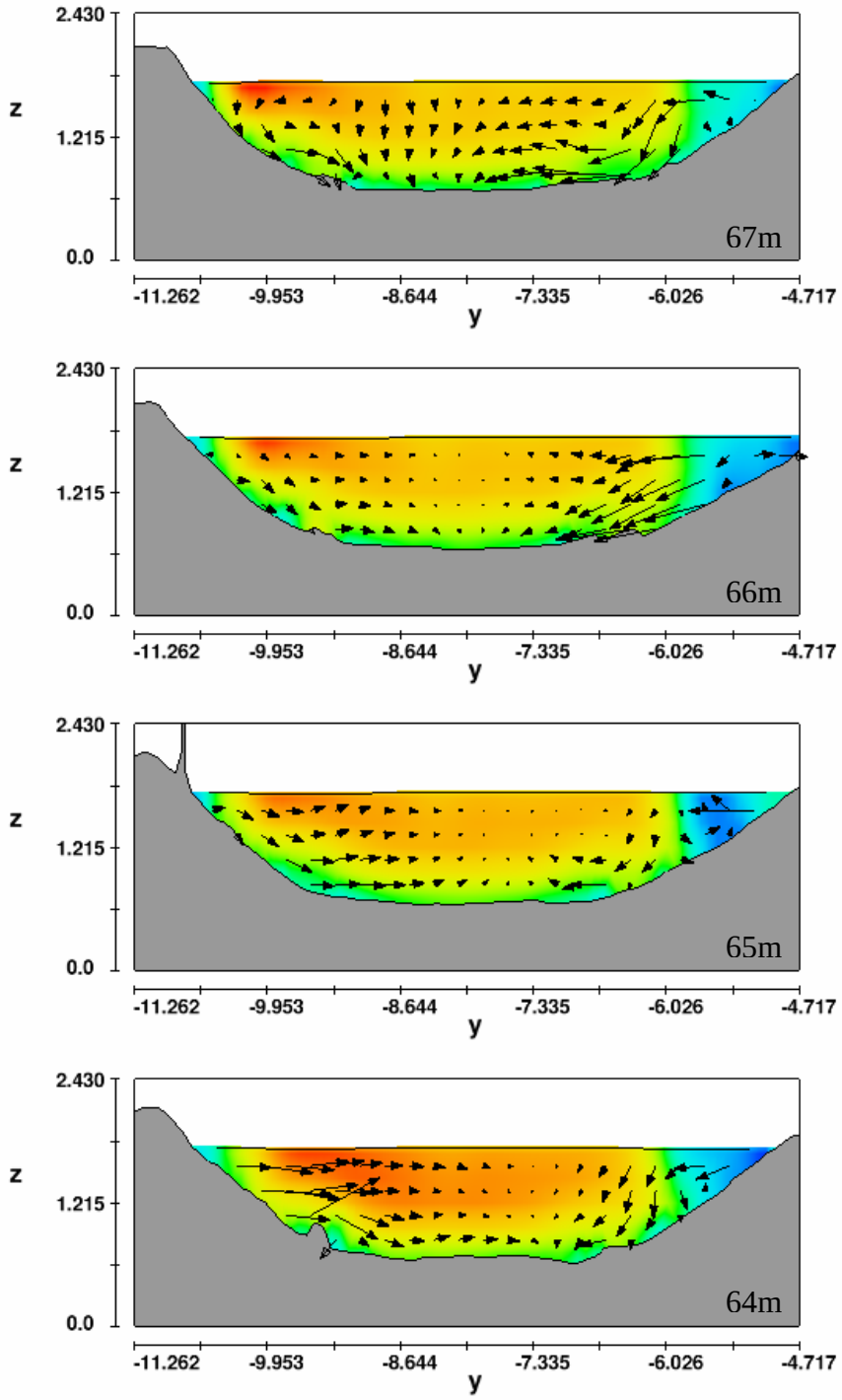
2.430
z
1.215
0.0
67m
-11.262
-9.953
-8.644
-7.335
-6.026
-4.717
y
2.430
z
1.215
0.0
66m
-11.262
-9.953
-8.644
-7.335
-6.026
-4.717
y
2.430
z
1.215
0.0
65m
-11.262
-9.953
-8.644
-7.335
-6.026
-4.717
y
2.430
z
1.215
0.0
64m
-11.262
-9.953
-8.644
-7.335
-6.026
-4.717
y

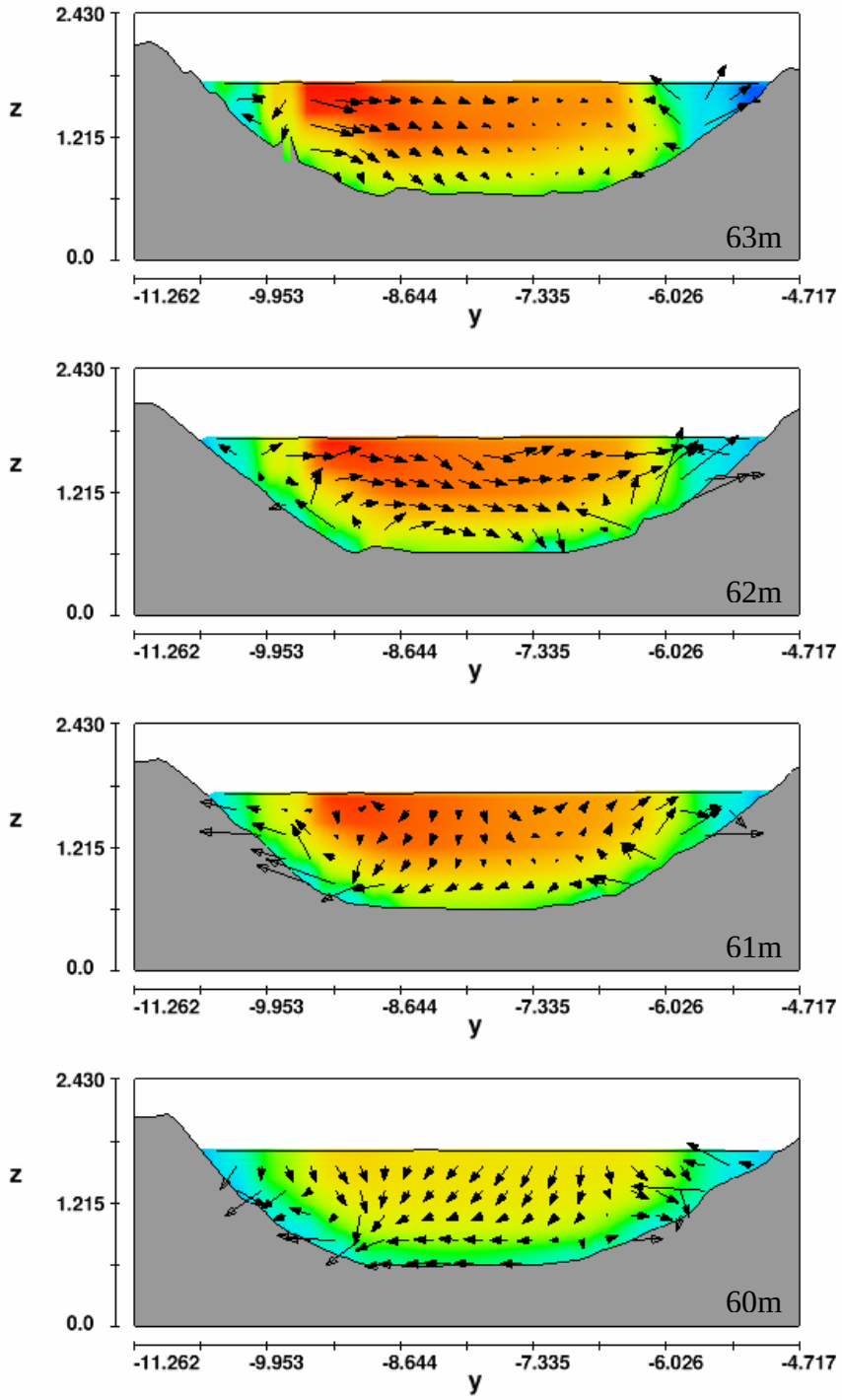
2.430
z
1.215
0.0
63m
-11.262
-9.953
-8.644
-7.335
-6.026
-4.717
y
2.430
z
1.215
0.0
62m
-11.262
-9.953
-8.644
-7.335
-6.026
-4.717
y
2.430
z
1.215
0.0
61m
-11.262
-9.953
-8.644
-7.335
-6.026
-4.717
y
2.430
z
1.215
0.0
60m
-11.262
-9.953
-8.644
-7.335
-6.026
-4.717
y

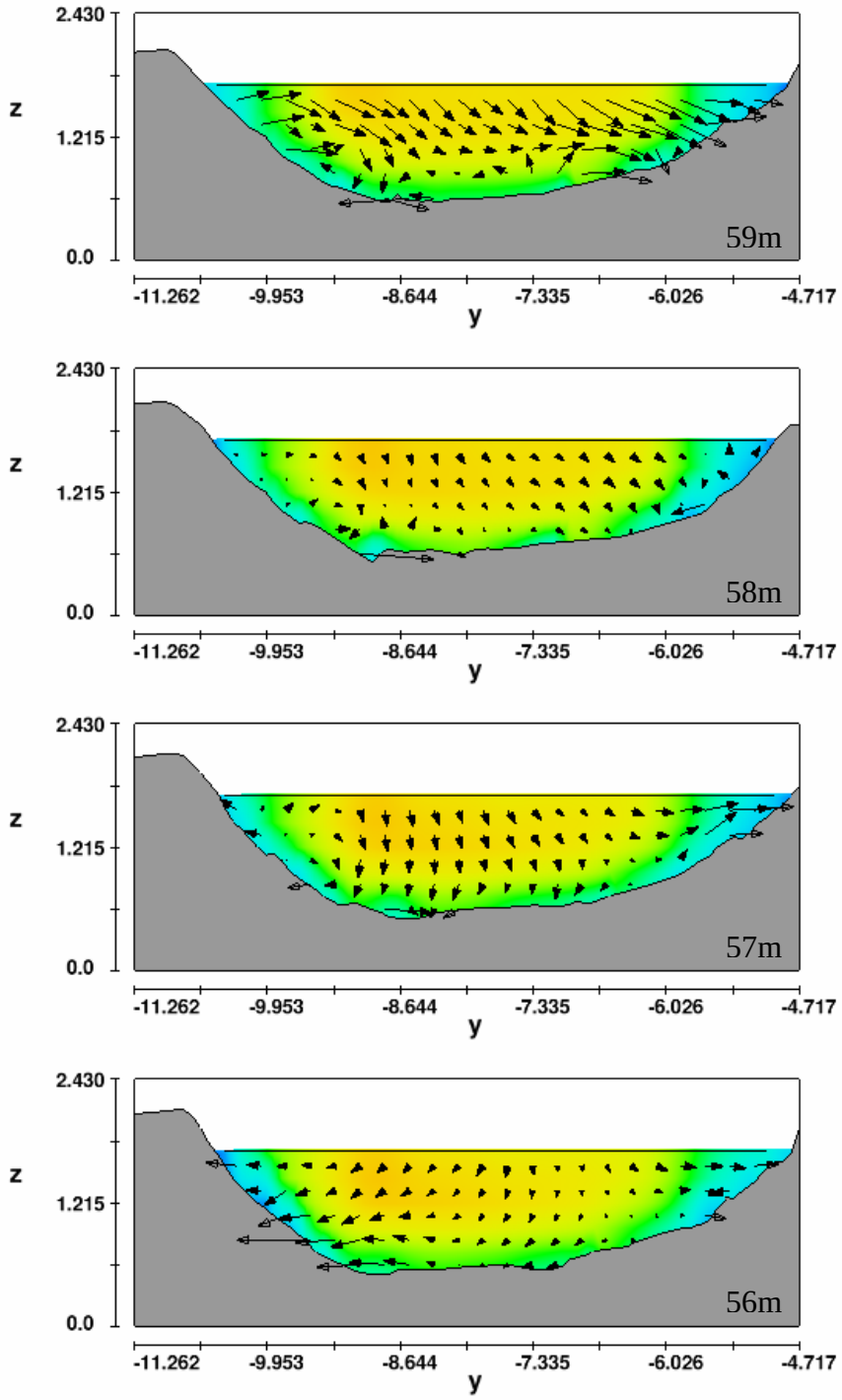
2.430
z
1.215
0.0
59m
-11.262
-9.953
-8.644
-7.335
-6.026
-4.717
y
2.430
z
1.215
0.0
58m
-11.262
-9.953
-8.644
-7.335
-6.026
-4.717
y
2.430
z
1.215
0.0
57m
-11.262
-9.953
-8.644
-7.335
-6.026
-4.717
y
2.430
z
1.215
0.0
56m
-11.262
-9.953
-8.644
-7.335
-6.026
-4.717
y

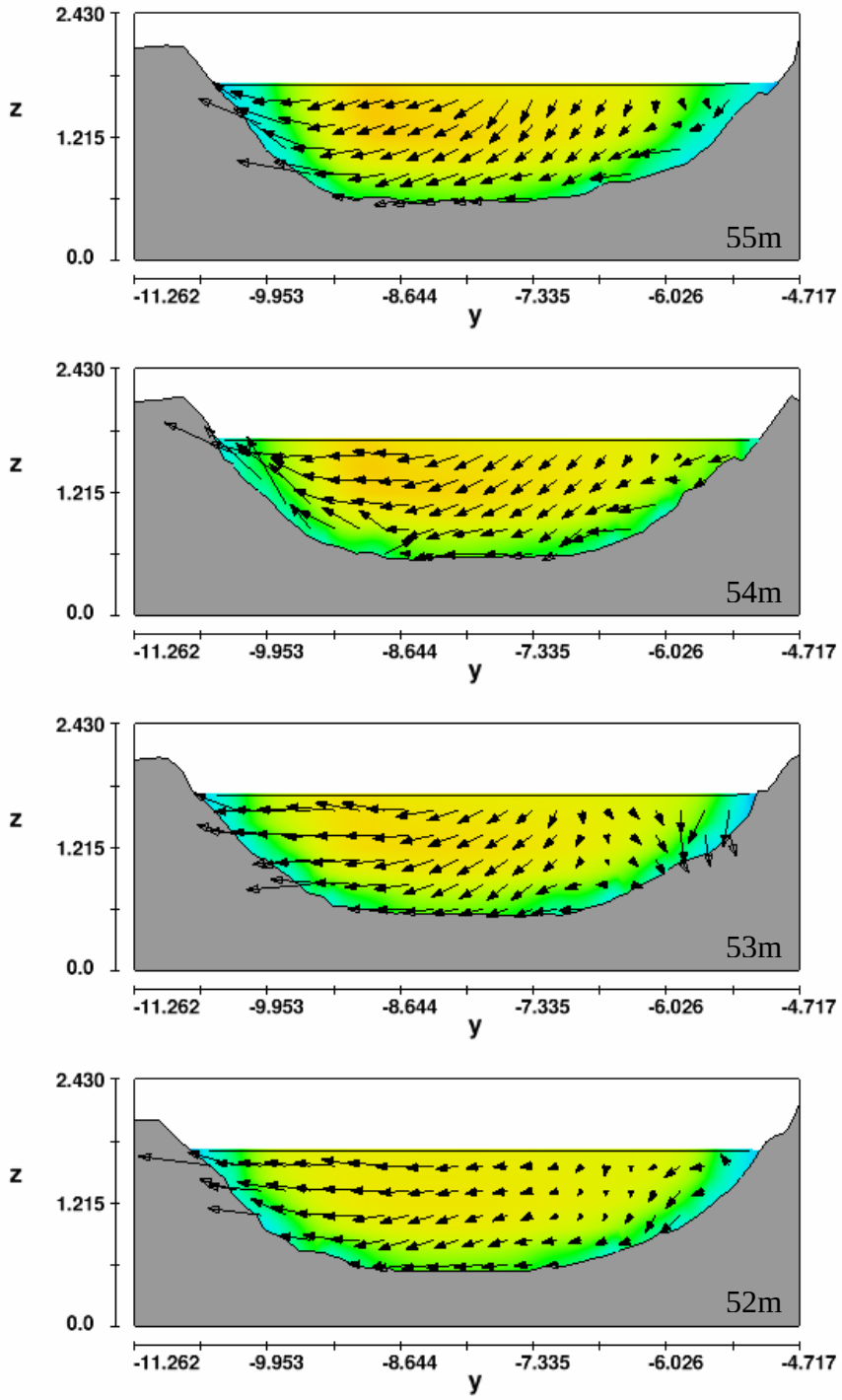
2.430
z
1.215
0.0
55m
-11.262
-9.953
-8.644
-7.335
-6.026
-4.717
y
2.430
z
1.215
0.0
54m
-11.262
-9.953
-8.644
-7.335
-6.026
-4.717
y
2.430
z
1.215
0.0
53m
-11.262
-9.953
-8.644
-7.335
-6.026
-4.717
y
2.430
z
1.215
0.0
52m
-11.262
-9.953
-8.644
-7.335
-6.026
-4.717
y

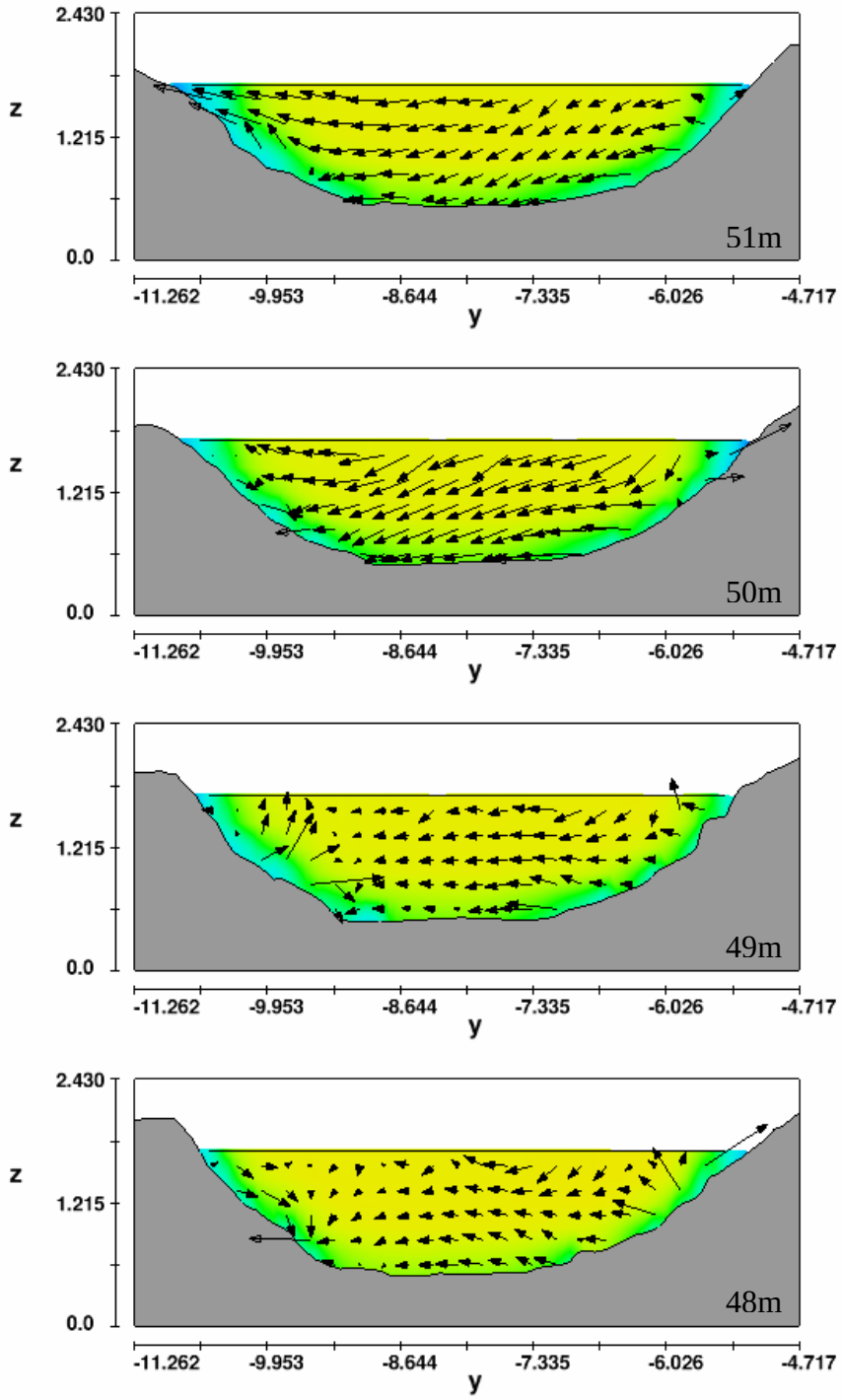
2.430
z
1.215
0.0
51m
-11.262
-9.953
-8.644
-7.335
-6.026
-4.717
y
2.430
z
1.215
0.0
50m
-11.262
-9.953
-8.644
-7.335
-6.026
-4.717
y
2.430
z
1.215
0.0
49m
-11.262
-9.953
-8.644
-7.335
-6.026
-4.717
y
2.430
z
1.215
0.0
48m
-11.262
-9.953
-8.644
-7.335
-6.026
-4.717
y

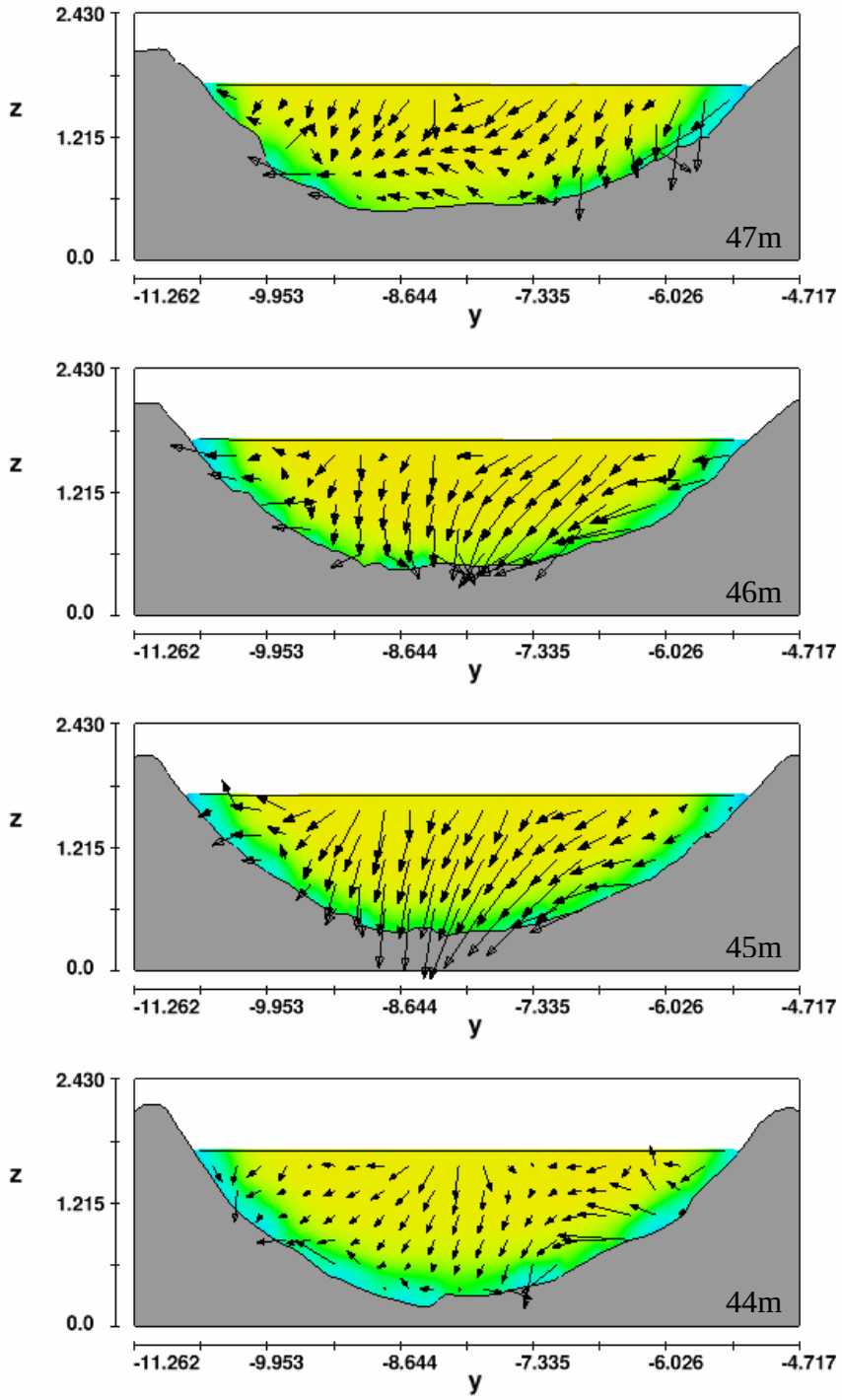
2.430
z
1.215
0.0
47m
-11.262
-9.953
-8.644
-7.335
-6.026
-4.717
y
2.430
z
1.215
0.0
46m
-11.262
-9.953
-8.644
-7.335
-6.026
-4.717
y
2.430
z
1.215
0.0
45m
-11.262
-9.953
-8.644
-7.335
-6.026
-4.717
y
2.430
z
1.215
0.0
44m
-11.262
-9.953
-8.644
-7.335
-6.026
-4.717
y

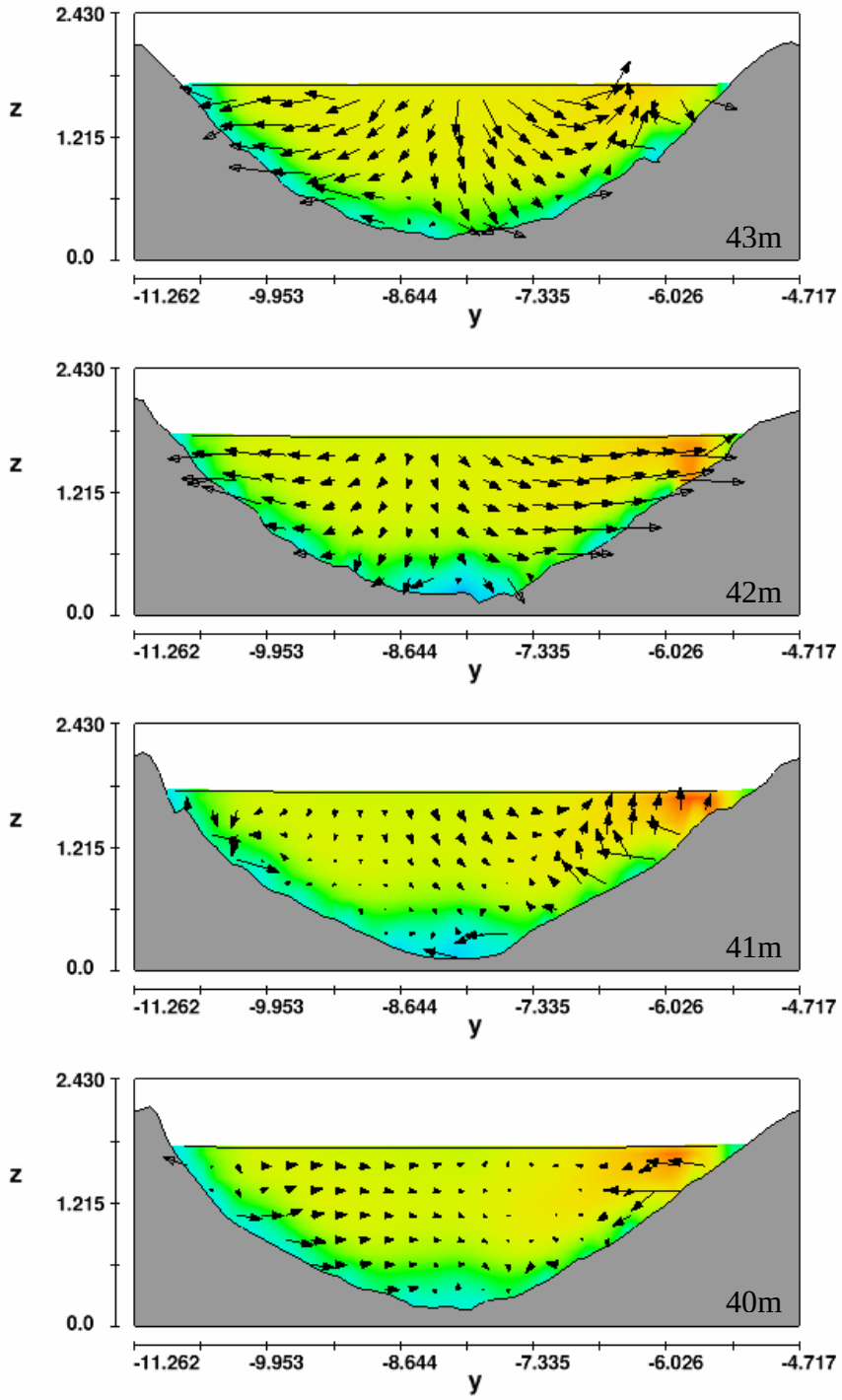
2.430
z
1.215
0.0
43m
-11.262
-9.953
-8.644
-7.335
-6.026
-4.717
y
2.430
z
1.215
0.0
42m
-11.262
-9.953
-8.644
-7.335
-6.026
-4.717
y
2.430
z
1.215
0.0
41m
-11.262
-9.953
-8.644
-7.335
-6.026
-4.717
y
2.430
z
1.215
0.0
40m
-11.262
-9.953
-8.644
-7.335
-6.026
-4.717
y

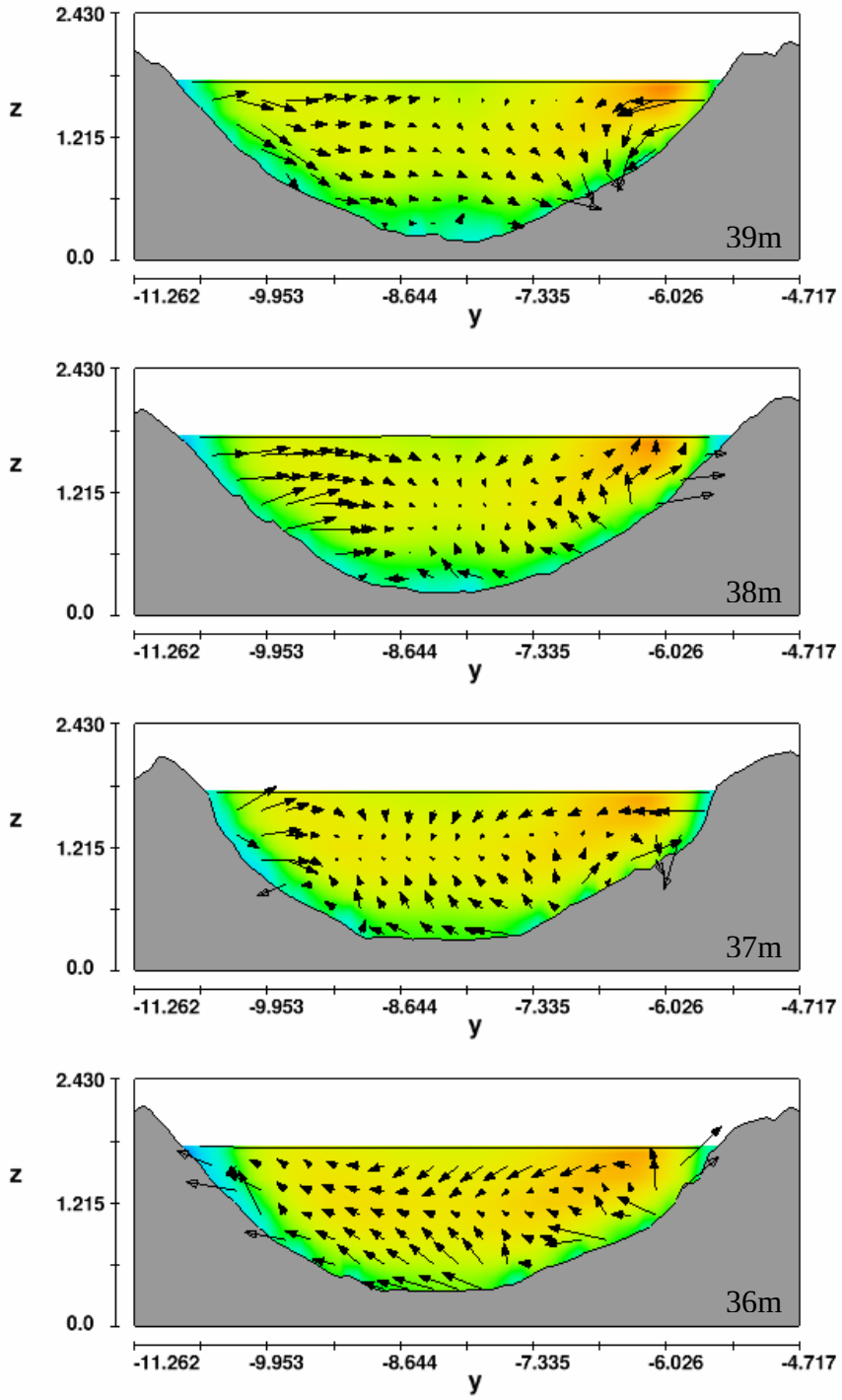
2.430
z
1.215
0.0
39m
-11.262
-9.953
-8.644
-7.335
-6.026
-4.717
y
2.430
z
1.215
0.0
38m
-11.262
-9.953
-8.644
-7.335
-6.026
-4.717
y
2.430
z
1.215
0.0
37m
-11.262
-9.953
-8.644
-7.335
-6.026
-4.717
y
2.430
z
1.215
0.0
36m
-11.262
-9.953
-8.644
-7.335
-6.026
-4.717
y

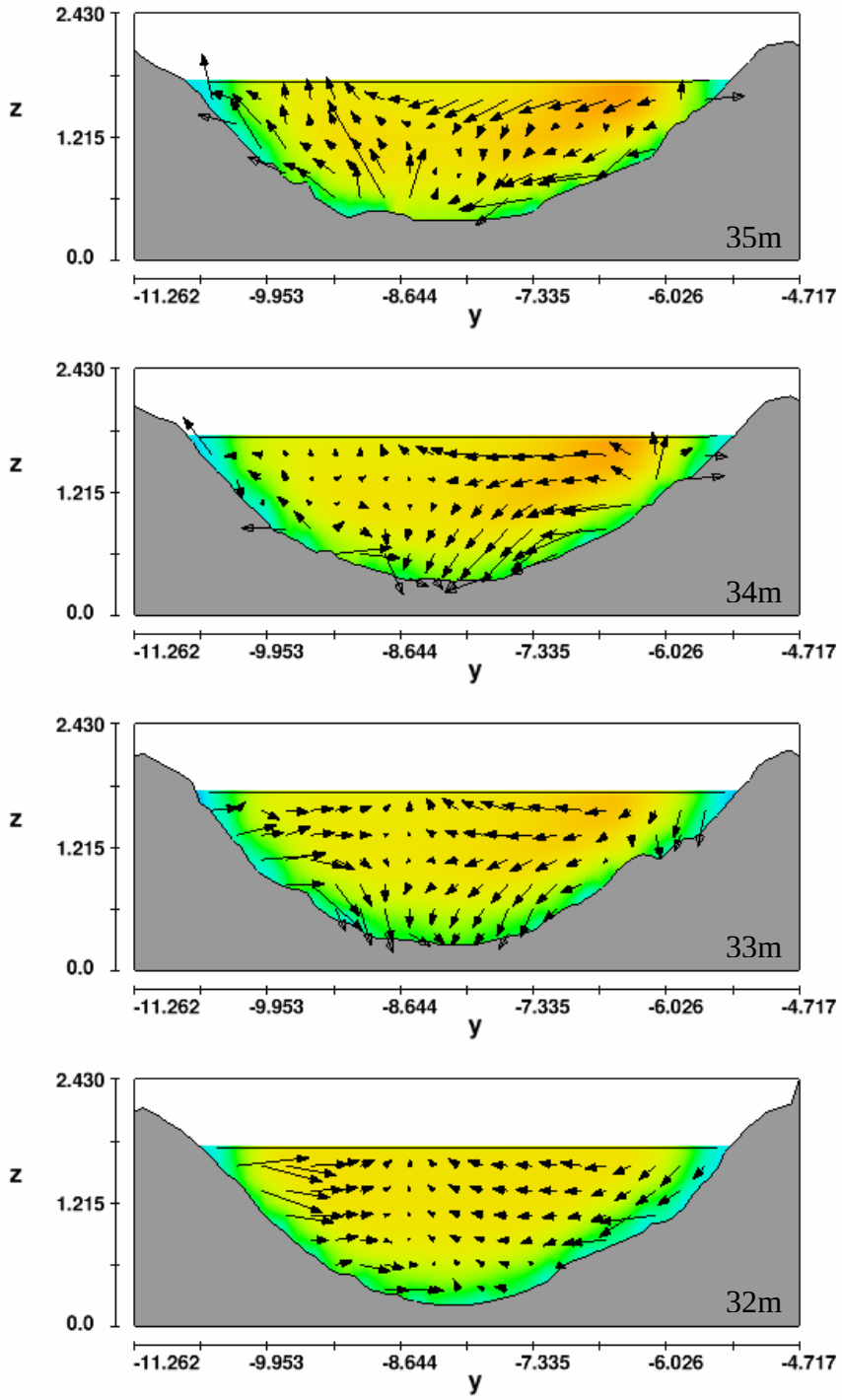
2.430
z
1.215
0.0
35m
-11.262
-9.953
-8.644
-7.335
-6.026
-4.717
y
2.430
z
1.215
0.0
34m
-11.262
-9.953
-8.644
-7.335
-6.026
-4.717
y
2.430
z
1.215
0.0
33m
-11.262
-9.953
-8.644
-7.335
-6.026
-4.717
y
2.430
z
1.215
0.0
32m
-11.262
-9.953
-8.644
-7.335
-6.026
-4.717
y

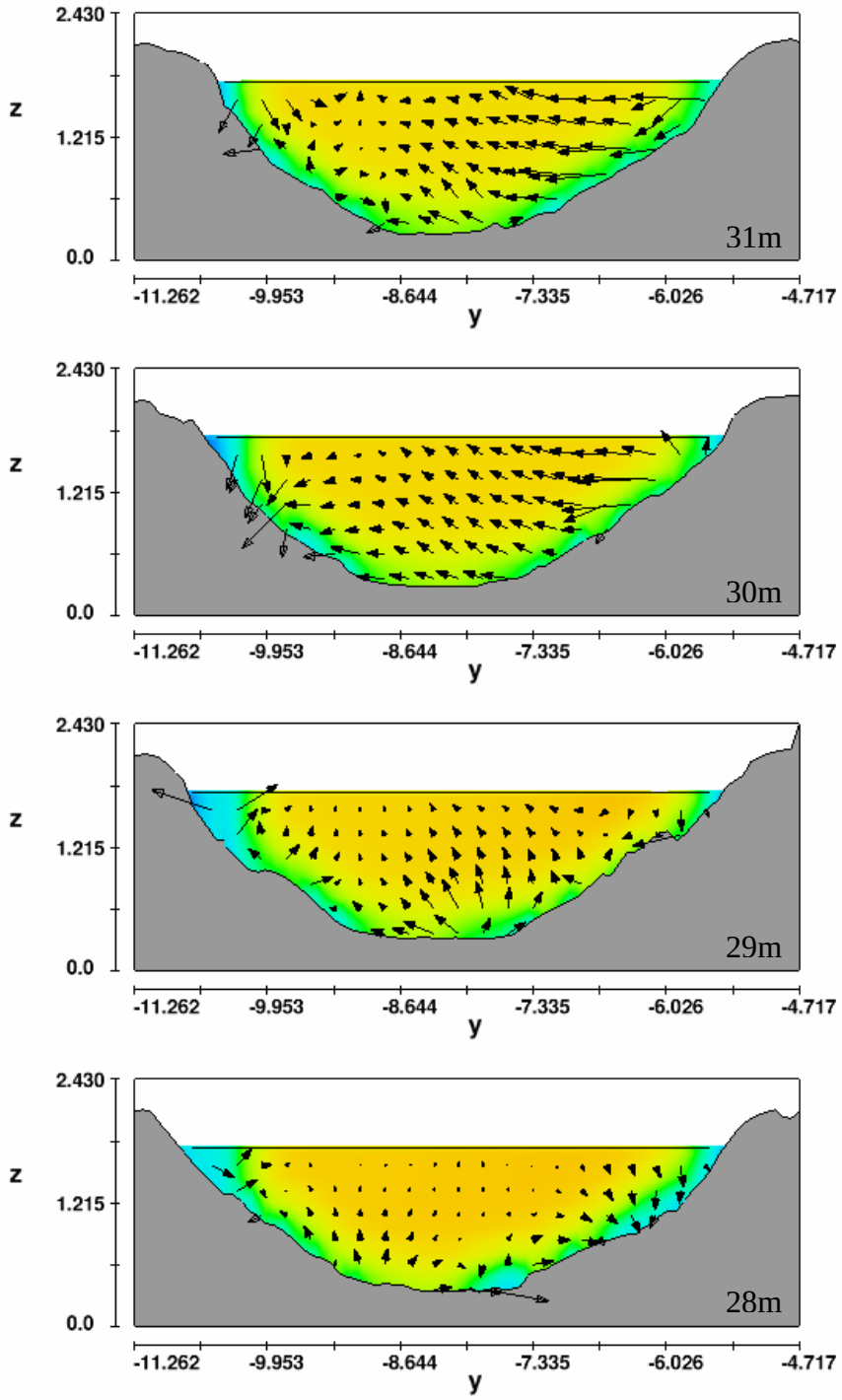
2.430
z
1.215
0.0
31m
-11.262
-9.953
-8.644
-7.335
-6.026
-4.717
y
2.430
z
1.215
0.0
30m
-11.262
-9.953
-8.644
-7.335
-6.026
-4.717
y
2.430
z
1.215
0.0
29m
-11.262
-9.953
-8.644
-7.335
-6.026
-4.717
y
2.430
z
1.215
0.0
28m
-11.262
-9.953
-8.644
-7.335
-6.026
-4.717
y

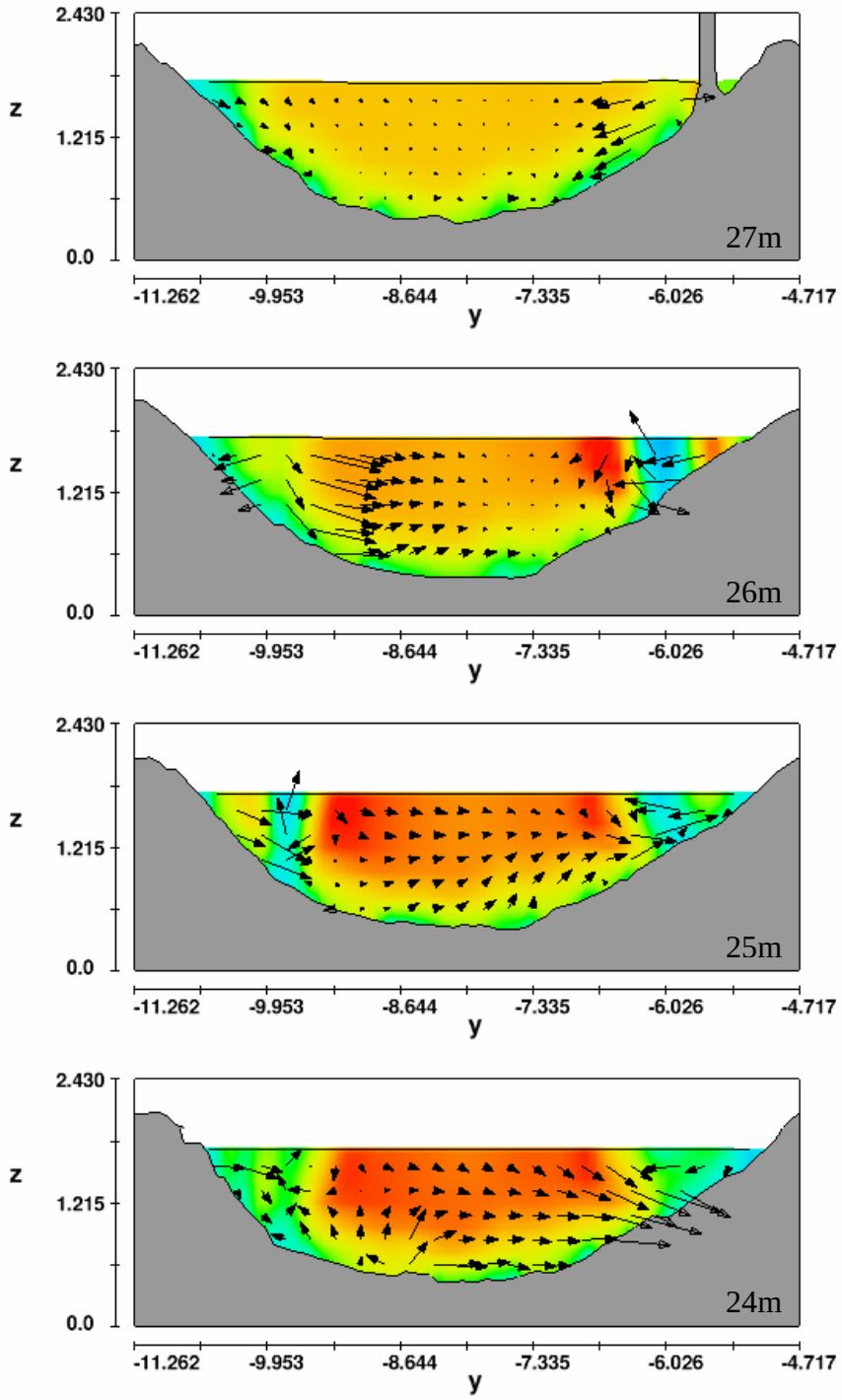
2.430
z
1.215
0.0
27m
-11.262
-9.953
-8.644
-7.335
-6.026
-4.717
y
2.430
z
1.215
0.0
26m
-11.262
-9.953
-8.644
-7.335
-6.026
-4.717
y
2.430
z
1.215
0.0
25m
-11.262
-9.953
-8.644
-7.335
-6.026
-4.717
y
2.430
z
1.215
0.0
24m
-11.262
-9.953
-8.644
-7.335
-6.026
-4.717
y

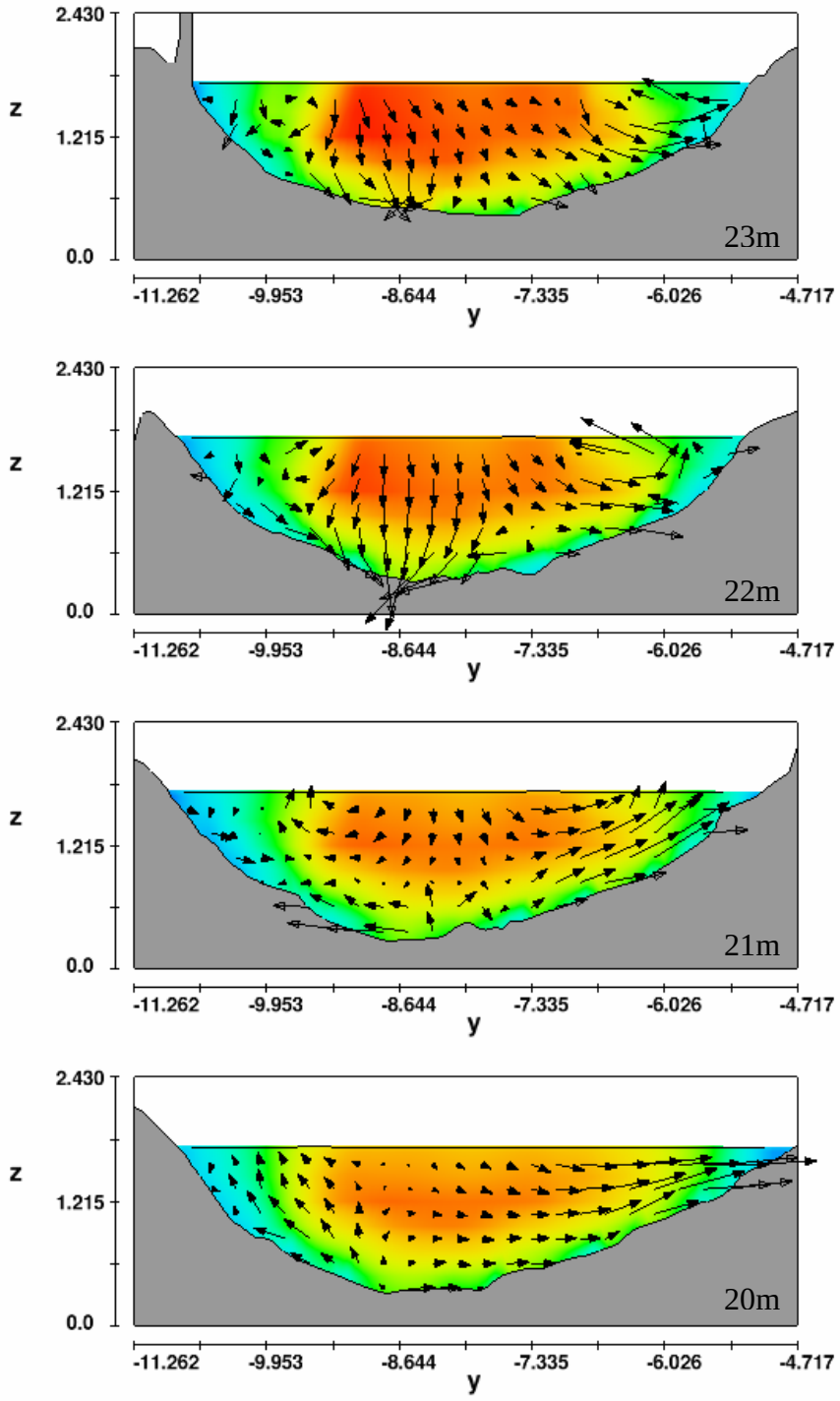
2.430
z
1.215
0.0
23m
-11.262
-9.953
-8.644
-7.335
-6.026
-4.717
y
2.430
z
1.215
0.0
22m
-11.262
-9.953
-8.644
-7.335
-6.026
-4.717
y
2.430
z
1.215
0.0
21m
-11.262
-9.953
-8.644
-7.335
-6.026
-4.717
y
2.430
z
1.215
0.0
20m
-11.262
-9.953
-8.644
-7.335
-6.026
-4.717
y

Vita

Frank Dworak was born in Chicago Illinois on April 23, 1971. He graduated from Bloom Trail High School in Chicago Heights, IL in June 1989. He pursued a career in carpentry before going to the University of Montana, where he graduated with a Bachelor's degree in Biology during May of 1997. Frank then returned to college at the University of Tennessee in pursuit of a Bachelor's degree in Civil Engineering. He graduated at the top of his class in May 2004 and continued his education after being invited into the graduate program at the University of Tennessee. He will receive his Master's of Science degree in Environmental Engineering in December 2005, majoring in Water Resources Engineering.